

Finding flavon

Gauhar Abbas^{a1}
 Ashutosh Kumar Alok^{b2}
 Neetu Raj Singh Chundawat^{b3}
 Najimuddin Khan^{c4}
 Neelam Singh^{a5}

^a *Department of Physics, Indian Institute of Technology (BHU), Varanasi 221005, India*

^b *Indian Institute of Technology Jodhpur, Jodhpur 342037, India*

^c *Department of Physics, Aligarh Muslim University, Aligarh-202002, India*

Abstract

We conduct a comprehensive investigation into the flavour phenomenology and collider signatures of flavon of $\mathcal{Z}_N \times \mathcal{Z}_M$ flavour symmetries for the soft symmetry-breaking scenario and a new symmetry-conserving mechanism at the high-luminosity LHC, high energy LHC, and a 100 TeV hadron collider. The flavour physics of quark and leptonic observables places different bounds on the parameter space of flavons of $\mathcal{Z}_N \times \mathcal{Z}_M$ flavour symmetries. On the collider side, the decay $t \rightarrow ca$ can be probed by the high-luminosity LHC, high energy LHC, and a 100 TeV hadron collider for the $\mathcal{Z}_8 \times \mathcal{Z}_{22}$ flavour symmetry. The inclusive production signatures can be used to probe the flavon of all the $\mathcal{Z}_N \times \mathcal{Z}_M$ flavour symmetries for the soft symmetry-breaking scenario for a heavy flavon at a 100 TeV collider. Flavons of all the $\mathcal{Z}_N \times \mathcal{Z}_M$ flavour symmetries can be probed at high energy LHC and a 100 TeV collider for a low mass in the case of soft symmetry-breaking. The di-flavon production is within reach of the high-luminosity LHC, high energy LHC, and a 100 TeV collider only for a light flavon. The 14 TeV high-luminosity LHC can probe only the $\mathcal{Z}_2 \times \mathcal{Z}_5$ and $\mathcal{Z}_8 \times \mathcal{Z}_{22}$ flavour symmetries for a few specific inclusive signatures. The symmetry-conserving scenario remains beyond the detection capabilities of any collider.

¹email: gauhar.phy@iitbhu.ac.in

²email: akalok@iitj.ac.in

³email: chundawat.1@iitj.ac.in

⁴email: nkhan.ph@amu.ac.in

⁵email: neelamsingh.rs.phy19@iitbhu.ac.in

1 Introduction

The enigma of fermion masses and quark mixing has persisted since the advent of the Standard Model [1, 2]. This challenge has been further exacerbated by the inclusion of neutrino masses and mixing. Potential resolutions to this issue may arise from various theoretical frameworks. Among these are the dark technicolor model, which addresses the problem through hierarchical vacuum expectation values (VEVs) manifested as sequential multi-fermion chiral condensates [3, 4, 5, 6], continuous flavour symmetries [7, 8, 9, 10, 11, 12, 13, 14, 15, 16, 17, 18, 19], discrete symmetries [20, 21, 22, 23], and alternative frameworks [24, 25, 26, 27].

The $\mathcal{Z}_N \times \mathcal{Z}_M$ flavour symmetry [20] is capable of explaining the masses and mixing of fermions through the different realizations of the Froggatt-Nielsen (FN) mechanism [7]. This symmetry is a subset of a more generic $\mathcal{Z}_N \times \mathcal{Z}_M \times \mathcal{Z}_P$ flavour symmetry, which naturally emerges in a dark technicolour framework [4, 1].

The FN mechanism is built upon the idea that an Abelian flavour symmetry $U(1)_F$ can differentiate among the different flavours among inter and intra-fermionic generations of the SM. A flavon field, χ , is employed for this purpose, which couples with the top quark at tree-level, and the masses of other fermions originate from the higher dimensional non-renormalizable operators constructed using the flavon field and choosing the appropriate charges of the fields under the flavour symmetry $U(1)_F$. For instance, if the charges of the fermions fields ψ_i^c and ψ_j are θ_i and θ_j , respectively, under the $U(1)_F$ flavour symmetry, and the Higgs field is assigned zero charge, the Yukawa Lagrangian for the masses of fermions takes the form of non-renormalizable operators,

$$\begin{aligned} \mathcal{O} &= y \left(\frac{\chi}{\Lambda} \right)^{(\theta_i + \theta_j)} \bar{\psi} \varphi \psi, \\ &= y \epsilon^{(\theta_i + \theta_j)} \bar{\psi} \varphi \psi = Y \bar{\psi} \varphi \psi \end{aligned} \quad (1)$$

where y denotes the dimensionless coupling constant, Λ represents the scale of the flavour symmetry, $\epsilon = \frac{\langle \chi \rangle}{\Lambda}$, $Y = y \epsilon^{(\theta_i + \theta_j)}$ stands for the effective Yukawa coupling, and the transformation of the gauge singlet flavon scalar field χ under the $SU(3)_c \times SU(2)_L \times U(1)_Y$ symmetry of the SM is given by,

$$\chi : (1, 1, 0). \quad (2)$$

The VEV of the flavon field χ breaks the $U(1)_F$ flavour symmetry spontaneously. The scale Λ , where the higher dimension operators appearing in equation 1 get renormalized, is not predicted by the FN mechanism, and it can be anywhere between the weak and the Planck scale. The essential requirement for the FN mechanism is that the flavour symmetry is broken in a way such that the ratio $\frac{\langle \chi \rangle}{\Lambda} < 1$.

The flavour phenomenology of the flavon field is determined by the scale Λ . The flavon field can impact flavour observables such as neutral meson mixing and CP -violation, meson decays, and charged lepton flavour violating effects. These effects could be detectable if the scale Λ is relatively low, closer to the weak scale. In such a scenario, it would also be possible to investigate the direct production of flavons in hadron colliders, like the Large Hadron Collider (LHC). Therefore, a critical question is how low the scale Λ can be, while still satisfying constraints from flavour physics data. This question also hinges on the nature of the flavour symmetry implementing the FN mechanism. For a continuous symmetry such as the $U(1)_F$ flavour symmetry, it is essential to determine whether it is a global or gauged symmetry. If $U(1)_F$ is a gauged symmetry, the flavour and collider phenomenology of the flavon field will include contributions from the exchange of the corresponding gauge boson. Conversely, a global $U(1)_F$ flavour symmetry would face the issue of a massless Goldstone boson.

The $\mathcal{Z}_N \times \mathcal{Z}_M$ flavour symmetry creates the FN mechanism through the product of two discrete symmetries. This results in a flavour structure of the SM, which is written in terms of the small parameter ϵ . The neutrino masses and mixing can also be recovered in this framework [21]. The theoretical origin of the $\mathcal{Z}_N \times \mathcal{Z}_M$ flavour symmetry may be traced back to an underlying Abelian or non-Abelian continuous symmetry or their products. For instance, in the dark technicolour framework, this symmetry is the result of the breaking of the two $U(1)$ axial symmetries [4, 1].

The flavour phenomenology of two simple prototypes of the $\mathcal{Z}_N \times \mathcal{Z}_M$ flavour symmetries is investigated in reference [21] where $N = 2$ and $M = 5, 9$ are used. The choice $N = 2$ is inspired by the use of the discrete \mathcal{Z}_2 symmetry in different scenarios, such as the two-Higgs-doublet model (2HDM) and the minimal supersymmetric

SM (MSSM), as well as the left-right symmetric mirror models [28, 29, 30, 31]. There are extensive phenomenological investigations of the flavon field in literature. For instance, for flavour phenomenology, see references [21, 32, 33, 34, 35, 36], and for collider studies, see the references [37, 38, 39, 40, 41, 42, 22, 43, 44].

In this work, we conduct a comprehensive investigation into the flavour phenomenology and collider signatures of the flavon associated with $\mathcal{Z}_N \times \mathcal{Z}_M$ flavour symmetries, extending beyond established prototypes. We examine quark flavour constraints through neutral meson mixing and decays and derive constraints on the flavon of $\mathcal{Z}_N \times \mathcal{Z}_M$ flavour symmetries from a wide range of observables in diverse decay channels, specifically focusing on the quark-level transition $b \rightarrow s\mu^+\mu^-$. Additionally, we investigate the muon forward-backward asymmetry in $B \rightarrow K\mu^+\mu^-$ decays, which is predicted to be zero within the SM. Furthermore, we explore the bounds from future sensitivities of lepton flavour violation experiments such as MEG-II, Mu3e, PRISM/PRIME, DeeMe, Mu2e, and COMET. We demonstrate that these upcoming experiments have the potential to constrain the parameter space of the flavon associated with $\mathcal{Z}_N \times \mathcal{Z}_M$ flavour symmetries by orders of magnitude compared to existing limits.

In the conventional approach, flavour and collider studies of flavon physics involve imparting mass to the pseudoscalar component of the flavon field through a soft symmetry-breaking term [21, 32, 33, 35, 36]. We investigate the flavour phenomenology and collider signatures of the flavon associated with $\mathcal{Z}_N \times \mathcal{Z}_M$ flavour symmetries using both the conventional approach and a novel symmetry-conserving mass mechanism for the pseudoscalar component of the flavon field. This novel scenario proves to be highly predictive.

For the collider signatures, our primary focus is on the High Luminosity LHC (HL-LHC), the High-Energy Large Hadron Collider (HE-LHC) [45], and a future high-luminosity 100 TeV hadron collider such as FCC-hh [46]. We classify the search for flavons into low and high-mass regions, with the low-mass region being particularly sensitive to the new symmetry-conserving mass mechanism of the pseudoscalar flavon. We utilize inclusive decay channels such as $\ell\ell$, $b\bar{b}$, and $t\bar{t}$, as well as associative production channels like $t\bar{t}a \rightarrow t\bar{t}t\bar{t}$, $gg \rightarrow abb \rightarrow \tau\tau b\bar{b}$, and $gb \rightarrow ab \rightarrow \tau\tau b$ to identify the flavon of different $\mathcal{Z}_N \times \mathcal{Z}_M$ flavour symmetries. Additionally, we investigate di-flavon production for both light and heavy flavon to determine the sensitivities of flavon models associated with $\mathcal{Z}_N \times \mathcal{Z}_M$ flavour symmetries. Throughout our investigation, we do not assume any specific ultraviolet (UV) completion of the $\mathcal{Z}_N \times \mathcal{Z}_M$ flavour symmetries, and we conduct our phenomenological studies in a model-independent manner.

This work will be presented along the following track: In section 2, we discuss different $\mathcal{Z}_N \times \mathcal{Z}_M$ flavour symmetries and their motivations. The scalar potential with the soft symmetry-breaking and the symmetry-conserving scenarios is presented in section 3. In section 4, bounds on the parameter space of the flavon of different $\mathcal{Z}_N \times \mathcal{Z}_M$ flavour symmetries from quark flavour physics are derived. We discuss constraints from lepton flavour violation experiments in section 5. We discuss the hadron collider physics of the flavon of the $\mathcal{Z}_N \times \mathcal{Z}_M$ flavour symmetries in section 6. In section 7, we summarize this work.

2 The $\mathcal{Z}_N \times \mathcal{Z}_M$ flavour symmetry

In this section, we present different realizations of the $\mathcal{Z}_N \times \mathcal{Z}_M$ flavour symmetry, for which we investigate the flavour phenomenology and collider signatures of the flavon field. A minimal form of the $\mathcal{Z}_N \times \mathcal{Z}_M$ flavour symmetry, $\mathcal{Z}_2 \times \mathcal{Z}_5$, was first proposed in reference [20], and flavour bounds on this minimal form, along with a non-minimal form, $\mathcal{Z}_2 \times \mathcal{Z}_9$, are derived in reference [4].

The theoretical origin of the $\mathcal{Z}_N \times \mathcal{Z}_M$ flavour symmetry may come from spontaneous breaking of a $U(1) \times U(1)$ symmetry, which could be a global or a local symmetry. It is also possible that this symmetry contains only one $U(1)$ factor as a local symmetry. The crucial difference between the FN mechanism based on the $\mathcal{Z}_N \times \mathcal{Z}_M$ flavour symmetry and the FN mechanism based on a $U(1)$ symmetry is that the $\mathcal{Z}_N \times \mathcal{Z}_M$ flavour symmetry may also originate from the breaking of a global $U(1)_A \times U(1)_A$ symmetry. This keeps apart the FN mechanism based on the $\mathcal{Z}_N \times \mathcal{Z}_M$ flavour symmetry from that based on the conventional $U(1)$ symmetry. Such a theoretical scenario is discussed in the appendix.

The FN mechanism is produced by imposing the $\mathcal{Z}_N \times \mathcal{Z}_M$ flavour symmetry on the SM. This provides the following mass Lagrangian for fermions,

$$-\mathcal{L}_{\text{Yukawa}} = \left[\frac{\chi(\text{or } \chi^\dagger)}{\Lambda} \right]^{n_{ij}^u} y_{ij}^u \bar{\psi}_{L_i}^q \tilde{\varphi} \psi_{R_j}^u + \left[\frac{\chi(\text{or } \chi^\dagger)}{\Lambda} \right]^{n_{ij}^d} y_{ij}^d \bar{\psi}_{L_i}^q \varphi \psi_{R_j}^d$$

$$+ \left[\frac{\chi(\text{or } \chi^\dagger)}{\Lambda} \right]^{n_{ij}} y_{ij}^\ell \bar{\psi}_{L_i}^\ell \varphi \psi_{R_j}^\ell + \text{H.c.}, \quad (3)$$

The complex singlet scalar field χ acquires VEV $\langle \chi \rangle = f$, and the Lagrangian corresponding to the SM fermions (charged leptons and quarks) mass is given by

$$= Y_{ij}^u \bar{\psi}_{L_i}^q \tilde{\varphi} \psi_{R_j}^u + Y_{ij}^d \bar{\psi}_{L_i}^q \varphi \psi_{R_j}^d + Y_{ij}^\ell \bar{\psi}_{L_i}^\ell \varphi \psi_{R_j}^\ell + \text{H.c.}, \quad (4)$$

where i and j show the generation indices, ψ_L^q, ψ_L^ℓ are left-handed doublets of the quark and leptonic fields, $\psi_R^u, \psi_R^d, \psi_R^\ell$ are the right-handed up, down-type quarks and leptons, $\tilde{\varphi} = -i\sigma_2 \varphi^*$, φ represent the SM Higgs doublet, and σ_2 is the second Pauli matrix. The couplings Y_{ij} stand for the effective Yukawa couplings such that $Y_{ij} = y_{ij} \epsilon^{n_{ij}}$, where $\frac{\langle \chi \rangle}{\Lambda} = \frac{f}{\sqrt{2}\Lambda} = \epsilon < 1$.

2.1 $\mathcal{Z}_2 \times \mathcal{Z}_5$ flavour symmetry

The first minimal realization of the $\mathcal{Z}_N \times \mathcal{Z}_M$ flavour symmetry is the $\mathcal{Z}_2 \times \mathcal{Z}_5$ flavour symmetry. The transformations of the scalar and fermionic fields under this symmetry are provided in table 1.

Fields	\mathcal{Z}_2	\mathcal{Z}_5
u_R, c_R, t_R	+	ω^2
$d_R, s_R, b_R, e_R, \mu_R, \tau_R$	-	ω
$\psi_{L_1}^q$	+	ω
$\psi_{L_2}^q$	+	ω^4
$\psi_{L_3}^q$	+	ω^2
$\psi_{L_1}^\ell$	+	ω
$\psi_{L_2}^\ell$	+	ω^4
$\psi_{L_3}^\ell$	+	ω^2
χ	-	ω
φ	+	1

Table 1: The charges of left and right-handed fermions of three families of the SM, right-handed neutrinos, Higgs, and singlet scalar fields under \mathcal{Z}_2 and \mathcal{Z}_5 symmetries, where ω is the fifth root of unity.

The $\mathcal{Z}_2 \times \mathcal{Z}_5$ flavour symmetry enables us to write the mass Lagrangian for charged fermions as,

$$\begin{aligned} -\mathcal{L}_{\text{Yukawa}} &= \left(\frac{\chi}{\Lambda}\right)^4 y_{11}^u \bar{\psi}_{L_1}^q \tilde{\varphi} u_R + \left(\frac{\chi}{\Lambda}\right)^4 y_{12}^u \bar{\psi}_{L_1}^q \tilde{\varphi} c_R + \left(\frac{\chi}{\Lambda}\right)^4 y_{13}^u \bar{\psi}_{L_1}^q \tilde{\varphi} t_R + \left(\frac{\chi}{\Lambda}\right)^2 y_{21}^u \bar{\psi}_{L_2}^q \tilde{\varphi} u_R \\ &+ \left(\frac{\chi}{\Lambda}\right)^2 y_{22}^u \bar{\psi}_{L_2}^q \tilde{\varphi} c_R + \left(\frac{\chi}{\Lambda}\right)^2 y_{23}^u \bar{\psi}_{L_2}^q \tilde{\varphi} t_R + y_{31}^u \bar{\psi}_{L_3}^q \tilde{\varphi} u_R + y_{32}^u \bar{\psi}_{L_3}^q \tilde{\varphi} c_R + y_{33}^u \bar{\psi}_{L_3}^q \tilde{\varphi} t_R \\ &+ \left(\frac{\chi}{\Lambda}\right)^5 y_{11}^d \bar{\psi}_{L_1}^q \varphi d_R + \left(\frac{\chi}{\Lambda}\right)^5 y_{12}^d \bar{\psi}_{L_1}^q \varphi s_R + \left(\frac{\chi}{\Lambda}\right)^5 y_{13}^d \bar{\psi}_{L_1}^q \varphi b_R + \left(\frac{\chi}{\Lambda}\right)^3 y_{21}^d \bar{\psi}_{L_2}^q \varphi d_R \\ &+ \left(\frac{\chi}{\Lambda}\right)^3 y_{22}^d \bar{\psi}_{L_2}^q \varphi s_R + \left(\frac{\chi}{\Lambda}\right)^3 y_{23}^d \bar{\psi}_{L_2}^q \varphi b_R + \left(\frac{\chi}{\Lambda}\right)^3 y_{31}^d \bar{\psi}_{L_3}^q \varphi d_R + \left(\frac{\chi}{\Lambda}\right)^3 y_{32}^d \bar{\psi}_{L_3}^q \varphi s_R \\ &+ \left(\frac{\chi}{\Lambda}\right)^3 y_{33}^d \bar{\psi}_{L_3}^q \varphi b_R + \left(\frac{\chi}{\Lambda}\right)^5 y_{11}^\ell \bar{\psi}_{L_1}^\ell \varphi e_R + \left(\frac{\chi}{\Lambda}\right)^5 y_{12}^\ell \bar{\psi}_{L_1}^\ell \varphi \mu_R + \left(\frac{\chi}{\Lambda}\right)^5 y_{13}^\ell \bar{\psi}_{L_1}^\ell \varphi \tau_R \\ &+ \left(\frac{\chi}{\Lambda}\right)^3 y_{21}^\ell \bar{\psi}_{L_2}^\ell \varphi e_R + \left(\frac{\chi}{\Lambda}\right)^3 y_{22}^\ell \bar{\psi}_{L_2}^\ell \varphi \mu_R + \left(\frac{\chi}{\Lambda}\right)^3 y_{23}^\ell \bar{\psi}_{L_2}^\ell \varphi \tau_R + \left(\frac{\chi}{\Lambda}\right)^3 y_{31}^\ell \bar{\psi}_{L_3}^\ell \varphi e_R \\ &+ \left(\frac{\chi}{\Lambda}\right)^3 y_{32}^\ell \bar{\psi}_{L_3}^\ell \varphi \mu_R + \left(\frac{\chi}{\Lambda}\right)^3 y_{33}^\ell \bar{\psi}_{L_3}^\ell \varphi \tau_R + \text{H.c.} \end{aligned}$$

The mass matrices for up- and down-type quarks and charged leptons read,

$$\mathcal{M}_u = \frac{v}{\sqrt{2}} \begin{pmatrix} y_{11}^u \epsilon^4 & y_{12}^u \epsilon^4 & y_{13}^u \epsilon^4 \\ y_{21}^u \epsilon^2 & y_{22}^u \epsilon^2 & y_{23}^u \epsilon^2 \\ y_{31}^u & y_{32}^u & y_{33}^u \end{pmatrix}, \mathcal{M}_d = \frac{v}{\sqrt{2}} \begin{pmatrix} y_{11}^d \epsilon^5 & y_{12}^d \epsilon^5 & y_{13}^d \epsilon^5 \\ y_{21}^d \epsilon^3 & y_{22}^d \epsilon^3 & y_{23}^d \epsilon^3 \\ y_{31}^d \epsilon & y_{32}^d \epsilon & y_{33}^d \epsilon \end{pmatrix}, \mathcal{M}_\ell = \frac{v}{\sqrt{2}} \begin{pmatrix} y_{11}^\ell \epsilon^5 & y_{12}^\ell \epsilon^5 & y_{13}^\ell \epsilon^5 \\ y_{21}^\ell \epsilon^3 & y_{22}^\ell \epsilon^3 & y_{23}^\ell \epsilon^3 \\ y_{31}^\ell \epsilon & y_{32}^\ell \epsilon & y_{33}^\ell \epsilon \end{pmatrix}, \quad (5)$$

where $\epsilon = 0.1$ can produce the required masses of the fermions.

The masses of the charged fermions can be written as[47],

$$\{m_t, m_c, m_u\} \simeq \{|y_{33}^u|, |y_{22}^u - \frac{y_{23}^u y_{32}^u}{y_{33}^u}| \epsilon^2, \quad (6)$$

$$|y_{11}^u - \frac{y_{12}^u y_{21}^u}{|y_{22}^u - y_{23}^u y_{32}^u / y_{33}^u}| - \frac{y_{13}^u |y_{31}^u y_{22}^u - y_{21}^u y_{32}^u| - y_{31}^u y_{12}^u y_{23}^u}{|y_{22}^u - y_{23}^u y_{32}^u / y_{33}^u| |y_{33}^u|} \epsilon^4 \} v / \sqrt{2},$$

$$\{m_b, m_s, m_d\} \simeq \{|y_{33}^d| \epsilon, |y_{22}^d - \frac{y_{23}^d y_{32}^d}{y_{33}^d}| \epsilon^3, \quad (7)$$

$$|y_{11}^d - \frac{y_{12}^d y_{21}^d}{|y_{22}^d - y_{23}^d y_{32}^d / y_{33}^d}| - \frac{y_{13}^d |y_{31}^d y_{22}^d - y_{21}^d y_{32}^d| - y_{31}^d y_{12}^d y_{23}^d}{|y_{22}^d - y_{23}^d y_{32}^d / y_{33}^d| |y_{33}^d|} \epsilon^5 \} v / \sqrt{2},$$

$$\{m_\tau, m_\mu, m_e\} \simeq \{|y_{33}^\ell| \epsilon, |y_{22}^\ell - \frac{y_{23}^\ell y_{32}^\ell}{y_{33}^\ell}| \epsilon^3, \quad (8)$$

$$|y_{11}^\ell - \frac{y_{12}^\ell y_{21}^\ell}{|y_{22}^\ell - y_{23}^\ell y_{32}^\ell / y_{33}^\ell}| - \frac{y_{13}^\ell |y_{31}^\ell y_{22}^\ell - y_{21}^\ell y_{32}^\ell| - y_{31}^\ell y_{12}^\ell y_{23}^\ell}{|y_{22}^\ell - y_{23}^\ell y_{32}^\ell / y_{33}^\ell| |y_{33}^\ell|} \epsilon^5 \} v / \sqrt{2}, \quad (9)$$

The quark mixing angles are [48],

$$\sin \theta_{12} \simeq |V_{us}| \simeq \left| \frac{y_{12}^d}{y_{22}^d} - \frac{y_{12}^u}{y_{22}^u} \right| \epsilon^2, \sin \theta_{23} \simeq |V_{cb}| \simeq \left| \frac{y_{23}^d}{y_{33}^d} - \frac{y_{23}^u}{y_{33}^u} \right| \epsilon^2,$$

$$\sin \theta_{13} \simeq |V_{ub}| \simeq \left| \frac{y_{13}^d}{y_{33}^d} - \frac{y_{12}^u y_{23}^d}{y_{22}^u y_{33}^d} - \frac{y_{13}^u}{y_{33}^u} \right| \epsilon^4. \quad (10)$$

2.2 $\mathcal{Z}_2 \times \mathcal{Z}_9$ flavour symmetry

A non-minimal realization of the $\mathcal{Z}_N \times \mathcal{Z}_M$ flavour symmetry is the $\mathcal{Z}_2 \times \mathcal{Z}_9$ flavour symmetry. The scalar and fermionic fields transform under this symmetry, as given in table 2.

Fields	\mathcal{Z}_2	\mathcal{Z}_9
u_R, t_R	+	1
c_R	+	ω^4
$d_R, s_R, b_R, e_R, \mu_R, \tau_R$	-	ω^3
$\psi_{L_1}^q$	+	ω
$\psi_{L_2}^q$	+	ω^8
$\psi_{L_3}^q$	+	1
$\psi_{L_1}^\ell$	+	ω
$\psi_{L_2}^\ell$	+	ω^8
$\psi_{L_3}^\ell$	+	ω^6
χ	-	ω
φ	+	1

Table 2: The charges of left and right-handed fermions of three families of the SM, right-handed neutrinos, Higgs, and singlet scalar field under \mathcal{Z}_2 and \mathcal{Z}_9 symmetries, where ω is the ninth root of unity.

After imposing the $\mathcal{Z}_2 \times \mathcal{Z}_9$ flavour symmetry on the SM, the mass Lagrangian for charged fermions reads as,

$$\begin{aligned}
-\mathcal{L}_{\text{Yukawa}} &= \left(\frac{\chi^\dagger}{\Lambda}\right)^8 y_{11}^u \bar{\psi}_{L_1}^q \tilde{\varphi} u_R + \left(\frac{\chi}{\Lambda}\right)^6 y_{12}^u \bar{\psi}_{L_1}^q \tilde{\varphi} c_R + \left(\frac{\chi^\dagger}{\Lambda}\right)^8 y_{13}^u \bar{\psi}_{L_1}^q \tilde{\varphi} t_R + \left(\frac{\chi}{\Lambda}\right)^8 y_{21}^u \bar{\psi}_{L_2}^q \tilde{\varphi} u_R \\
&+ \left(\frac{\chi}{\Lambda}\right)^4 y_{22}^u \bar{\psi}_{L_2}^q \tilde{\varphi} c_R + \left(\frac{\chi}{\Lambda}\right)^8 y_{23}^u \bar{\psi}_{L_2}^q \tilde{\varphi} t_R + y_{31}^u \bar{\psi}_{L_3}^q \tilde{\varphi} u_R + \left(\frac{\chi^\dagger}{\Lambda}\right)^4 y_{32}^u \bar{\psi}_{L_3}^q \tilde{\varphi} c_R + y_{33}^u \bar{\psi}_{L_3}^q \tilde{\varphi} t_R \\
&+ \left(\frac{\chi}{\Lambda}\right)^7 y_{11}^d \bar{\psi}_{L_1}^q \varphi d_R + \left(\frac{\chi}{\Lambda}\right)^7 y_{12}^d \bar{\psi}_{L_1}^q \varphi s_R + \left(\frac{\chi}{\Lambda}\right)^7 y_{13}^d \bar{\psi}_{L_1}^q \varphi b_R + \left(\frac{\chi}{\Lambda}\right)^5 y_{21}^d \bar{\psi}_{L_2}^q \varphi d_R \\
&+ \left(\frac{\chi}{\Lambda}\right)^5 y_{22}^d \bar{\psi}_{L_2}^q \varphi s_R + \left(\frac{\chi}{\Lambda}\right)^5 y_{23}^d \bar{\psi}_{L_2}^q \varphi b_R + \left(\frac{\chi^\dagger}{\Lambda}\right)^3 y_{31}^d \bar{\psi}_{L_3}^q \varphi d_R + \left(\frac{\chi^\dagger}{\Lambda}\right)^3 y_{32}^d \bar{\psi}_{L_3}^q \varphi s_R \\
&+ \left(\frac{\chi^\dagger}{\Lambda}\right)^3 y_{33}^d \bar{\psi}_{L_3}^q \varphi b_R + \left(\frac{\chi}{\Lambda}\right)^7 y_{11}^\ell \bar{\psi}_{L_1}^\ell \varphi e_R + \left(\frac{\chi}{\Lambda}\right)^7 y_{12}^\ell \bar{\psi}_{L_1}^\ell \varphi \mu_R + \left(\frac{\chi}{\Lambda}\right)^7 y_{13}^\ell \bar{\psi}_{L_1}^\ell \varphi \tau_R \\
&+ \left(\frac{\chi}{\Lambda}\right)^5 y_{21}^\ell \bar{\psi}_{L_2}^\ell \varphi e_R + \left(\frac{\chi}{\Lambda}\right)^5 y_{22}^\ell \bar{\psi}_{L_2}^\ell \varphi \mu_R + \left(\frac{\chi}{\Lambda}\right)^5 y_{23}^\ell \bar{\psi}_{L_2}^\ell \varphi \tau_R + \left(\frac{\chi}{\Lambda}\right)^3 y_{31}^\ell \bar{\psi}_{L_3}^\ell \varphi e_R \\
&+ \left(\frac{\chi}{\Lambda}\right)^3 y_{32}^\ell \bar{\psi}_{L_3}^\ell \varphi \mu_R + \left(\frac{\chi}{\Lambda}\right)^3 y_{33}^\ell \bar{\psi}_{L_3}^\ell \varphi \tau_R + \text{H.c.}
\end{aligned}$$

The mass matrices for up and down-type quarks and charged leptons read,

$$\mathcal{M}_u = \frac{v}{\sqrt{2}} \begin{pmatrix} y_{11}^u \epsilon^8 & y_{12}^u \epsilon^6 & y_{13}^u \epsilon^8 \\ y_{21}^u \epsilon^8 & y_{22}^u \epsilon^4 & y_{23}^u \epsilon^8 \\ y_{31}^u & y_{32}^u \epsilon^4 & y_{33}^u \end{pmatrix}, \mathcal{M}_d = \frac{v}{\sqrt{2}} \begin{pmatrix} y_{11}^d \epsilon^7 & y_{12}^d \epsilon^7 & y_{13}^d \epsilon^7 \\ y_{21}^d \epsilon^5 & y_{22}^d \epsilon^5 & y_{23}^d \epsilon^5 \\ y_{31}^d \epsilon^3 & y_{32}^d \epsilon^3 & y_{33}^d \epsilon^3 \end{pmatrix}, \mathcal{M}_\ell = \frac{v}{\sqrt{2}} \begin{pmatrix} y_{11}^\ell \epsilon^7 & y_{12}^\ell \epsilon^7 & y_{13}^\ell \epsilon^7 \\ y_{21}^\ell \epsilon^5 & y_{22}^\ell \epsilon^5 & y_{23}^\ell \epsilon^5 \\ y_{31}^\ell \epsilon^3 & y_{32}^\ell \epsilon^3 & y_{33}^\ell \epsilon^3 \end{pmatrix}. \quad (11)$$

where $\epsilon = 0.225$ is chosen to produce the masses of fermions.

The masses of charged fermions are approximately [47],

$$\{m_t, m_c, m_u\} \simeq \{|y_{33}^u|, |y_{22}^u \epsilon^4 - \frac{y_{23}^u y_{32}^u}{|y_{33}^u|} \epsilon^{12}|, \quad (12)$$

$$\left| y_{11}^u \epsilon^8 - \frac{y_{12}^u y_{21}^u}{|y_{22}^u|} \epsilon^{10} - \frac{y_{13}^u |y_{31}^u y_{22}^u - y_{21}^u y_{32}^u|}{|y_{22}^u| |y_{33}^u|} \epsilon^8 \right| v / \sqrt{2},$$

$$\{m_b, m_s, m_d\} \simeq \{|y_{33}^d| \epsilon^3, |y_{22}^d - \frac{y_{23}^d y_{32}^d}{|y_{33}^d|} \epsilon^5, \quad (13)$$

$$\left| y_{11}^d - \frac{y_{12}^d y_{21}^d}{|y_{22}^d - y_{23}^d y_{32}^d / y_{33}^d|} - \frac{y_{13}^d |y_{31}^d y_{22}^d - y_{21}^d y_{32}^d| - y_{31}^d y_{12}^d y_{23}^d}{|y_{22}^d - y_{23}^d y_{32}^d / y_{33}^d| |y_{33}^d|} \right| \epsilon^7 \} v / \sqrt{2},$$

$$\{m_\tau, m_\mu, m_e\} \simeq \{|y_{33}^\ell| \epsilon^3, |y_{22}^\ell - \frac{y_{23}^\ell y_{32}^\ell}{|y_{33}^\ell|} \epsilon^5, \quad (14)$$

$$\left| y_{11}^\ell - \frac{y_{12}^\ell y_{21}^\ell}{|y_{22}^\ell - y_{23}^\ell y_{32}^\ell / y_{33}^\ell|} - \frac{y_{13}^\ell |y_{31}^\ell y_{22}^\ell - y_{21}^\ell y_{32}^\ell| - y_{31}^\ell y_{12}^\ell y_{23}^\ell}{|y_{22}^\ell - y_{23}^\ell y_{32}^\ell / y_{33}^\ell| |y_{33}^\ell|} \right| \epsilon^7 \} v / \sqrt{2}, \quad (15)$$

The quark mixing angles are identical to that of the minimal $\mathcal{Z}_2 \times \mathcal{Z}_5$ flavour symmetry.

2.3 $\mathcal{Z}_2 \times \mathcal{Z}_{11}$ flavour symmetry

The next non-minimal realization of the $\mathcal{Z}_N \times \mathcal{Z}_M$ flavour symmetry is the $\mathcal{Z}_2 \times \mathcal{Z}_{11}$ flavour symmetry. The $\mathcal{Z}_2 \times \mathcal{Z}_{11}$ flavour symmetry, in this work, is chosen to probe a relatively large value of the parameter ϵ which is 0.27. The scalar and fermionic fields transform under this symmetry, as shown in table 3.

The mass Lagrangian for charged fermions after imposing $\mathcal{Z}_2 \times \mathcal{Z}_{11}$ flavour symmetry on the SM reads,

$$-\mathcal{L}_{\text{Yukawa}} = \left(\frac{\chi}{\Lambda}\right)^{10} y_{11}^u \bar{\psi}_{L_1}^q \tilde{\varphi} u_R + \left(\frac{\chi}{\Lambda}\right)^{10} y_{12}^u \bar{\psi}_{L_1}^q \tilde{\varphi} c_R + \left(\frac{\chi}{\Lambda}\right)^{12} y_{13}^u \bar{\psi}_{L_1}^q \tilde{\varphi} t_R + \left(\frac{\chi^\dagger}{\Lambda}\right)^6 y_{21}^u \bar{\psi}_{L_2}^q \tilde{\varphi} u_R$$

Fields	\mathcal{Z}_2	\mathcal{Z}_{11}
u_R, c_R	+	ω^2
t_R	+	1
$d_R, s_R, b_R, e_R, \mu_R, \tau_R$	-	ω^3
ψ_L^1	+	ω
ψ_L^2	+	ω^7
ψ_L^3	+	1
χ	-	ω
φ	+	1
σ	+	ω^4

Table 3: The charges of left and right-handed fermions of three families of the SM, right-handed neutrinos, Higgs, and singlet scalar fields under \mathcal{Z}_2 and \mathcal{Z}_{11} symmetries where ω is the eleventh root of unity.

$$\begin{aligned}
& + \left(\frac{\chi^\dagger}{\Lambda}\right)^6 y_{22}^u \bar{\psi}_{L_2}^q \tilde{\varphi} c_R + \left(\frac{\chi^\dagger}{\Lambda}\right)^4 y_{23}^u \bar{\psi}_{L_2}^q \tilde{\varphi} t_R + \left(\frac{\chi^\dagger}{\Lambda}\right)^2 y_{31}^u \bar{\psi}_{L_3}^q \tilde{\varphi} u_R + \left(\frac{\chi^\dagger}{\Lambda}\right)^2 y_{32}^u \bar{\psi}_{L_3}^q \tilde{\varphi} c_R \\
& + y_{33}^u \bar{\psi}_{L_3}^q \tilde{\varphi} t_R + \left(\frac{\chi}{\Lambda}\right)^9 y_{11}^d \bar{\psi}_{L_1}^q \varphi d_R + \left(\frac{\chi}{\Lambda}\right)^9 y_{12}^d \bar{\psi}_{L_1}^q \varphi s_R + \left(\frac{\chi}{\Lambda}\right)^9 y_{13}^d \bar{\psi}_{L_1}^q \varphi b_R + \left(\frac{\chi^\dagger}{\Lambda}\right)^7 y_{21}^d \bar{\psi}_{L_2}^q \varphi d_R \\
& + \left(\frac{\chi^\dagger}{\Lambda}\right)^7 y_{22}^d \bar{\psi}_{L_2}^q \varphi s_R + \left(\frac{\chi^\dagger}{\Lambda}\right)^7 y_{23}^d \bar{\psi}_{L_2}^q \varphi b_R + \left(\frac{\chi^\dagger}{\Lambda}\right)^3 y_{31}^d \bar{\psi}_{L_3}^q \varphi d_R + \left(\frac{\chi^\dagger}{\Lambda}\right)^3 y_{32}^d \bar{\psi}_{L_3}^q \varphi s_R \\
& + \left(\frac{\chi^\dagger}{\Lambda}\right)^3 y_{33}^d \bar{\psi}_{L_3}^q \varphi b_R + \left(\frac{\chi}{\Lambda}\right)^9 y_{11}^\ell \bar{\psi}_{L_1}^\ell \varphi e_R + \left(\frac{\chi}{\Lambda}\right)^9 y_{12}^\ell \bar{\psi}_{L_1}^\ell \varphi \mu_R + \left(\frac{\chi}{\Lambda}\right)^9 y_{13}^\ell \bar{\psi}_{L_1}^\ell \varphi \tau_R \\
& + \left(\frac{\chi^\dagger}{\Lambda}\right)^7 y_{21}^\ell \bar{\psi}_{L_2}^\ell \varphi e_R + \left(\frac{\chi^\dagger}{\Lambda}\right)^7 y_{22}^\ell \bar{\psi}_{L_2}^\ell \varphi \mu_R + \left(\frac{\chi^\dagger}{\Lambda}\right)^7 y_{23}^\ell \bar{\psi}_{L_2}^\ell \varphi \tau_R + \left(\frac{\chi^\dagger}{\Lambda}\right)^3 y_{31}^\ell \bar{\psi}_{L_3}^\ell \varphi e_R \\
& + \left(\frac{\chi^\dagger}{\Lambda}\right)^3 y_{32}^\ell \bar{\psi}_{L_3}^\ell \varphi \mu_R + \left(\frac{\chi^\dagger}{\Lambda}\right)^3 y_{33}^\ell \bar{\psi}_{L_3}^\ell \varphi \tau_R + \text{H.c.}
\end{aligned}$$

The mass matrices for up- and down-type quarks and charged leptons turn out to be,

$$\mathcal{M}_u = \frac{v}{\sqrt{2}} \begin{pmatrix} y_{11}^u \epsilon^{10} & y_{12}^u \epsilon^{10} & y_{13}^u \epsilon^{12} \\ y_{21}^u \epsilon^6 & y_{22}^u \epsilon^6 & y_{23}^u \epsilon^4 \\ y_{31}^u \epsilon^2 & y_{32}^u \epsilon^2 & y_{33}^u \end{pmatrix}, \mathcal{M}_d = \frac{v}{\sqrt{2}} \begin{pmatrix} y_{11}^d \epsilon^9 & y_{12}^d \epsilon^9 & y_{13}^d \epsilon^9 \\ y_{21}^d \epsilon^7 & y_{22}^d \epsilon^7 & y_{23}^d \epsilon^7 \\ y_{31}^d \epsilon^3 & y_{32}^d \epsilon^3 & y_{33}^d \epsilon^3 \end{pmatrix}, \mathcal{M}_\ell = \frac{v}{\sqrt{2}} \begin{pmatrix} y_{11}^\ell \epsilon^9 & y_{12}^\ell \epsilon^9 & y_{13}^\ell \epsilon^9 \\ y_{21}^\ell \epsilon^7 & y_{22}^\ell \epsilon^7 & y_{23}^\ell \epsilon^7 \\ y_{31}^\ell \epsilon^3 & y_{32}^\ell \epsilon^3 & y_{33}^\ell \epsilon^3 \end{pmatrix}. \quad (16)$$

The masses of quarks and charged leptons are approximately [47],

$$\{m_t, m_c, m_u\} \simeq \{|y_{33}^u|, \left|y_{22}^u - \frac{y_{23}^u y_{32}^u}{|y_{33}^u|}\right| \epsilon^6, \quad (17)$$

$$\left|y_{11}^u - \frac{y_{12}^u y_{21}^u}{|y_{22}^u - y_{23}^u y_{32}^u / y_{33}^u|} - \frac{y_{13}^u |y_{31}^u y_{22}^u - y_{21}^u y_{32}^u| - y_{31}^u y_{12}^u y_{23}^u}{|y_{22}^u - y_{23}^u y_{32}^u / y_{33}^u| |y_{33}^u|}\right| \epsilon^{10} \} v / \sqrt{2},$$

$$\{m_b, m_s, m_d\} \simeq \{|y_{33}^d| \epsilon^3, \left|y_{22}^d - \frac{y_{23}^d y_{32}^d}{|y_{33}^d|}\right| \epsilon^7, \quad (18)$$

$$\left|y_{11}^d - \frac{y_{12}^d y_{21}^d}{|y_{22}^d - y_{23}^d y_{32}^d / y_{33}^d|} - \frac{y_{13}^d |y_{31}^d y_{22}^d - y_{21}^d y_{32}^d| - y_{31}^d y_{12}^d y_{23}^d}{|y_{22}^d - y_{23}^d y_{32}^d / y_{33}^d| |y_{33}^d|}\right| \epsilon^9 \} v / \sqrt{2},$$

$$\{m_\tau, m_\mu, m_e\} \simeq \{|y_{33}^\ell| \epsilon^3, \left|y_{22}^\ell - \frac{y_{23}^\ell y_{32}^\ell}{|y_{33}^\ell|}\right| \epsilon^7, \quad (19)$$

$$\left|y_{11}^\ell - \frac{y_{12}^\ell y_{21}^\ell}{|y_{22}^\ell - y_{23}^\ell y_{32}^\ell / y_{33}^\ell|} - \frac{y_{13}^\ell |y_{31}^\ell y_{22}^\ell - y_{21}^\ell y_{32}^\ell| - y_{31}^\ell y_{12}^\ell y_{23}^\ell}{|y_{22}^\ell - y_{23}^\ell y_{32}^\ell / y_{33}^\ell| |y_{33}^\ell|}\right| \epsilon^9 \} v / \sqrt{2}, \quad (20)$$

The mixing angles of quarks are found to be [48],

$$\begin{aligned}\sin \theta_{12} \simeq |V_{us}| &\simeq \left| \frac{y_{12}^d}{y_{22}^d} \epsilon^2 - \frac{y_{12}^u}{y_{22}^u} \epsilon^4 \right|, \sin \theta_{23} \simeq |V_{cb}| \simeq \left| \frac{y_{23}^d}{y_{33}^d} - \frac{y_{23}^u}{y_{33}^u} \right| \epsilon^4, \\ \sin \theta_{13} \simeq |V_{ub}| &\simeq \left| \frac{y_{13}^d}{y_{33}^d} \epsilon^6 - \frac{y_{12}^u y_{23}^d}{y_{22}^u y_{33}^d} \epsilon^8 \right|.\end{aligned}\quad (21)$$

The mixing angles in this have a consistent hierarchical pattern of the order $(\epsilon^2, \epsilon^4, \epsilon^6)$. However, to produce the observed values of the fermionic masses and mixing angles, we need a relatively large value of the parameter ϵ .

2.4 The $\mathcal{Z}_8 \times \mathcal{Z}_{22}$ flavour symmetry

This symmetry can provide the so-called flavonic dark matter [49], and is inspired by the hierarchical VEVs model[3, 4], where the mass of the top quark originates from the dimension-5 operator. The transformations of fermionic and scalar fields under this symmetry are given in table 4.

Fields	\mathcal{Z}_8	\mathcal{Z}_{22}	Fields	\mathcal{Z}_8	\mathcal{Z}_{22}	Fields	\mathcal{Z}_8	\mathcal{Z}_{22}	Fields	\mathcal{Z}_8	\mathcal{Z}_{22}	Fields	\mathcal{Z}_8	\mathcal{Z}_{22}
u_R	ω^2	ω^2	c_R	ω^5	ω^5	t_R	ω^6	ω^6	d_R	ω^3	ω^3	s_R	ω^4	ω^4
b_R	ω^4	ω^4	$\psi_{L,1}^q$	ω^2	ω^{10}	$\psi_{L,2}^q$	ω	ω^9	$\psi_{L,3}^q$	ω^7	ω^7	$\psi_{L,1}^\ell$	ω^3	ω^3
$\psi_{L,2}^\ell$	ω^2	ω^2	$\psi_{L,3}^\ell$	ω^2	ω^2	e_R	ω^2	ω^{16}	μ_R	ω^5	ω^{19}	τ_R	ω^7	ω^{21}
ν_{eR}	ω^2	1	$\nu_{\mu R}$	ω^5	ω^3	$\nu_{\tau R}$	ω^6	ω^4	χ	ω	ω	φ	1	1

Table 4: The charges of the SM and the flavon fields under the $\mathcal{Z}_8 \times \mathcal{Z}_{22}$ symmetry, where ω is the 8th and 22nd root of unity.

The $\mathcal{Z}_8 \times \mathcal{Z}_{22}$ symmetry allows us to write mass Lagrangian for the charged fermions as,

$$\begin{aligned}-\mathcal{L}_{\text{Yukawa}} &= \left(\frac{\chi}{\Lambda}\right)^8 y_{11}^u \bar{\psi}_{L_1}^q \tilde{\varphi} u_R + \left(\frac{\chi}{\Lambda}\right)^5 y_{12}^u \bar{\psi}_{L_1}^q \tilde{\varphi} c_R + \left(\frac{\chi}{\Lambda}\right)^4 y_{13}^u \bar{\psi}_{L_1}^q \tilde{\varphi} t_R + \left(\frac{\chi}{\Lambda}\right)^7 y_{21}^u \bar{\psi}_{L_2}^q \tilde{\varphi} u_R \\ &+ \left(\frac{\chi}{\Lambda}\right)^4 y_{22}^u \bar{\psi}_{L_2}^q \tilde{\varphi} c_R + \left(\frac{\chi}{\Lambda}\right)^3 y_{23}^u \bar{\psi}_{L_2}^q \tilde{\varphi} t_R + \left(\frac{\chi}{\Lambda}\right)^5 y_{31}^u \bar{\psi}_{L_3}^q \tilde{\varphi} u_R + \left(\frac{\chi}{\Lambda}\right)^2 y_{32}^u \bar{\psi}_{L_3}^q \tilde{\varphi} c_R \\ &+ \left(\frac{\chi}{\Lambda}\right) y_{33}^u \bar{\psi}_{L_3}^q \tilde{\varphi} t_R + \left(\frac{\chi}{\Lambda}\right)^7 y_{11}^d \bar{\psi}_{L_1}^q \varphi d_R + \left(\frac{\chi}{\Lambda}\right)^6 y_{12}^d \bar{\psi}_{L_1}^q \varphi s_R + \left(\frac{\chi}{\Lambda}\right)^6 y_{13}^d \bar{\psi}_{L_1}^q \varphi b_R + \left(\frac{\chi}{\Lambda}\right)^6 y_{21}^d \bar{\psi}_{L_2}^q \varphi d_R \\ &+ \left(\frac{\chi}{\Lambda}\right)^5 y_{22}^d \bar{\psi}_{L_2}^q \varphi s_R + \left(\frac{\chi}{\Lambda}\right)^5 y_{23}^d \bar{\psi}_{L_2}^q \varphi b_R + \left(\frac{\chi}{\Lambda}\right)^4 y_{31}^d \bar{\psi}_{L_3}^q \varphi d_R + \left(\frac{\chi}{\Lambda}\right)^3 y_{32}^d \bar{\psi}_{L_3}^q \varphi s_R \\ &+ \left(\frac{\chi}{\Lambda}\right)^3 y_{33}^d \bar{\psi}_{L_3}^q \varphi b_R + \left(\frac{\chi}{\Lambda}\right)^9 y_{11}^\ell \bar{\psi}_{L_1}^\ell \varphi e_R + \left(\frac{\chi}{\Lambda}\right)^6 y_{12}^\ell \bar{\psi}_{L_1}^\ell \varphi \mu_R + \left(\frac{\chi}{\Lambda}\right)^4 y_{13}^\ell \bar{\psi}_{L_1}^\ell \varphi \tau_R \\ &+ \left(\frac{\chi}{\Lambda}\right)^8 y_{21}^\ell \bar{\psi}_{L_2}^\ell \varphi e_R + \left(\frac{\chi}{\Lambda}\right)^5 y_{22}^\ell \bar{\psi}_{L_2}^\ell \varphi \mu_R + \left(\frac{\chi}{\Lambda}\right)^3 y_{23}^\ell \bar{\psi}_{L_2}^\ell \varphi \tau_R + \left(\frac{\chi}{\Lambda}\right)^8 y_{31}^\ell \bar{\psi}_{L_3}^\ell \varphi e_R \\ &+ \left(\frac{\chi}{\Lambda}\right)^5 y_{32}^\ell \bar{\psi}_{L_3}^\ell \varphi \mu_R + \left(\frac{\chi}{\Lambda}\right)^3 y_{33}^\ell \bar{\psi}_{L_3}^\ell \varphi \tau_R + \text{H.c.}\end{aligned}$$

The mass matrices of the up and down-type quarks and charged leptons take the forms,

$$\mathcal{M}_u = \frac{v}{\sqrt{2}} \begin{pmatrix} y_{11}^u \epsilon^8 & y_{12}^u \epsilon^5 & y_{13}^u \epsilon^4 \\ y_{21}^u \epsilon^7 & y_{22}^u \epsilon^4 & y_{23}^u \epsilon^3 \\ y_{31}^u \epsilon^5 & y_{32}^u \epsilon^2 & y_{33}^u \epsilon \end{pmatrix}, \mathcal{M}_d = \frac{v}{\sqrt{2}} \begin{pmatrix} y_{11}^d \epsilon^7 & y_{12}^d \epsilon^6 & y_{13}^d \epsilon^6 \\ y_{21}^d \epsilon^6 & y_{22}^d \epsilon^5 & y_{23}^d \epsilon^5 \\ y_{31}^d \epsilon^4 & y_{32}^d \epsilon^3 & y_{33}^d \epsilon^3 \end{pmatrix}, \mathcal{M}_\ell = \frac{v}{\sqrt{2}} \begin{pmatrix} y_{11}^\ell \epsilon^9 & y_{12}^\ell \epsilon^6 & y_{13}^\ell \epsilon^4 \\ y_{21}^\ell \epsilon^8 & y_{22}^\ell \epsilon^5 & y_{23}^\ell \epsilon^3 \\ y_{31}^\ell \epsilon^8 & y_{32}^\ell \epsilon^5 & y_{33}^\ell \epsilon^3 \end{pmatrix}, \quad (22)$$

where $\epsilon = 0.225$ produces the masses and mixing of fermions.

The masses of charged fermions are given by [47],

$$\{m_t, m_c, m_u\} \simeq \left\{ |y_{33}^u| \epsilon, \left| y_{22}^u - \frac{y_{23}^u y_{32}^u}{y_{33}^u} \right| \epsilon^4, \right. \quad (23)$$

$$\left\{ m_b, m_s, m_d \right\} \simeq \left\{ |y_{33}^d| \epsilon^3, \left| y_{22}^d - \frac{y_{23}^d y_{32}^d}{y_{33}^d} \right| \epsilon^5, \left| y_{11}^u - \frac{y_{12}^u y_{21}^u}{y_{22}^u - y_{23}^u y_{32}^u / y_{33}^u} - \frac{y_{13}^u (y_{31}^u y_{22}^u - y_{21}^u y_{32}^u) - y_{31}^u y_{12}^u y_{23}^u}{(y_{22}^u - y_{23}^u y_{32}^u / y_{33}^u) y_{33}^u} \right| \epsilon^8 \right\} v / \sqrt{2}, \quad (24)$$

$$\left\{ m_\tau, m_\mu, m_e \right\} \simeq \left\{ |y_{33}^l| \epsilon^3, \left| y_{22}^l - \frac{y_{23}^l y_{32}^l}{y_{33}^l} \right| \epsilon^5, \left| y_{11}^d - \frac{y_{12}^d y_{21}^d}{y_{22}^d - y_{23}^d y_{32}^d / y_{33}^d} - \frac{y_{13}^d (y_{31}^d y_{22}^d - y_{21}^d y_{32}^d) - y_{31}^d y_{12}^d y_{23}^d}{(y_{22}^d - y_{23}^d y_{32}^d / y_{33}^d) y_{33}^d} \right| \epsilon^7 \right\} v / \sqrt{2},$$

$$\left\{ y_{11}^l - \frac{y_{12}^l y_{21}^l}{y_{22}^l - y_{23}^l y_{32}^l / y_{33}^l} - \frac{y_{13}^l (y_{31}^l y_{22}^l - y_{21}^l y_{32}^l) - y_{31}^l y_{12}^l y_{23}^l}{(y_{22}^l - y_{23}^l y_{32}^l / y_{33}^l) y_{33}^l} \right\} \epsilon^9 v / \sqrt{2}. \quad (25)$$

The mixing angles of quarks can be written as[47],

$$\begin{aligned} \sin \theta_{12} \simeq |V_{us}| &\simeq \left| \frac{y_{12}^d}{y_{22}^d} - \frac{y_{12}^u}{y_{22}^u} \right| \epsilon, \quad \sin \theta_{23} \simeq |V_{cb}| \simeq \left| \frac{y_{23}^d}{y_{33}^d} - \frac{y_{23}^u}{y_{33}^u} \right| \epsilon^2, \\ \sin \theta_{13} \simeq |V_{ub}| &\simeq \left| \frac{y_{13}^d}{y_{33}^d} - \frac{y_{12}^u y_{23}^d}{y_{22}^u y_{33}^d} - \frac{y_{13}^u}{y_{33}^u} \right| \epsilon^3. \end{aligned} \quad (26)$$

3 The scalar potential

The scalar potential of the model acquires the following form,

$$-\mathcal{L}_{\text{potential}} = -\mu^2 \varphi^\dagger \varphi + \lambda (\varphi^\dagger \varphi)^2 - \mu_\chi^2 \chi^* \chi + \lambda_\chi (\chi^* \chi)^2 + \lambda_{\varphi\chi} (\chi^* \chi) (\varphi^\dagger \varphi). \quad (27)$$

In the phenomenological investigation, we assume $\lambda_{\varphi\chi} = 0$, i.e., no Higgs-flavon mixing. The effects of this coupling are explored in reference [38]. We parametrize the scalar fields as,

$$\chi = \frac{f + s + i a}{\sqrt{2}}, \quad \varphi = \begin{pmatrix} G^+ \\ \frac{v+h+iG^0}{\sqrt{2}} \end{pmatrix}. \quad (28)$$

We have the SM VEV given by $\langle \phi \rangle = v (\equiv v_{SM}) \simeq 246$ GeV and $\langle \chi \rangle = f$. Here, G^+, G^0 are the Goldstone modes, which become the longitudinal components of the gauge bosons and give them mass after the electroweak symmetry is spontaneously broken.

3.1 Softly broken scalar potential

In the conventional approach [21, 32, 33, 35, 36], we can provide mass to the pseudoscalar component of the flavon field by adding the following term to the scalar potential, which breaks the $\mathcal{Z}_N \times \mathcal{Z}_M$ flavour symmetry softly,

$$V_\rho = \rho \chi^2 + \text{H.c.} \quad (29)$$

The parameter ρ is complex, and its phase can be rotated away by redefining the flavon field χ resulting in a real value of the VEV of the field χ .

The minimization conditions produce the masses of scalar and pseudoscalar flavons,

$$m_s = \sqrt{\mu_\chi - 2\rho} = \sqrt{\lambda_\chi} f \quad \text{and} \quad m_a = \sqrt{-2\rho}. \quad (30)$$

The mass of the pseudoscalar flavon depends on the soft-breaking parameter ρ , and is a free parameter of the model.

3.2 Symmetry-conserving scalar potential

The $\mathcal{Z}_N \times \mathcal{Z}_M$ flavour symmetry presents a novel scenario that simultaneously addresses the flavour problem and dark matter within a unified and generic framework [49]. This is achieved by formulating the flavon potential as,

$$V_\lambda = -\lambda \frac{\chi^{\tilde{N}}}{\Lambda^{\tilde{N}-4}} + \text{H.c.}, \quad (31)$$

where \tilde{N} is the least common multiple of N and M .

Upon the $\mathcal{Z}_N \times \mathcal{Z}_M$ flavour symmetry breaking by the VEV $\langle \chi \rangle$, the flavonic Goldstone boson (a) receives the potential,

$$V_{\tilde{N}} = -\frac{1}{4} |\lambda| \epsilon^{\tilde{N}-4} f^4 \cos\left(\tilde{N} \frac{a}{f} + \alpha\right), \quad (32)$$

where $\lambda = |\lambda| e^{i\alpha}$.

The axial flavon mass now turns out to be,

$$m_a^2 = \frac{1}{8} |\lambda| \tilde{N}^2 \epsilon^{\tilde{N}-4} f^2, \quad (33)$$

which depends on the symmetry breaking scale and is no longer an arbitrary free parameter of the model.

3.3 Couplings of flavon to fermions

Now, using equation 28, we can write

$$\frac{\chi}{\Lambda} = \epsilon \left[1 + \frac{s + ia}{f} \right]. \quad (34)$$

For obtaining the couplings of the scalar and pseudoscalar couplings to fermionic pair, we write the effective Yukawa couplings in the following form,

$$Y_{ij}^f \left(\frac{v+h}{\sqrt{2}} \right) = y_{ij}^f \left(\frac{\chi}{\Lambda} \right)^{n_{ij}^f} \left(\frac{v+h}{\sqrt{2}} \right) \cong y_{ij}^f \epsilon^{n_{ij}^f} \frac{v}{\sqrt{2}} \left[1 + \frac{n_{ij}^f (s+ia)}{f} + \frac{h}{v} \right] = \mathcal{M}_f \left[1 + \frac{n_{ij}^f (s+ia)}{f} + \frac{h}{v} \right], \quad (35)$$

where $f = u, d, \ell$, and n_{ij}^f denote the power of the ϵ , which appears in the mass matrices \mathcal{M}_f .

We keep only the linear terms of the flavon field components s and a in equation 35 in our phenomenological analysis. The higher-order terms are not relevant for the analysis given in this work. The couplings of the scalar and pseudoscalar components s and a of the flavon field to the fermionic pair are derived from the matrix $n_{ij}^f \mathcal{M}_f$, which cannot be diagonalized. This results in the non-diagonal flavour-changing and CP -violating interactions of the flavon field.

The couplings of the scalar component of the flavon field are obtained as,

$$y_{ij} = y_{s f_{iL} f_{jR}} = -i y_{a f_{iL} f_{jR}}. \quad (36)$$

4 Quark flavour physics constraints on the flavon of the $\mathcal{Z}_N \times \mathcal{Z}_M$ flavour symmetries

In this section, we thoroughly investigate the bounds on the parameter space of the $\mathcal{Z}_N \times \mathcal{Z}_M$ flavour symmetries using the quark-flavour physics data. We shall present the bounds on the flavon VEV f and mass of the pseudoscalar field m_a in both soft symmetry-breaking as well as symmetry-preserving scenarios.

4.1 Neutral meson mixing

The neutral meson-antimeson mixing receives a contribution from the FCNC interactions occurring at the tree-level due to the non-diagonal couplings of the flavon to fermions. This contribution can be incorporated by writing the following $\Delta F = 2$ effective Hamiltonian,

$$\begin{aligned} \mathcal{H}_{\text{NP}}^{\Delta F=2} = & C_1^{ij} (\bar{q}_L^i \gamma_\mu q_L^j)^2 + \tilde{C}_1^{ij} (\bar{q}_R^i \gamma_\mu q_R^j)^2 + C_2^{ij} (\bar{q}_R^i q_L^j)^2 + \tilde{C}_2^{ij} (\bar{q}_L^i q_R^j)^2 \\ & + C_4^{ij} (\bar{q}_R^i q_L^j) (\bar{q}_L^i q_R^j) + C_5^{ij} (\bar{q}_L^i \gamma_\mu q_L^j) (\bar{q}_R^i \gamma^\mu q_R^j) + \text{H.c.}, \end{aligned} \quad (37)$$

where $q_{R,L} = \frac{1 \pm \gamma_5}{2} q$, and we do not show the colour indices for simplicity.

G_F	1.166×10^{-5} GeV [50]	v	246.22 GeV [50]
$\alpha_s [M_Z]$	0.1184 [51]	m_u	$(2.16^{+0.49}_{-0.26}) \times 10^{-3}$ GeV [50]
M_W	80.387 ± 0.016 GeV [50]	m_d	$(4.67^{+0.48}_{-0.17}) \times 10^{-3}$ GeV [50]
f_K	159.8 MeV [52]	m_c	1.27 ± 0.02 GeV [50]
m_K	497.611 ± 0.013 MeV [50]	m_s	$93.4^{+8.6}_{-3.4}$ GeV [50]
\hat{B}_K	0.7625 [51]	m_t	172.69 ± 0.30 GeV [50]
B_1^K	0.60(6) [52]	m_b	$4.18^{+0.03}_{-0.02}$ GeV [50]
B_2^K	0.66(4) [52]	$m_c(m_c)$	1.275 GeV
B_3^K	1.05(12) [52]	$m_b(m_b)$	4.18 GeV
B_4^K	1.03(6) [52]	$m_t(m_t)$	162.883 GeV
B_5^K	0.73(10) [52]	α	1/137.035 [50]
η_1	1.87 ± 0.76 [53]	e	0.302862 GeV
η_2	0.574 [54]	m_e	0.51099 MeV [50]
η_3	0.496 ± 0.047 [55]	m_μ	105.65837 MeV [50]
f_{B_s}	230.3 MeV [51]	m_τ	1776.86 ± 0.12 MeV [50]
m_{B_s}	5366.88 MeV [50]	τ_μ	2.196811×10^{-6} sec [50]
\hat{B}_{B_s}	1.232[51]	τ_τ	$(290.3 \pm 0.5) \times 10^{-15}$ sec [50]
$B_1^{B_s}$	0.86(2) $^{(+5)}_{(-4)}$ [56]	m_p	938.272 MeV [50]
$B_2^{B_s}$	0.83(2)(4) [56]	m_n	939.565 MeV [50]
$B_3^{B_s}$	1.03(4)(9) [56]	m_D	1864.83 MeV [50]
$B_4^{B_s}$	1.17(2) $^{(+5)}_{(-7)}$ [56]	f_D	212 MeV[51]
$B_5^{B_s}$	1.94(3) $^{(+23)}_{(-7)}$ [56]	B_1^D	0.861 [57]
η_{2B}	0.551 [54]	B_2^D	0.82 [57]
f_{B_d}	190.0 MeV [51]	B_3^D	1.07 [57]
m_{B_d}	5279.65 MeV [50]	B_4^D	1.08 [57]
\hat{B}_{B_d}	1.222[51]	B_5^D	1.455 [57]
$B_1^{B_d}$	0.87(4) $^{(+5)}_{(-4)}$ [56]	τ_{B_d}	$(1.520 \pm 0.004) \times 10^{-12}$ sec [58]
$B_2^{B_d}$	0.82(3)(4) [56]	τ_{B_s}	$(1.505 \pm 0.005) \times 10^{-12}$ sec [58]
$B_3^{B_d}$	1.02(6)(9) [56]	τ_{K_L}	$(5.116 \pm 0.021) \times 10^{-8}$ sec [50]
$B_4^{B_d}$	1.16(3) $^{(+5)}_{(-7)}$ [56]	τ_D	$(410.1 \pm 1.5) \times 10^{-15}$ sec [50]
$B_5^{B_d}$	1.91(4) $^{(+22)}_{(-7)}$ [56]		

Table 5: The numerical values of the used input parameters in this work.

The Wilson coefficients corresponding to the tree-level contribution to neutral meson mixing due to the flavon exchange read as [59, 60],

$$\begin{aligned} C_2^{ij} &= -(y_{ji}^*)^2 \left(\frac{1}{m_s^2} - \frac{1}{m_a^2} \right) \\ \tilde{C}_2^{ij} &= -y_{ij}^2 \left(\frac{1}{m_s^2} - \frac{1}{m_a^2} \right) \end{aligned}$$

$$C_4^{ij} = -\frac{y_{ij}y_{ji}}{2} \left(\frac{1}{m_s^2} + \frac{1}{m_a^2} \right), \quad (38)$$

where m_s and m_a represent the masses of scalar and pseudoscalar degrees of the flavon field.

We evolve down the Wilson coefficients C_i from a scale Λ to the hadronic scales, used in the lattice computations of the corresponding matrix elements [52, 56, 57], 4.6 GeV for bottom mesons, 2.8 GeV for charmed mesons, and 2 GeV for kaons. The renormalization group running of the matrix elements is performed using the procedure discussed in reference [57], and matrix elements are adopted from reference [52, 56]. Thus, the $B_q - \bar{B}_q$ mixing amplitudes beyond the SM can be written as [57],

$$\langle \bar{B}_q | \mathcal{H}_{\text{eff}}^{\Delta B=2} | B_q \rangle_i = \sum_{j=1}^5 \sum_{r=1}^5 \left(b_j^{(r,i)} + \eta c_j^{(r,i)} \right) \eta^{a_j} C_i(\Lambda) \langle \bar{B}_q | Q_r^{bq} | B_q \rangle, \quad (39)$$

where $q = d, s$, $\eta = \alpha_s(\Lambda)/\alpha_s(m_t)$, a_j , $b_j^{(r,i)}$, $c_j^{(r,i)}$ denote the so-called magic numbers taken from reference [61], and α_s is the strong coupling constant. A similar expression can be written for the $D^0 - \bar{D}^0$ for which the magic numbers are present in reference [57]. The corresponding expression for the $K^0 - \bar{K}^0$ mixing reads as [57],

$$\langle \bar{K}^0 | \mathcal{H}_{\text{eff}}^{\Delta S=2} | K^0 \rangle_i = \sum_{j=1}^5 \sum_{r=1}^5 \left(b_j^{(r,i)} + \eta c_j^{(r,i)} \right) \eta^{a_j} C_i(\Lambda) R_r \langle \bar{K}^0 | Q_1^{sd} | K^0 \rangle, \quad (40)$$

where R_r denotes the ratio of the matrix elements of NP operators over that of the SM [62]. The numerical values of R_r can be found in reference [57]. For the $K^0 - \bar{K}^0$ mixing, the magic numbers are used from reference [52].

For constraining the flavon mass and the VEV, we use the experimental measurements of the mixing observables of the $K^0 - \bar{K}^0$ mixing, which is given as [57],

$$C_{\epsilon_K} = \frac{\text{Im} \langle K^0 | \mathcal{H}_{\text{eff}}^{\Delta F=2} | \bar{K}^0 \rangle}{\text{Im} \langle K^0 | \mathcal{H}_{\text{SM}}^{\Delta F=2} | \bar{K}^0 \rangle} = 1.12_{-0.25}^{+0.27}, \quad C_{\Delta m_K} = \frac{\text{Re} \langle K^0 | \mathcal{H}_{\text{eff}}^{\Delta F=2} | \bar{K}^0 \rangle}{\text{Re} \langle K^0 | \mathcal{H}_{\text{SM}}^{\Delta F=2} | \bar{K}^0 \rangle} = 0.93_{-0.42}^{+1.14}, \quad (41)$$

where $\mathcal{H}_{\text{eff}}^{\Delta F=2}$ represents the SM and flavon contributions, and $\mathcal{H}_{\text{SM}}^{\Delta F=2}$ denotes only the SM contribution.

The $B_q - \bar{B}_q$ mixing observables are,

$$C_{B_q} e^{2i\phi_{B_q}} = \frac{\text{Im} \langle B_q^0 | \mathcal{H}^{\Delta F=2} | \bar{B}_q^0 \rangle}{\text{Im} \langle B_q^0 | \mathcal{H}_{\text{SM}}^{\Delta F=2} | \bar{B}_q^0 \rangle},$$

where $q = s, d$ for the B_s and B_d mixing, respectively. We use the following measurements at 95 % CL limits in this work [57],

$$\begin{aligned} C_{B_s} &= 1.110 \pm 0.090 [0.942, 1.288], & \phi_{B_s}^o &= 0.42 \pm 0.89 [-1.35, 2.21] \\ C_{B_d} &= 1.05 \pm 0.11 [0.83, 1.29], & \phi_{B_d}^o &= -2.0 \pm 1.8 [-6.0, 1.5]. \end{aligned}$$

We write the new physics contributions to neutral meson mixing in the following form,

$$M_{12}^{d,s,K} = (M_{12}^{d,s,K})_{\text{SM}} (1 + h_{d,s,K} e^{2i\sigma_{d,s,K}}). \quad (42)$$

The following future sensitivity phases are adopted in this work [63]:

1. Phase I which corresponds to $50fb^{-1}$ LHCb and $50ab^{-1}$ Belle II (late 2020s);
2. Phase II which corresponds to $300fb^{-1}$ LHCb and $250ab^{-1}$ Belle II (late 2030s).

In table 6, we show the expected sensitivities to the observables $C_{\Delta m_K}$ and C_{B_q} in the future phase I and II of the LHCb and the Belle II.

Now, we discuss the bounds on the parameter space of the flavon of the $\mathcal{Z}_N \times \mathcal{Z}_M$ flavour symmetries arising from the neutral meson mixing. We discuss these bounds simultaneously for the soft symmetry-breaking as

Observables	Phase I	Phase II	Ref.
h_d	0 – 0.04	0 – 0.028	[63]
h_s	0 – 0.036	0 – 0.025	[63]
h_K	0 – 0.3	–	[64]

Table 6: The future projected sensitivities of the neutral meson mixing.

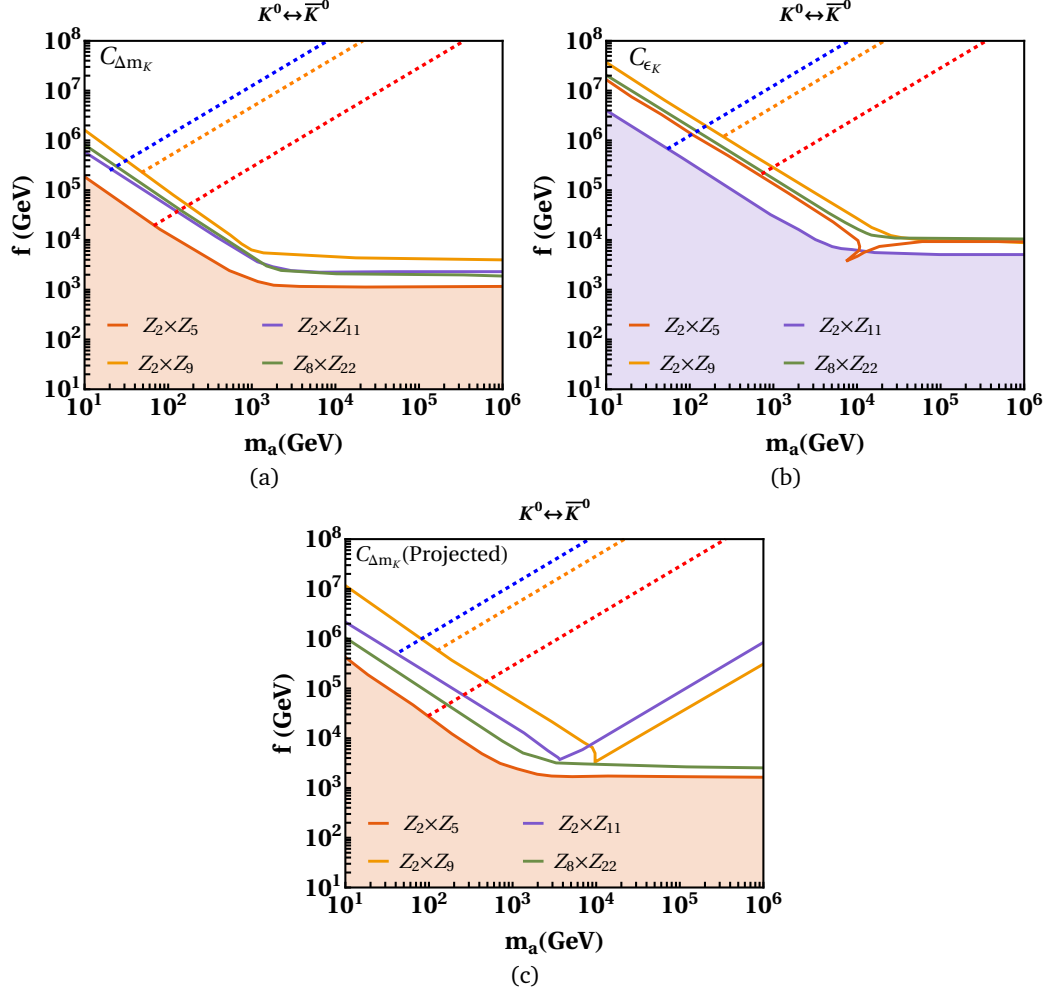


Figure 1: Bounds on the parameter space of the flavon of different $\mathcal{Z}_N \times \mathcal{Z}_M$ flavour symmetries in $f - m_a$ plane from the neutral-kaon oscillations. On the left, we show the constraints arising from the observable $C_{\Delta m_K}$, and on the right, the bounds from the observable C_{ϵ_K} are shown for the value $\lambda_\chi = 2$. Moreover, the continuous curves represent the soft symmetry-breaking framework, and dashed curves are for the symmetry-preserving scenario defined by equation 31.

well as the symmetry-conserving scenarios. In figure 1, we show the bounds on the parameter space of the flavon corresponding to different $\mathcal{Z}_N \times \mathcal{Z}_M$ flavour symmetries from neutral kaon mixing observable $C_{\Delta m_K}$ on the left, and that from the observable C_{ϵ_K} on the right for the quartic coupling $\lambda_\chi = 2$. The continuous curves show the soft symmetry-breaking scenario for different $\mathcal{Z}_N \times \mathcal{Z}_M$ flavour symmetries. On the other side, the dashed curves represent symmetry-conserving scenario defined by equation 31. In the case of the soft symmetry-breaking scenario, the region of the parameter space below the continuous curves is excluded by the corresponding observables. The symmetry-conserving scenario turns out to be extremely predictive in the sense

that the allowed flavon parameter space is only along the dashed straight lines, and the rest of the region is excluded by the corresponding observables.

Thus, we observe that the bounds from the observable $C_{\Delta m_K}$ are most stringent for the flavour symmetry $\mathcal{Z}_2 \times \mathcal{Z}_9$, shown by the region above yellow-coloured continuous curve in figure 1a. This is followed by the $\mathcal{Z}_2 \times \mathcal{Z}_{11}$ and $\mathcal{Z}_8 \times \mathcal{Z}_{22}$ flavour symmetries for which the allowed parameter space is almost similar, shown in figure 1a by the region above the violet and green coloured continuous curves, respectively. The bounds become more stringent when the observable C_{ϵ_K} is used as shown in figure 1b. The most stringent bounds continue to be for the $\mathcal{Z}_2 \times \mathcal{Z}_9$ flavour symmetry even from the observable C_{ϵ_K} . The bounds from the observable C_{ϵ_K} on the flavour symmetries $\mathcal{Z}_2 \times \mathcal{Z}_{11}$ and $\mathcal{Z}_8 \times \mathcal{Z}_{22}$ are very close and are more stringent than that of the minimal flavour symmetry $\mathcal{Z}_2 \times \mathcal{Z}_5$ shown by the red continuous curve. In figure 1c, we show the bounds on the parameter space of the flavon of different $\mathcal{Z}_N \times \mathcal{Z}_M$ flavour symmetries for the projected future sensitivities of the neutral meson mixing given in table 6 for the soft symmetry-breaking and symmetry-conserving scenario again by the solid continuous curves.

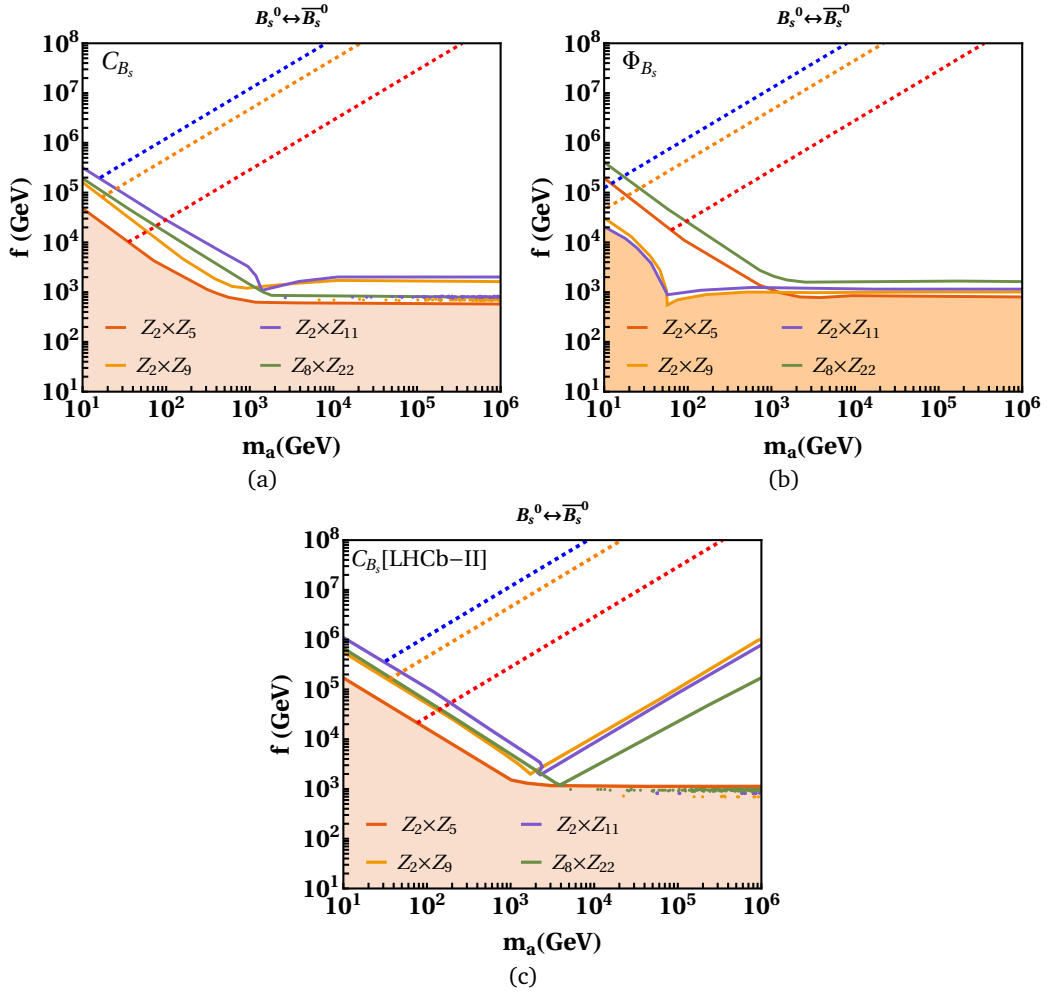


Figure 2: Bounds on the parameter space of the flavon of different $\mathcal{Z}_N \times \mathcal{Z}_M$ flavour symmetries in $f - m_a$ plane from the neutral B_s -meson mixing. On the left, we show the constraints arising from the observable C_{B_s} , and on the right, the bounds from the observable Φ_{B_s} are shown for the value $\lambda_\chi = 2$. Moreover, the continuous curves represent the soft symmetry-breaking framework, and dashed curves are for the symmetry-preserving scenario defined by equation 31.

For the symmetry-conserving scenario, the most stringent bounds from the observable $C_{\Delta m_K}$ again appear

for the $\mathcal{Z}_2 \times \mathcal{Z}_9$ flavour symmetry denoted by the orange dashed line in figure 1a. We must note that for the symmetry-conserving case, the dashed straight lines are the only allowed parameter space, and the rest of the region is excluded by the corresponding mixing observables. The bounds for the projected future sensitivities of the neutral meson mixing given in table 6 in the case of the symmetry-conserving scenario are shown by the dashed straight lines in figure 1c for different $\mathcal{Z}_N \times \mathcal{Z}_M$ flavour symmetries.

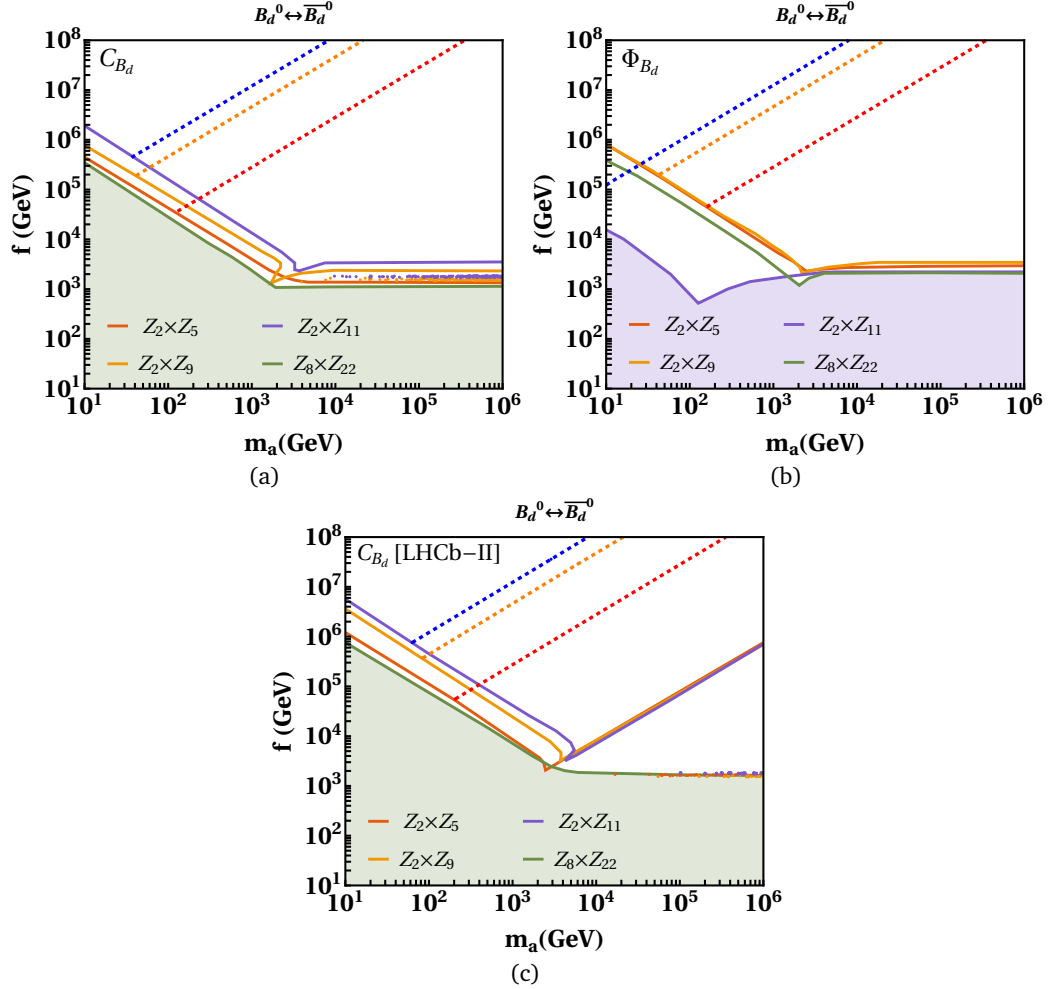


Figure 3: Bounds on the parameter space of the flavon of different $\mathcal{Z}_N \times \mathcal{Z}_M$ flavour symmetries in $f - m_a$ plane from the neutral B_s -meson mixing. On the left, we show the constraints arising from the observable C_{B_d} , and on the right, the bounds from the observable Φ_{B_d} are shown for the value $\lambda_\chi = 2$. Moreover, the continuous curves represent the soft symmetry-breaking framework, and dashed curves are for the symmetry-preserving scenario defined by equation 31.

The bounds on the parameter space of the flavon of the $\mathcal{Z}_N \times \mathcal{Z}_M$ flavour symmetries arising from the neutral B_s -meson mixing are represented in figure 2. On the left in figure 2a, we show the constraints on the parameter space of the flavon derived from the observable C_{B_s} . For the soft symmetry-breaking case, the bounds are depicted by the solid continuous curves, and the region below these curves is excluded by the experimental measurement of the observable C_{B_s} . We notice that the observable C_{B_s} , unlike the neutral-kaon mixing, which was more constraining to the $\mathcal{Z}_2 \times \mathcal{Z}_9$ flavour symmetry, place stronger bounds on the $\mathcal{Z}_2 \times \mathcal{Z}_{11}$ flavour symmetry for the flavon mass approximately below 1 TeV. Above the flavon mass 1 TeV, the bounds are similar for the $\mathcal{Z}_2 \times \mathcal{Z}_{11}$ and $\mathcal{Z}_2 \times \mathcal{Z}_9$ flavour symmetries. The observable Φ_{B_s} is more suitable to constrain the parameter space corresponding to the $\mathcal{Z}_8 \times \mathcal{Z}_{22}$ flavour symmetry, as observed in figure 2b. The future projected

sensitivity of the observable C_{B_s} in the LHCb phase-I further constrains the parameter space corresponding to the $\mathcal{Z}_2 \times \mathcal{Z}_{11}$ flavour symmetry for the flavon mass approximately up to 1 TeV. Above the flavon mass 1 TeV, the bounds are further stronger and again similar for the $\mathcal{Z}_2 \times \mathcal{Z}_{11}$ and $\mathcal{Z}_2 \times \mathcal{Z}_9$ flavour symmetries.

For the symmetry-conserving scenario, the most stringent constraints are derived for the symmetry $\mathcal{Z}_2 \times \mathcal{Z}_{11}$ from both the observables C_{B_s} and Φ_{B_s} , as shown by the dashed blue straight lines in figures 2a, 2b, and in 2c for the future projected sensitivity of the observable C_{B_s} in the LHCb phase-II. After the $\mathcal{Z}_2 \times \mathcal{Z}_{11}$ flavour symmetry, the parameter space corresponding to the flavon of the $\mathcal{Z}_2 \times \mathcal{Z}_9$ flavour symmetry receives the stronger bounds denoted by the orange dashed straight lines in figure 2.

In the case of the B_d -meson mixing, the observable C_{B_d} places the most stringent bounds on the parameter space of the flavon of the $\mathcal{Z}_2 \times \mathcal{Z}_{11}$ flavour symmetry for the soft symmetry-breaking scenario, as shown in figure 3a. This observation is similar to that obtained from the neutral B_s -meson mixing in figure 2. This feature continues to be seen even in the future projected sensitivity of the observable C_{B_d} in the LHCb phase-II, as shown in figure 3c. The bounds for the future projected sensitivity of the observable C_{B_d} in the LHCb phase-I are very similar to that of phase-II. Therefore, we do not show them in this work. On the other side, the observable Φ_{B_d} provides more stringent bounds on the parameter space of the flavon of the $\mathcal{Z}_2 \times \mathcal{Z}_{5,9}$ flavour symmetries for the soft symmetry-breaking scenario as shown in figure 3b.

In the symmetry-conserving scenario, the B_d -meson mixing places bounds on the parameter space of the flavon of $\mathcal{Z}_N \times \mathcal{Z}_M$ flavour symmetries similar to that of the B_s -meson mixing, as can be observed from figure 3a-3c, where the allowed parameter space is shown by dashed straight lines. The strongest bounds in this case turn out to be for the flavon of the $\mathcal{Z}_2 \times \mathcal{Z}_{11}$ flavour symmetry, followed by the flavon of the $\mathcal{Z}_2 \times \mathcal{Z}_9$ flavour symmetry.

Large hadronic uncertainties exist in the SM contribution of the $D^0 - \bar{D}^0$ mixing. For this reason, the flavon contribution to the $D^0 - \bar{D}^0$ mixing is chosen to lie within the 2σ experimental bound [65], that is,

$$|M_{12}^D| = |\langle D^0 | \mathcal{H}^{\Delta F=2} | \bar{D}^0 \rangle| < 7.5 \times 10^{-3} ps^{-1} \quad (43)$$

In figure 4, we show the bounds arising from the D -meson mixing. The D -meson mixing observable $|M_{12}^D|$ places robust bounds on the parameter space of the flavon of the $\mathcal{Z}_2 \times \mathcal{Z}_5$ flavour symmetry for the soft symmetry-breaking, as well as for the symmetry-preserving scenarios.

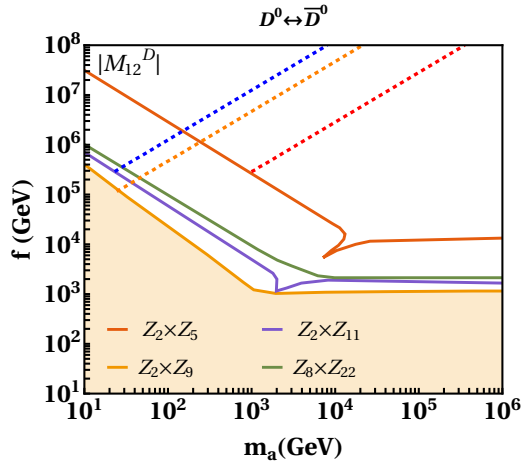


Figure 4: Bounds on the parameter space of the flavon of different $\mathcal{Z}_N \times \mathcal{Z}_M$ flavour symmetries in $f - m_a$ plane from the neutral $D^0 - \bar{D}^0$ meson mixing for the soft symmetry-breaking as well as for the symmetry-conserving scenarios for $\lambda_\chi = 2$.

4.2 Two body leptonic decays of pseudoscalar mesons

The two-body leptonic decays of a pseudoscalar meson into charged leptons can be described by the following effective Hamiltonian,

$$\mathcal{H}_{\text{eff}} = -\frac{G_F^2 m_W^2}{\pi^2} \left(C_S^{ij} (\bar{q}_i P_L q_j) \bar{\ell} \ell + \tilde{C}_S^{ij} (\bar{q}_i P_R q_j) \bar{\ell} \ell + C_P^{ij} (\bar{q}_i P_L q_j) \bar{\ell} \gamma_5 \ell + \tilde{C}_P^{ij} (\bar{q}_i P_R q_j) \bar{\ell} \gamma_5 \ell \right) + \text{H.c.} \quad (44)$$

The branching ratio for such a leptonic decay of meson can be written as,

$$\text{BR}(M \rightarrow \ell^+ \ell^-) = \frac{G_F^4 m_W^4}{8\pi^5} \beta m_M f_M^2 m_\ell^2 \tau_M \left(\left| \frac{m_M^2 (C_P^{ij} - \tilde{C}_P^{ij})}{2m_\ell(m_i + m_j)} - C_A^{\text{SM}} \right|^2 + \left| \frac{m_M^2 (C_S^{ij} - \tilde{C}_S^{ij})}{2m_\ell(m_i + m_j)} \right|^2 \beta^2 \right), \quad (45)$$

where $\beta(x) = \sqrt{1 - 4x^2}$ with $x = m_\ell/m_M$.

The tree-level contribution of the flavon to the corresponding Wilson coefficients reads as [59, 60],

$$\begin{aligned} C_S^{ij} &= \frac{\pi^2}{2G_F^2 m_W^2} \frac{2y_{\ell\ell} y_{ji}}{m_s^2} \\ \tilde{C}_S^{ij} &= \frac{\pi^2}{2G_F^2 m_W^2} \frac{2y_{\ell\ell} y_{ij}}{m_s^2} \\ C_P^{ij} &= \frac{\pi^2}{2G_F^2 m_W^2} \frac{2y_{\ell\ell} y_{ji}}{m_a^2} \\ \tilde{C}_P^{ij} &= \frac{\pi^2}{2G_F^2 m_W^2} \frac{2y_{\ell\ell} y_{ij}}{m_a^2}. \end{aligned} \quad (46)$$

In the SM, the two-body leptonic decays of a pseudoscalar meson into two charged leptons occur at one-loop, and their contribution is given by [60],

$$C_A^{\text{SM}} = -V_{tb}^* V_{ts} Y \left(\frac{m_t^2}{m_W^2} \right) - V_{cb}^* V_{cs} Y \left(\frac{m_c^2}{m_W^2} \right), \quad (47)$$

where $Y(x)$ is the Inami-Lim function, given by [66],

$$Y(x) = \eta_{\text{QCD}} \frac{x}{8} \left[\frac{4-x}{1-x} + \frac{3x}{(1-x)^2} \log x \right], \quad (48)$$

where $\eta_{\text{QCD}} = 1.0113$ shows the NLO QCD effects [67]. For B_d meson, the SM predictions can be obtained by replacing the indices in equation 47.

4.2.1 The $B_{s,d}$ meson decays

The HFLAV group provides the branching fraction of $B_s \rightarrow \mu^+ \mu^-$ to be [68],

$$\text{BR}(B_s \rightarrow \mu^+ \mu^-) = (3.45 \pm 0.29) \times 10^{-9}. \quad (49)$$

The branching ratio of the $B_d \rightarrow \mu^+ \mu^-$ decay is [69, 70],

$$\text{BR}(B_d \rightarrow \mu^+ \mu^-) < 2.6 \times 10^{-10}. \quad (50)$$

To convert the theoretical branching ratio of the B_s meson to the experimental branching ratio, we multiply by the factor $(1 - y_s)^{-1}$ [71], where $y_s = 0.088 \pm 0.014$ [72]. This is done due to the sizeable width difference of the B_s meson, and this correction can be ignored in the case of the B_d meson.

Observables	Current	LHCb-I	LHCb-II	CMS	ATLAS
$\text{BR}(B_s \rightarrow \mu^+ \mu^-) (\times 10^9)$	± 0.38	± 0.30	± 0.16	–	± 0.50
$\mathcal{R}_{\mu\mu}$	$\sim 70\%$	$\sim 34\%$	$\sim 10\%$	$\sim 21\%$	–
$\tau_{\mu\mu}$	$\sim 12\%$	± 0.16 ps	± 0.04 ps	–	–

Table 7: The values of the rare B decays observables for the current and expected experimental precision. The LHCb-I corresponds to $23fb^{-1}$, LHCb-II corresponds to $300fb^{-1}$, and the CMS and the ATLAS correspond to $3ab^{-1}$ [73, 74].

We note that the LHCb collaboration has also measured the ratio of the $\text{BR}(B_d \rightarrow \mu^+ \mu^-)$ and $\text{BR}(B_s \rightarrow \mu^+ \mu^-)$ branching fractions, $\mathcal{R}_{\mu\mu}$ [69, 70]. This observable can also be used to constrain the parameter space of flavon of different $\mathcal{Z}_N \times \mathcal{Z}_M$ flavour symmetries, and we shall show later that it provides the striking bounds of the parameter space of flavon of different $\mathcal{Z}_N \times \mathcal{Z}_M$ flavour symmetries. It should be noted that the ratio $\mathcal{R}_{\mu\mu}$ turns out to be an excellent observable to probe the minimal flavour violation [74]. Moreover, the effective lifetime, $\tau_{\mu\mu}$, of the $B_s \rightarrow \mu^+ \mu^-$ decay is also measured by the CMS [73]. The effective lifetime, $\tau_{\mu\mu}$ is capable of distinguishing between the contributions due to any possible new scalar and pseudoscalar mediators [74].

The ratio of branching fractions, $\mathcal{R}_{\mu\mu}$ is [69, 70],

$$\mathcal{R}_{\mu\mu} = \frac{\text{BR}(B_d \rightarrow \mu^+ \mu^-)}{\text{BR}(B_s \rightarrow \mu^+ \mu^-)} = 0.039_{-0.024-0.004}^{+0.030+0.006}. \quad (51)$$

The CMS has measured the effective lifetime $\tau_{\mu\mu}$ and the branching fraction of $B_s \rightarrow \mu^+ \mu^-$, which are [73],

$$\tau_{\mu\mu} = 1.83_{-0.20-0.04}^{+0.23+0.04} \text{ ps}, \quad (52)$$

$$\text{BR}(B_s \rightarrow \mu^+ \mu^-) = 3.83_{-0.36-0.16-0.13}^{+0.38+0.19+0.14} \times 10^{-9}. \quad (53)$$

The HFLAV measurement average of the effective lifetime $\tau_{\mu\mu}$ is [68],

$$\tau_{\mu\mu} = 2.00_{-0.26}^{+0.27} \text{ ps}, \quad (54)$$

with $\text{BR}(B_s \rightarrow \mu^+ \mu^-)$ given in equation 49.

We summarize the current and future sensitivities of these observables in table 7. The effective lifetime can be expressed as [75],

$$\tau_{\mu\mu} = \tau_{B_s} \frac{(B_s \rightarrow \mu^+ \mu^-)_{\text{experiment}}}{(B_s \rightarrow \mu^+ \mu^-)_{\text{theory}}}, \quad (55)$$

where the SM value of the final state dependent observable is $\mathcal{A}_{\Delta\Gamma}^f = 1$ [72].

4.2.2 The K_L meson decays

The short-distance (SD) part of $K_L \rightarrow \mu^+ \mu^-$ decay can be estimated in a reliable manner [59]. Its SM prediction is given in reference [59], and reads as,

$$C_A^{\text{SM}} = -V_{ts}^* V_{td} Y \left(\frac{m_t^2}{m_W^2} \right) - V_{cs}^* V_{cd} Y_{\text{NNL}}, \quad (56)$$

where at NNLO $Y_{\text{NNL}} = \lambda^4 P_c(Y)$, $\lambda = |V_{us}|$ and $P_c(Y) = 0.113 \pm 0.017$ [76]. The short-distance contribution is extracted from the experimental measurement, and its upper limit is [60],

$$\text{BR}(K_L \rightarrow \mu^+ \mu^-)_{\text{SD}} < 2.5 \times 10^{-9}. \quad (57)$$

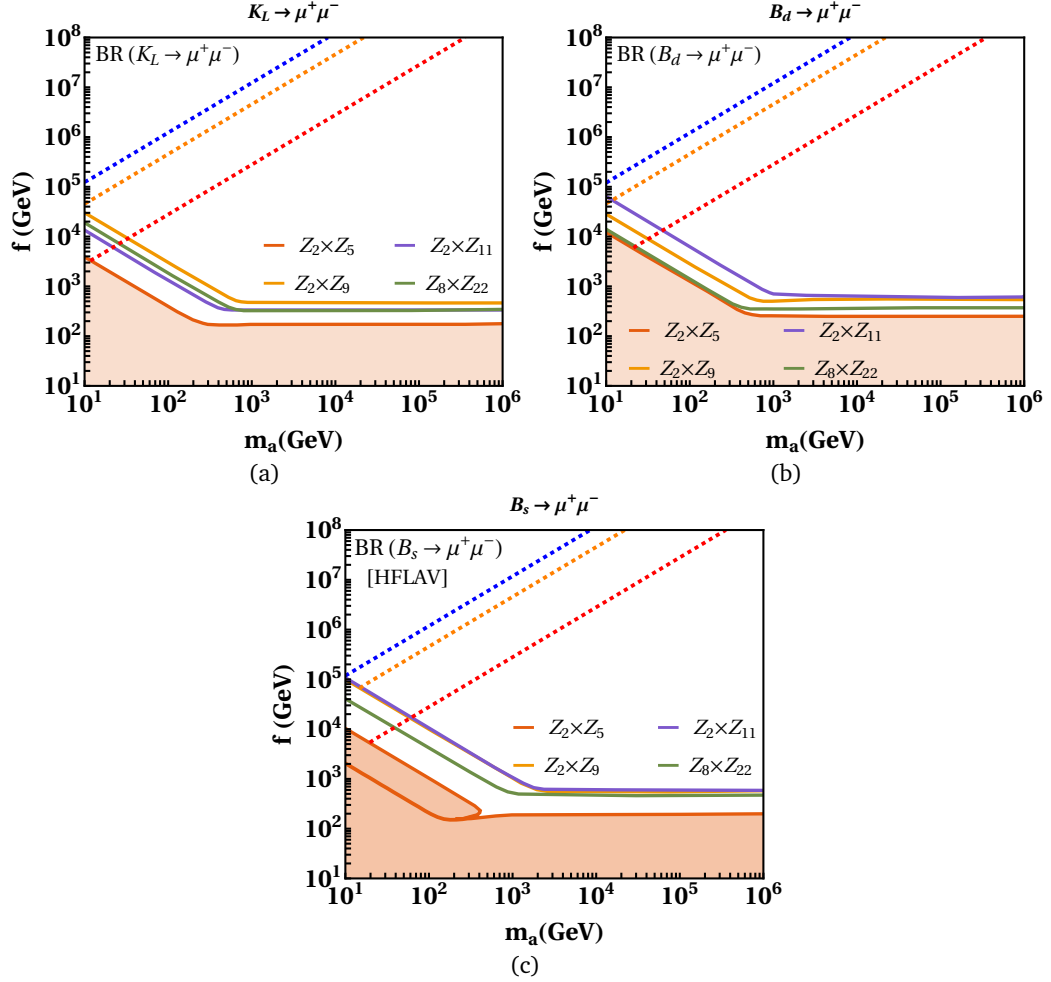


Figure 5: The coloured region represents the excluded parameter space for the flavon of all four $\mathcal{Z}_N \times \mathcal{Z}_M$ flavour symmetries by the limits on branching ratios $\text{BR}(K_L \rightarrow \mu^+ \mu^-)_{\text{SD}}$, $\text{BR}(B_d \rightarrow \mu^+ \mu^-)$ and the $\text{BR}(B_s \rightarrow \mu^+ \mu^-)$ for the soft symmetry-breaking scenario. The dashed line represents the allowed parameter space by the same observables for symmetry-conserving scenario, with $\lambda_\chi = 2$ for both the scenarios.

4.2.3 The D meson decays

The SM contribution of the $D \rightarrow \mu^+ \mu^-$ decay is marred by the large non-perturbative effects. Therefore, we assume that the flavon contribution to this decay rate lies within the experimental upper bound on the branching ratio, given at 90% C.L.[77],

$$\text{BR}(D \rightarrow \mu^+ \mu^-) < 6.2 \times 10^{-9}. \quad (58)$$

In figure 5, we show the bounds on the parameter space of flavon of different $\mathcal{Z}_N \times \mathcal{Z}_M$ flavour symmetries arising from the branching ratio of the $K_L \rightarrow \mu^+ \mu^-$ decay. In the case of the soft symmetry-breaking scenario, the branching ratio of the $K_L \rightarrow \mu^+ \mu^-$ decay imposes stronger bounds on the $\mathcal{Z}_2 \times \mathcal{Z}_9$ flavour symmetry. After this, the constraints are stronger for the $\mathcal{Z}_2 \times \mathcal{Z}_{11}$ flavour symmetry. The decay $B_d \rightarrow \mu^+ \mu^-$ constrains more parameter space of flavon of the $\mathcal{Z}_2 \times \mathcal{Z}_{11}$ flavour symmetry, followed by the $\mathcal{Z}_2 \times \mathcal{Z}_9$ flavour symmetry. On the other hand, branching ratio of the decay $B_s \rightarrow \mu^+ \mu^-$ bounds both the $\mathcal{Z}_2 \times \mathcal{Z}_9$ and $\mathcal{Z}_2 \times \mathcal{Z}_{11}$ flavour symmetries together with similar strength, while the bounds are comparatively weak in the case of $\mathcal{Z}_8 \times \mathcal{Z}_{22}$ flavour symmetry. In the symmetry-preserving scenario, all three decays place the stronger bounds on the

$\mathcal{Z}_2 \times \mathcal{Z}_{11}$ flavour symmetry. This is followed by the $\mathcal{Z}_2 \times \mathcal{Z}_9$ flavour symmetry, and $\mathcal{Z}_2 \times \mathcal{Z}_5$ flavour symmetry. We do not show the bounds from $BR(D \rightarrow \mu^+ \mu^-)$ as it imposes extremely weak constraint on the parameter space of all four $\mathcal{Z}_N \times \mathcal{Z}_M$ flavour symmetries.

The observable $\tau_{\mu\mu}$ places the strongest bounds on the parameter space of flavon of the $\mathcal{Z}_2 \times \mathcal{Z}_5$ flavour symmetry in the soft symmetry-breaking scenario, as observed in figure 6. This is followed by the flavon of the $\mathcal{Z}_2 \times \mathcal{Z}_{11}$ flavour symmetry. For the symmetry-conserving scenario, the most stringent constraints arise for the flavon of the $\mathcal{Z}_2 \times \mathcal{Z}_{11}$ flavour symmetry, followed by the flavon of the $\mathcal{Z}_2 \times \mathcal{Z}_9$ flavour symmetry. There is no substantial improvement over these bounds in the future projected sensitivities of the LHCb. Therefore, we do not show them in this work.

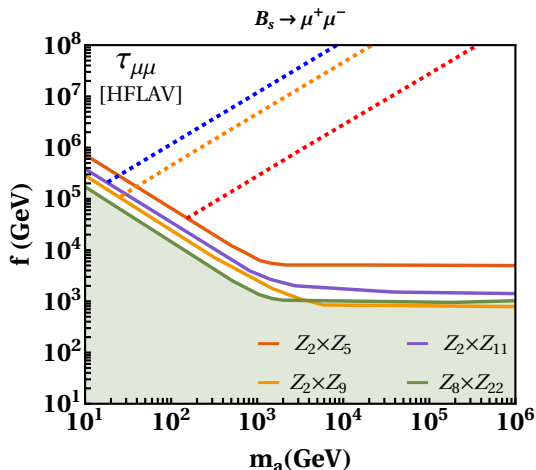


Figure 6: The allowed parameter space by the observable $\tau_{\mu\mu}$ for the flavon of different $\mathcal{Z}_N \times \mathcal{Z}_M$ flavour symmetries for the recent measurement.

The ratio $\mathcal{R}_{\mu\mu}$ is one of the most important observables to test the $\mathcal{Z}_N \times \mathcal{Z}_M$ flavour symmetries. Its future projected sensitivity will play a decisive role in constraining the parameter space of flavon of $\mathcal{Z}_N \times \mathcal{Z}_M$ flavour symmetries. The predictions from this observable are shown in figure 7.

In the case of soft symmetry-breaking scenario, the strongest bounds turn out to be for the $\mathcal{Z}_2 \times \mathcal{Z}_9$ and $\mathcal{Z}_2 \times \mathcal{Z}_{11}$ flavour symmetries for the current measurement of the observable $\mathcal{R}_{\mu\mu}$, as observed in figure 7a. This feature continues to grow stronger further in the future high luminosity phase-I of the LHCb, as can be seen in figure 7b. In the symmetry-conserving scenario, the parameter space of the flavon of the $\mathcal{Z}_2 \times \mathcal{Z}_{11}$ is more constrained than any other flavour symmetry for the current measurement as well as for the high luminosity phase-I of the LHCb, as can be seen in figure 7a and 7b. This is followed by the $\mathcal{Z}_2 \times \mathcal{Z}_9$ flavour symmetry.

The most dramatic bounds on the parameter space of the flavon of different $\mathcal{Z}_N \times \mathcal{Z}_M$ flavour symmetries arise from the future high luminosity phase-II of the LHCb, as can be seen in figure 7c. We emphasize to note that the colored stripes in this figure are allowed parameter space for the soft symmetry-breaking scenario, and the blank region is the excluded parameter space. We observe from 7c that the allowed parameter space is very narrow and different for $\mathcal{Z}_N \times \mathcal{Z}_M$ flavour symmetries for $m_a < 1$ TeV. The stripe corresponding to the $\mathcal{Z}_2 \times \mathcal{Z}_9$ flavour symmetry resides inside the stripe corresponding to the $\mathcal{Z}_2 \times \mathcal{Z}_5$ flavour symmetry in this case. Above $m_a > 1$ TeV, the stripes corresponding to the $\mathcal{Z}_2 \times \mathcal{Z}_9$ and $\mathcal{Z}_2 \times \mathcal{Z}_{11}$ flavour symmetries overlap around 10^4 TeV.

We obtain remarkable predictions in the case of the symmetry-conserving scenario. As evident from figure 7c, only $\mathcal{Z}_2 \times \mathcal{Z}_5$ and $\mathcal{Z}_2 \times \mathcal{Z}_{11}$ flavour symmetries barely survive in the future high luminosity phase-II of the LHCb. Thus, the future high luminosity phase-II of the LHCb will be crucial and decisive in ruling out the symmetry-conserving scenario discussed in this work.

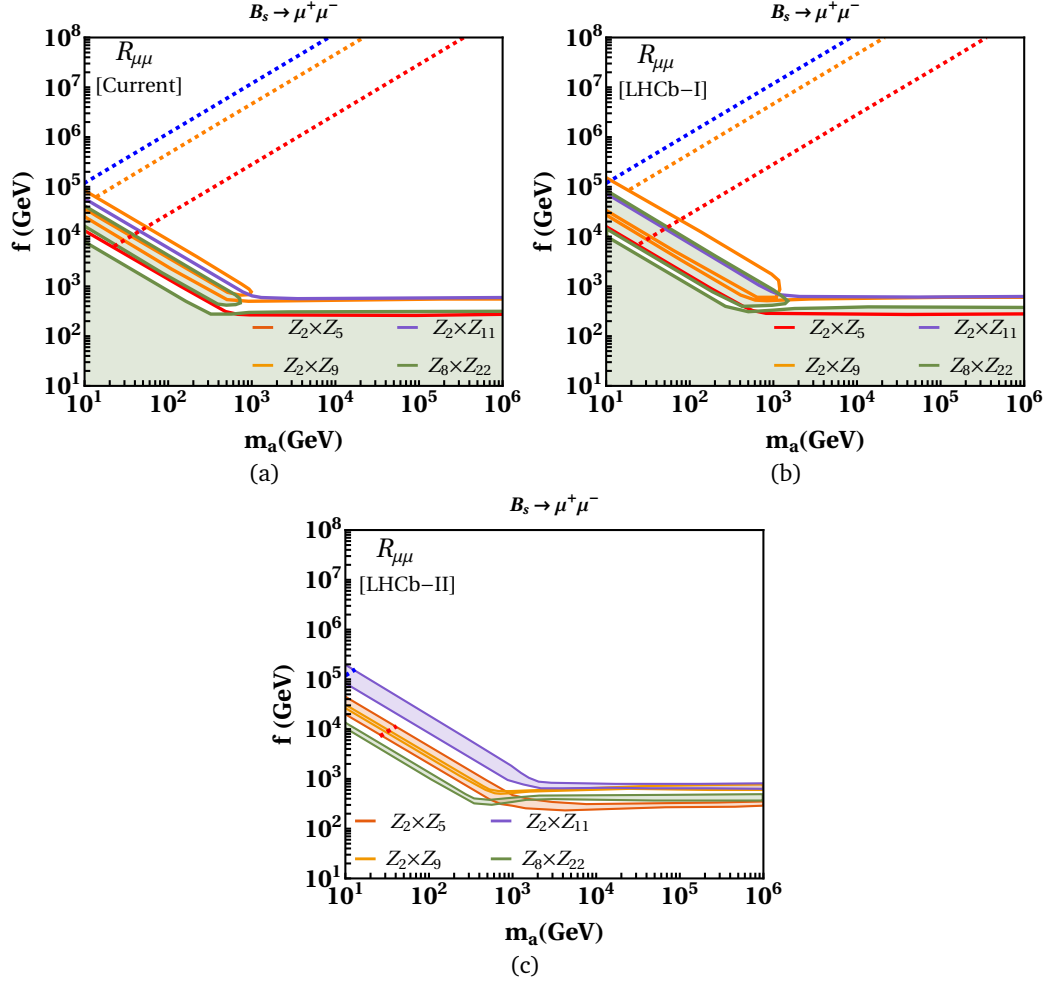


Figure 7: The blank region above the continuous curves in figure 7a and 7b shows the allowed $f - m_a$ parameter space of the flavon of different $\mathcal{Z}_N \times \mathcal{Z}_M$ models by current measurement as well as the future projected sensitivities in the LHCb Phase-I for the observable $\mathcal{R}_{\mu\mu}$, with $\lambda_\chi = 2$, in the soft symmetry-breaking scenario. The coloured region in figure 7c depicts the same allowed parameter space for projected sensitivities of $\mathcal{R}_{\mu\mu}$ in the LHCb Phase-II, while the dashed lines represent the allowed parameter space in the symmetry-conserving scenario.

4.3 Constraints from $b \rightarrow s\mu^+\mu^-$ transition

In this section, we explore constraints arising from a plethora of observables in diverse decay channels triggered by the quark-level transition $b \rightarrow s\mu^+\mu^-$. This also encompasses the branching ratio of $B_s \rightarrow \mu^+\mu^-$, which was addressed in the preceding sub-section. The effective Hamiltonian for $b \rightarrow s\mu^+\mu^-$ transition can be written as follows:

$$\mathcal{H}_{\text{eff}} = -\frac{4G_F}{\sqrt{2}} \frac{e^2}{16\pi^2} m_b V_{ts}^* V_{tb} \left[C_S^{\mu\mu} (\bar{s}_L b_R) (\bar{\mu}\mu) + C_S^{\prime\mu\mu} (\bar{s}_R b_L) (\bar{\mu}\mu) + C_P^{\mu\mu} (\bar{s}_L b_R) (\bar{\mu}\gamma_5\mu) + C_P^{\prime\mu\mu} (\bar{s}_R b_L) (\bar{\mu}\gamma_5\mu) \right]. \quad (59)$$

Here, $C_S^{\mu\mu}$, $C_P^{\mu\mu}$, $C_S^{\prime\mu\mu}$, and $C_P^{\prime\mu\mu}$ represent the new physics scalar/pseudoscalar Wilson coefficients (WCs). In the model under consideration, these WCs are generated at the tree level and are expressed in terms of model parameters. For various flavour symmetries, these WCs are given in Table 8.

These new physics WCs, which are complex, are subject to constraints imposed by a multitude of $b \rightarrow s\mu^+\mu^-$ observables (158 observables), which include:

WCs	$\mathcal{Z}_2 \times \mathcal{Z}_5$	$\mathcal{Z}_2 \times \mathcal{Z}_9$	$\mathcal{Z}_2 \times \mathcal{Z}_{11}$	$\mathcal{Z}_8 \times \mathcal{Z}_{22}$
$C_S^{\mu\mu}$	$\mathcal{N}(9\epsilon^6/m_s^2)y_{23}^d y_{22}^{\ell*}$	$\mathcal{N}(25\epsilon^{10}/m_s^2)y_{23}^d y_{22}^{\ell*}$	$\mathcal{N}(49\epsilon^{14}/m_s^2)y_{23}^d y_{22}^{\ell*}$	$\mathcal{N}(25\epsilon^{10}/m_s^2)y_{23}^d y_{22}^{\ell*}$
$C_S^{\prime\mu\mu}$	$\mathcal{N}(3\epsilon^4/m_s^2)y_{32}^{d*} y_{22}^{\ell*}$	$\mathcal{N}(15\epsilon^8/m_s^2)y_{32}^{d*} y_{22}^{\ell*}$	$\mathcal{N}(21\epsilon^{10}/m_s^2)y_{32}^{d*} y_{22}^{\ell*}$	$\mathcal{N}(15\epsilon^8/m_s^2)y_{32}^{d*} y_{22}^{\ell*}$
$C_P^{\mu\mu}$	$\mathcal{N}(9\epsilon^6/m_a^2)y_{23}^d y_{22}^{\ell*}$	$\mathcal{N}(25\epsilon^{10}/m_a^2)y_{23}^d y_{22}^{\ell*}$	$\mathcal{N}(49\epsilon^{14}/m_a^2)y_{23}^d y_{22}^{\ell*}$	$\mathcal{N}(25\epsilon^{10}/m_a^2)y_{23}^d y_{22}^{\ell*}$
$C_P^{\prime\mu\mu}$	$\mathcal{N}(3\epsilon^4/m_a^2)y_{32}^{d*} y_{22}^{\ell*}$	$\mathcal{N}(15\epsilon^8/m_a^2)y_{32}^{d*} y_{22}^{\ell*}$	$\mathcal{N}(21\epsilon^{10}/m_a^2)y_{32}^{d*} y_{22}^{\ell*}$	$\mathcal{N}(15\epsilon^8/m_a^2)y_{32}^{d*} y_{22}^{\ell*}$

Table 8: Scalar and pseudoscalar WCs for $b \rightarrow s\mu^+\mu^-$ decay in terms of model parameters for various flavour symmetries. Here $\mathcal{N} = -\frac{2\sqrt{2}\pi^2 v^2}{G_F m_b V_{tb} V_{ts}^* e^2 f^2}$ whereas the benchmark values of y_{23}^d (y_{32}^d), and y_{22}^{ℓ} couplings are given in the appendix for all four $\mathcal{Z}_N \times \mathcal{Z}_M$ flavour symmetries.

1. The branching ratio of $B_s \rightarrow \mu^+\mu^-$ [68, 78] and $B \rightarrow X_s\mu^+\mu^-$ in both low and high- q^2 bins [79]. Here, we consider the modified world average of the branching ratio of $B_s \rightarrow \mu^+\mu^-$ [78] obtained after the recent CMS update, which is based on the full Run 2 dataset [73]. The updated world average now aligns with the predictions of the SM.
2. The differential branching ratios of $B^0 \rightarrow K^{*0}\mu^+\mu^-$ [80, 81, 82], $B^+ \rightarrow K^{*+}\mu^+\mu^-$, $B^0 \rightarrow K^0\mu^+\mu^-$, $B^+ \rightarrow K^+\mu^+\mu^-$ [83, 81] and $B_s \rightarrow \phi\mu^+\mu^-$ [84] in various q^2 intervals. It should be noted that for all of these observables, as well as for other $b \rightarrow s\mu^+\mu^-$ observables utilized in our analysis, we have excluded measurements within the $6 \text{ GeV}^2 \leq q^2 \leq 14.0 \text{ GeV}^2$ bin.
3. In addition to branching fractions, our analysis incorporates various angular observables as constraints within the fit. These observables encompass the longitudinal polarization fraction f_L , forward-backward asymmetry A_{FB} , and $S_{3,4,5,7,8,9}$ observables measured in the $B^0 \rightarrow K^{*0}\mu^+\mu^-$ decay across multiple q^2 bins, as reported by the LHCb collaboration [85]. Furthermore, we include the observables f_L , P_1 , P'_4 , P'_5 , P'_6 , and P'_8 measured in $B^0 \rightarrow K^{*0}\mu^+\mu^-$ decay by ATLAS [86], along with P_1 and P'_5 measurements from CMS [87]. Additionally, measurements of f_L and A_{FB} by the CDF and CMS collaborations [81, 82] are also integrated into our fit.
4. The f_L and $P_1 - P'_8$ angular observables in $B^+ \rightarrow K^{*+}\mu^+\mu^-$ decay mode are also included [88] in the fit.
5. The fit also incorporates f_L , S_3 , S_4 , and S_7 observables obtained from the measurements of the $B_s \rightarrow \phi\mu^+\mu^-$ decay by the LHCb collaboration, as reported in [89].

The constraints on new physics couplings are obtained by performing a χ^2 fit using the CERN minimization code MINUIT [90]. The available experimental correlations [85, 88, 89], as well as theoretical correlations, are included in the analysis. The theoretical correlations, along with the expressions for various observables, are computed using flavio [91]. The observables in flavio are pre-implemented on the basis of refs. [92, 93]. For the fit, we closely follow the methodology adopted in [94, 95, 96].

The value of χ_{SM}^2 is 164.80, whereas the χ^2 at the best-fit point is 164.26, indicating that the addition of new physics in the form of scalar and pseudoscalar interactions only provides an extremely marginal improvement over the SM (Pull = 0.54). The fit results are (1σ allowed range of real and complex components of the WCs)

$$\begin{aligned}
C_S^{\mu\mu} &= [(-0.13, 0.13), (-0.13, 0.13)] \\
C_P^{\mu\mu} &= [(-0.07, 0.13), (-0.12, 0.12)] \\
C_S^{\prime\mu\mu} &= [(-0.11, 0.10), (-0.12, 0.12)] \\
C_P^{\prime\mu\mu} &= [(-0.07, 0.13), (-0.11, 0.11)].
\end{aligned} \tag{60}$$

The model-independent fit results for the Wilson coefficients of $b \rightarrow s\mu^+\mu^-$ obtained in equation 60 can be utilized to constrain free parameters for the different $\mathcal{Z}_N \times \mathcal{Z}_M$ symmetries, as shown in figure 8. In the case of soft symmetry-breaking, the region above the continuous curves represents the allowed parameter space, and it is evident that the bounds are weakest for the minimal $\mathcal{Z}_2 \times \mathcal{Z}_5$ flavour symmetry, while the $\mathcal{Z}_2 \times \mathcal{Z}_9$, $\mathcal{Z}_2 \times \mathcal{Z}_{11}$, and $\mathcal{Z}_8 \times \mathcal{Z}_{22}$ impose almost similar constraints on the free parameters. In the symmetry-conserving scenario, the corresponding allowed parameter space for $\mathcal{Z}_2 \times \mathcal{Z}_{5,9,11}$ models are represented by the dashed straight lines, among which, the parameter space for the flavon of $\mathcal{Z}_2 \times \mathcal{Z}_{11}$ is most constrained.

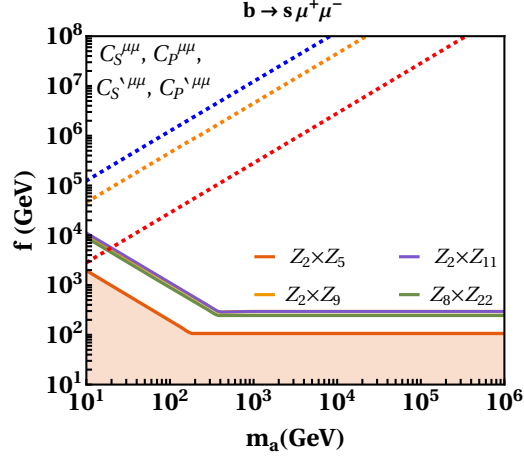


Figure 8: Bounds on the $f - m_a$ parameter space of the flavon of different $\mathcal{Z}_N \times \mathcal{Z}_M$ models by obtained limits on $C_S^{\mu\mu}$, $C_P^{\mu\mu}$, $C_S^{\prime\mu\mu}$ and $C_P^{\prime\mu\mu}$ as in equation 60 for the soft symmetry-breaking as well as symmetry-conserving scenario.

4.4 Muon forward-backward asymmetry in $B \rightarrow K\mu^+\mu^-$

Within the framework of the SM, the muon forward-backward asymmetry in the context of $B \rightarrow K\mu^+\mu^-$ decay is inherently predicted to have a value of approximately zero. This prediction holds even when considering the effects of new physics scenarios involving vector-axial vector interactions. However, it's noteworthy that if new physics manifests in the form of scalar or pseudoscalar interactions, it has the potential to introduce a non-zero value to A_{FB} [97, 98]. Given this intriguing possibility, it is prudent to investigate this observable within the framework of flavons. Such an exploration could yield valuable insights into whether the new physics parameter space allowed in the context of this model has the potential to enhance A_{FB} to a value that can be measured experimentally.

The muon forward-backward asymmetry in $B \rightarrow K\mu^+\mu^-$ is given by [97]

$$A_{FB} = \frac{\int_{q_{\min}^2}^{q_{\max}^2} b_\mu(q^2) dq^2}{\int_{q_{\min}^2}^{q_{\max}^2} (2a_\mu(q^2) + \frac{2}{3}c_\mu(q^2)) dq^2}, \quad (61)$$

where

$$a_\mu(q^2) = N(q^2) \left[q^2 |F_P|^2 + \frac{\lambda}{4} (|F_V|^2 + |F_A|^2) + 2m_\mu (m_B^2 - m_K^2 + q^2) \text{Re}(F_P F_A^*) + 4m_\mu^2 m_B^2 |F_A|^2 \right], \quad (62)$$

$$b_\mu(q^2) = 2N(q^2) \left[m_\mu \beta_\mu \sqrt{\lambda_K} \text{Re}(F_S F_V^*) \right], \quad (63)$$

$$c_\mu(q^2) = -\frac{\lambda}{4} \beta_\mu^2 N(q^2) (|F_V|^2 + |F_A|^2), \quad (64)$$

with

$$N(q^2) = \frac{G_F^2 \alpha |V_{tb} V_{ts}^*|^2}{512 \pi^5 m_B^3} \beta_\mu \lambda_K f_+(q^2). \quad (65)$$

Here $\lambda = m_B^4 + m_K^4 + q^4 - 2(m_B^2 m_K^2 + m_B^2 q^2 + m_K^2 q^2)$ and $\beta_\mu = \sqrt{1 - 4m_\mu^2/q^2}$. The F functions are written in terms of WCs and form-factors as

$$F_A = C_{10}, \quad (66)$$

$$F_V = C_9 + \frac{2m_B T_P(q^2)}{M_B f_+(q^2)}, \quad (67)$$

$$F_S = \frac{M_B^2 - M_K^2}{2(m_b - m_s)} \frac{f_0(q^2)}{f_+(q^2)} m_b \left(C_S^{\mu\mu} + C_S^{\prime\mu\mu} \right), \quad (68)$$

$$F_P = \frac{M_B^2 - M_K^2}{2(m_b - m_s)} \frac{f_0(q^2)}{f_+(q^2)} m_b \left(C_P^{\mu\mu} + C_P^{\prime\mu\mu} \right) + m_\mu C_{10} \left[\frac{M_B^2 - M_K^2}{q^2} \left(\frac{f_0(q^2)}{f_+(q^2)} - 1 \right) - 1 \right] \quad (69)$$

Here $f_0(q^2)$ and $f_+(q^2)$ are $B \rightarrow K$ form-factors whereas $C_{9,10}$ are SM WCs. The function $T_P(q^2)$ in the expression of F_V incorporates contributions from virtual one-photon exchange between the hadrons and the lepton pair, in addition to the hard scattering contributions [97]. At low- q^2 values, all form factors simplify to a single soft form factor [99, 100]. It is evident that in the absence of new physics scalar and pseudoscalar couplings, the muon-forward backward asymmetry remains zero. Consequently, in the current scenario, we anticipate a non-zero value for A_{FB} . Nonetheless, it would be intriguing to determine whether the constraints imposed by the new physics scalar and pseudoscalar couplings, as derived from the existing $b \rightarrow s\mu^+\mu^-$ data, permit any meaningful enhancements or not.

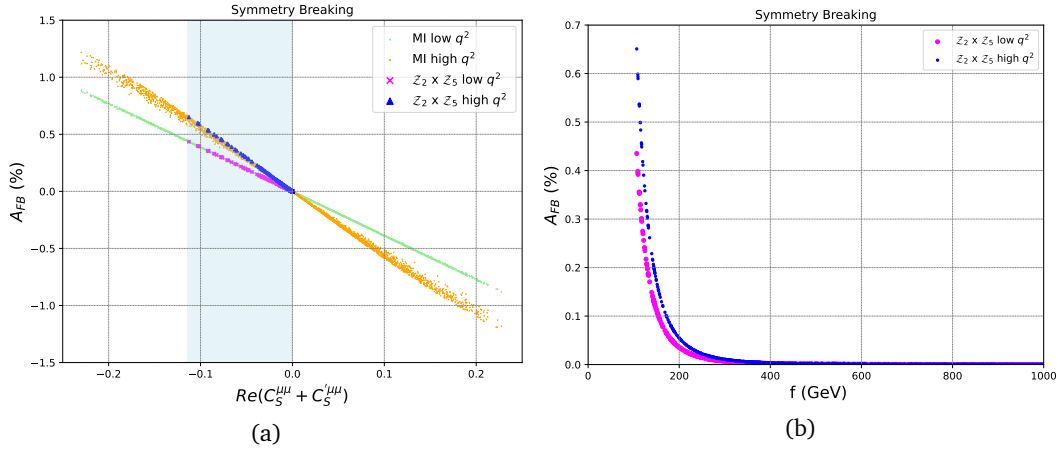


Figure 9: Predictions for the muon FB asymmetry in the $B^+ \rightarrow K^+\mu^+\mu^-$ decay.

Utilizing the model-independent constraints on the new physics scalar and pseudoscalar couplings as derived in the previous sub-section, the FB asymmetry in both the low and high- q^2 regions is illustrated in Fig. 9. The figure clearly demonstrates that the existing $b \rightarrow s\mu^+\mu^-$ data permits an enhancement in A_{FB} , reaching up to a percent level.

We now explore the prediction of A_{FB} within the flavon model, considering both symmetry-conserving and symmetry-breaking scenarios. In the symmetry-conserving scenario, the flavon masses, as discussed in equation 33, are dependent on its VEV (f). Therefore, for all these symmetries, f serves as the sole free parameter. It is observed that, in order to satisfy the model-independent constraints on scalar as well as pseudoscalar couplings derived in eq. 60, the values of f need to be large. This holds true for all four flavour symmetries. However, such large values of f result in exceedingly small values of $C_S^{\mu\mu}$ and $C_S^{\prime\mu\mu}$ couplings, leading to predicted values of A_{FB} that are too negligible to be observed.

In the scenario of symmetry breaking, both f and m_a serve as free parameters. The parameter space of $(m_a - f)$ is constrained by eq. 60. For all flavour symmetries except $\mathcal{Z}_2 \times \mathcal{Z}_5$, the constraints derived from eq. 60 limits the $(m_a - f)$ parameter space to such an extent that any significant enhancement in A_{FB} is precluded. The prediction of A_{FB} for the $\mathcal{Z}_2 \times \mathcal{Z}_5$ flavour symmetry is illustrated in Fig. 9. As depicted in the left panel of the figure, A_{FB} can be enhanced by up to half a percent level, both in the low and high- q^2 regions. This enhancement is smaller as compared to the model independent results because the allowed $(C_S^{\mu\mu} + C_S^{\prime\mu\mu})$ values (indicated by the light blue band), which are pertinent to A_{FB} , are more restrictive compared to the model-independent bounds. The right panel displays A_{FB} as a function of the parameter f . It is apparent from the plot that a meaningful enhancement of A_{FB} is achievable only for smaller values of f , specifically $f < 200$ GeV.

5 Leptonic flavour physics of the flavon of the $\mathcal{Z}_N \times \mathcal{Z}_M$ flavour symmetries

The current and future experiments on the charged lepton flavour violation (CLFV) processes have a great potential to place stringent bounds on the parameter space of the flavon of the $\mathcal{Z}_N \times \mathcal{Z}_M$ flavour symmetries, and even may provide an improvement over the constraints arising from the quark flavour physics. The sensitivities of the CLFV processes for the current as well as future projected experiments are shown in table 9.

Observables	Current sensitivity	Ref.	Future projection	Ref.
$\text{BR}(\mu \rightarrow e\gamma)$	$< 4.2 \times 10^{-13}$	MEG [101]	6×10^{-14}	MEGII [102]
$\text{BR}(\tau \rightarrow e\gamma)$	$< 3.3 \times 10^{-8}$	Babar [103]	$\sim 10^{-9}$	Belle II [104]
$\text{BR}(\tau \rightarrow \mu\gamma)$	$< 4.4 \times 10^{-8}$	Babar [103]	$\sim 10^{-9}$	Belle II [104]
$\text{BR}(\mu \rightarrow e)^{\text{Au}}$	$< 7 \times 10^{-13}$	SINDRUM II [105]	–	–
$\text{BR}(\mu \rightarrow e)^{\text{Al}}$	–	–	3×10^{-15}	COMET Phase-I [106, 107]
$\text{BR}(\mu \rightarrow e)^{\text{Al}}$	–	–	6×10^{-17}	COMET Phase-II [106]
$\text{BR}(\mu \rightarrow e)^{\text{Al}}$	–	–	6×10^{-17}	Mu2e [108]
$\text{BR}(\mu \rightarrow e)^{\text{Al}}$	–	–	3×10^{-18}	Mu2e II [107]
$\text{BR}(\mu \rightarrow e)^{\text{Si}}$	–	–	2×10^{-14}	DeeMe [109]
$\text{BR}(\mu \rightarrow e)^{\text{Ti}}$	–	–	$\sim 10^{-20} - 10^{-18}$	PRISM/PRIME [110, 111]
$\text{BR}(\mu \rightarrow e\bar{e}e)$	$< 1.0 \times 10^{-12}$	SINDRUM [112]	$\sim 10^{-16}$	Mu3e [113]
$\text{BR}(\tau \rightarrow 3\mu)$	$< 2.1 \times 10^{-8}$	Belle [114]	$\sim 10^{-9}$	Belle II [104]
$\text{BR}(\tau \rightarrow 3e)$	$< 2.7 \times 10^{-8}$	Belle [114]	$\sim 10^{-9}$	Belle II [104]

Table 9: Experimental upper limits on various Leptonic flavour violation (LFV) processes.

5.1 Radiative leptonic decays

We write the following effective Lagrangian for the radiative leptonic decays,

$$\mathcal{L}_{\text{eff}} = m_{\ell'} C_T^L \bar{\ell} \sigma^{\rho\lambda} P_L \ell' F_{\rho\lambda} + m_{\ell'} C_T^R \bar{\ell} \sigma^{\rho\lambda} P_R \ell' F_{\rho\lambda}. \quad (70)$$

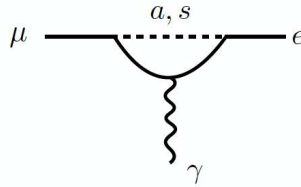


Figure 10: Feynman diagram representing $\mu \rightarrow e\gamma$ decay.

The branching ratio of the radiative leptonic decays is given by,

$$\text{BR}(\ell' \rightarrow \ell\gamma) = \frac{m_{\ell'}^5}{4\pi\Gamma_{\ell'}} (|C_T^L|^2 + |C_T^R|^2). \quad (71)$$

The radiative leptonic decays receive the one-loop contribution, as shown in figure 10. The Wilson coefficients corresponding to the one-loop contribution read as [33],

$$C_T^L = (C_T^R)^* = \frac{e}{32\pi^2} \sum_{k=e,\mu,\tau} \left\{ \frac{1}{6} \left(y_{\ell k}^* y_{\ell' k} + \frac{m_{\ell}}{m_k} y_{k\ell}^* y_{k\ell'} \right) \left(\frac{1}{m_s^2} - \frac{1}{m_a^2} \right) \right\}$$

$$- y_{\ell k} y_{k \ell'} \frac{m_k}{m_{\ell'}} \left[\frac{1}{m_s^2} \left(\frac{3}{2} + \log \frac{m_{\ell'}^2}{m_s^2} \right) - \frac{1}{m_a^2} \left(\frac{3}{2} + \log \frac{m_{\ell'}^2}{m_a^2} \right) \right] \}. \quad (72)$$

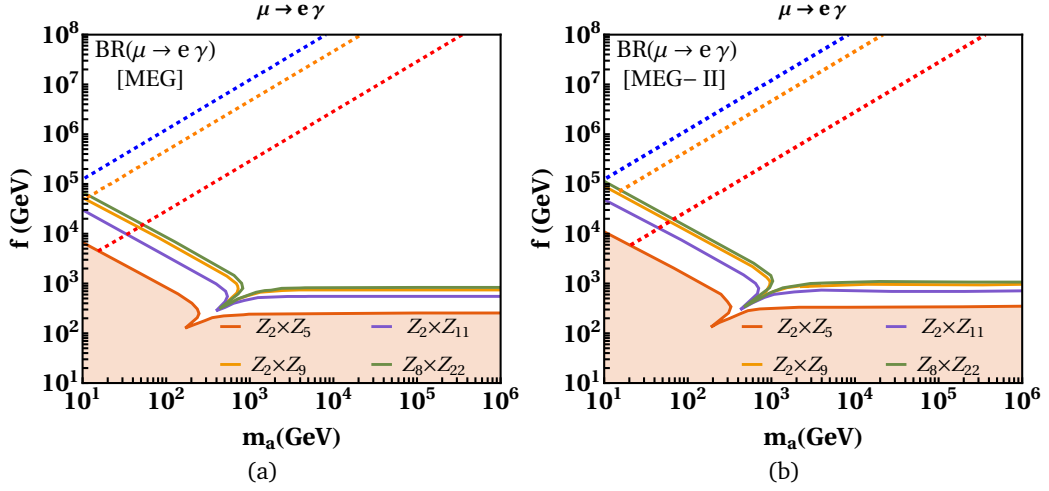


Figure 11: Bounds on the $f - m_a$ parameter space of the flavon of different $\mathcal{Z}_N \times \mathcal{Z}_M$ models by $\text{BR}(\mu \rightarrow e \gamma)$ for current as well as projected measurements from MEG and MEG-II experiments. The region above continuous curves represents the allowed parameter space for the corresponding $\mathcal{Z}_N \times \mathcal{Z}_M$ flavour symmetries in the soft symmetry-breaking scenario. The dashed lines show the allowed parameter space in the symmetry-conserving scenario. For both the scenario, $\lambda_\chi = 2$.

The radiative leptonic decays impose the most stringent constraints on the parameter space of flavon of the $\mathcal{Z}_8 \times \mathcal{Z}_{22}$ and $\mathcal{Z}_2 \times \mathcal{Z}_9$ flavour symmetries in the soft symmetry-breaking scenario, as observed in figure 11a and 11b for the MEG and MEG-II experiments. This is followed by the $\mathcal{Z}_2 \times \mathcal{Z}_{11}$ flavour symmetry. For the symmetry-conserving case, the strongest bounds arise for the flavon of the $\mathcal{Z}_2 \times \mathcal{Z}_{11}$ flavour symmetry, followed by the flavon of the $\mathcal{Z}_2 \times \mathcal{Z}_9$ flavour symmetry.

5.2 $A \mu \rightarrow A e$ conversion

We write the following effective Lagrangian describing $A \mu \rightarrow A e$ conversion,

$$\mathcal{L}_{\text{eff}} = C_{qq}^{VL} \bar{e} \gamma^\nu P_L \mu P_L \bar{q} \gamma_\nu q + m_\mu m_q C_{qq}^{SL} \bar{e} P_R \mu \bar{q} q + m_\mu \alpha_s C_{gg}^L \bar{e} P_R \mu G_{\rho\nu} G^{\rho\nu} + (R \leftrightarrow L), \quad (73)$$

Moreover, the dipole operators given in equation (70) provide additional contribution to $A \mu \rightarrow A e$ conversion. We show the Feynman diagram for $A \mu \rightarrow A e$ conversion in figure 12. The Wilson coefficients for the diagram on the left in figure 12 are given by [33],

$$\begin{aligned} C_{qq}^{SL} &= \left(\frac{1}{m_s^2} + \frac{1}{m_a^2} \right) y_{\mu e}^* \text{Re}(y_{qq}), \\ C_{qq}^{SR} &= \left(\frac{1}{m_s^2} - \frac{1}{m_a^2} \right) y_{e\mu} \text{Re}(y_{qq}). \end{aligned} \quad (74)$$

The nucleon-level Wilson coefficients which include the nuclear effects of quarks inside the nucleons as well as the contribution of the Feynman diagram on the right side of figure 12 can be written as,

$$\begin{aligned} \tilde{C}_p^{VL} &= \sum_{q=u,d} C_{qq}^{VL} f_{V_q}^p, \\ \tilde{C}_p^{SL} &= \sum_{q=u,d,s} C_{qq}^{SL} f_q^p - \sum_{Q=c,b,t} C_{QQ}^{SL} f_{\text{heavy}}^p, \end{aligned} \quad (75)$$

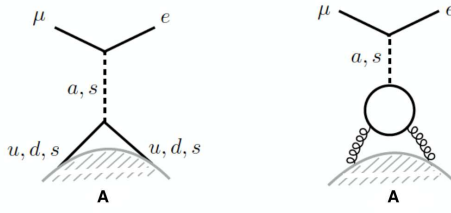


Figure 12: Feynman diagram showing $A \mu \rightarrow A e$ conversion.

where the proton quark content is parameterized by the vector and scalar couplings $f_{V_q}^p, f_q^p$, and $f_{\text{heavy}}^p = 2/27(1 - f_u^p - f_d^p - f_s^p)$ [115]. For right-handed operators, analogous expressions can be obtained by replacing L with R , and for the neutron p is replaced by n . The contribution of the vector operators is much less than that of the scalar operators. Therefore, it can be ignored [33]. We use the numerical values of vector and scalar couplings given in references [116, 117], which are obtained after using the lattice average given in reference [118],

$$\begin{aligned}
 f_u^p &= 0.0191 & f_u^n &= 0.0171, \\
 f_d^p &= 0.0363 & f_d^n &= 0.0404, \\
 f_s^p &= f_s^n & &= 0.043.
 \end{aligned} \tag{76}$$

After including nuclear effects, the $A \mu \rightarrow A e$ conversion rate reads as [33],

$$\Gamma_{A \mu \rightarrow A e} = \frac{m_\mu^5}{4} \left| C_T^L D + 4 \left[m_\mu m_p \tilde{C}_p^{SL} + \tilde{C}_p^{VL} V^p + (p \rightarrow n) \right] \right|^2 + L \rightarrow R, \tag{77}$$

where the dimensionless coefficients $D, S^{p,n}$, and $V^{p,n}$ are functions of the overlap integrals of the initial state muon and the final-state electron wave functions with the target nucleus. We use their numerical values given in table 10 [119].

Target	D	S^p	S^n	V^p	V^n	$\Gamma_{\text{capt}} [10^6 \text{s}^{-1}]$
Au	0.189	0.0614	0.0918	0.0974	0.146	13.06
Al	0.0362	0.0155	0.0167	0.0161	0.0173	0.705
Si	0.0419	0.0179	0.0179	0.0187	0.0187	0.871
Ti	0.0864	0.0368	0.0435	0.0396	0.0468	2.59

Table 10: Numerical values of the dimensionless coefficients $D, S^{p,n}$, $V^{p,n}$ and the muon capture rate for different nuclei where Γ_{capt} denotes the muon capture rate.

The most stringent constraints from the $A \mu \rightarrow A e$ conversion rate on the parameter space of flavon of $\mathcal{Z}_N \times \mathcal{Z}_M$ flavour symmetries arise for the $\mathcal{Z}_8 \times \mathcal{Z}_{22}$ and $\mathcal{Z}_2 \times \mathcal{Z}_{9,11}$ flavour symmetries. The bounds from the future experiments are remarkably stronger than the existing limits. This can be seen in figure 13 for different ongoing and future experiments. This is followed by the $\mathcal{Z}_2 \times \mathcal{Z}_5$ flavour symmetries. In the symmetry-conserving scenario, the most stringent bounds are for the $\mathcal{Z}_2 \times \mathcal{Z}_{11}$ flavour symmetry, followed by the $\mathcal{Z}_2 \times \mathcal{Z}_{9,5}$ flavour symmetries.

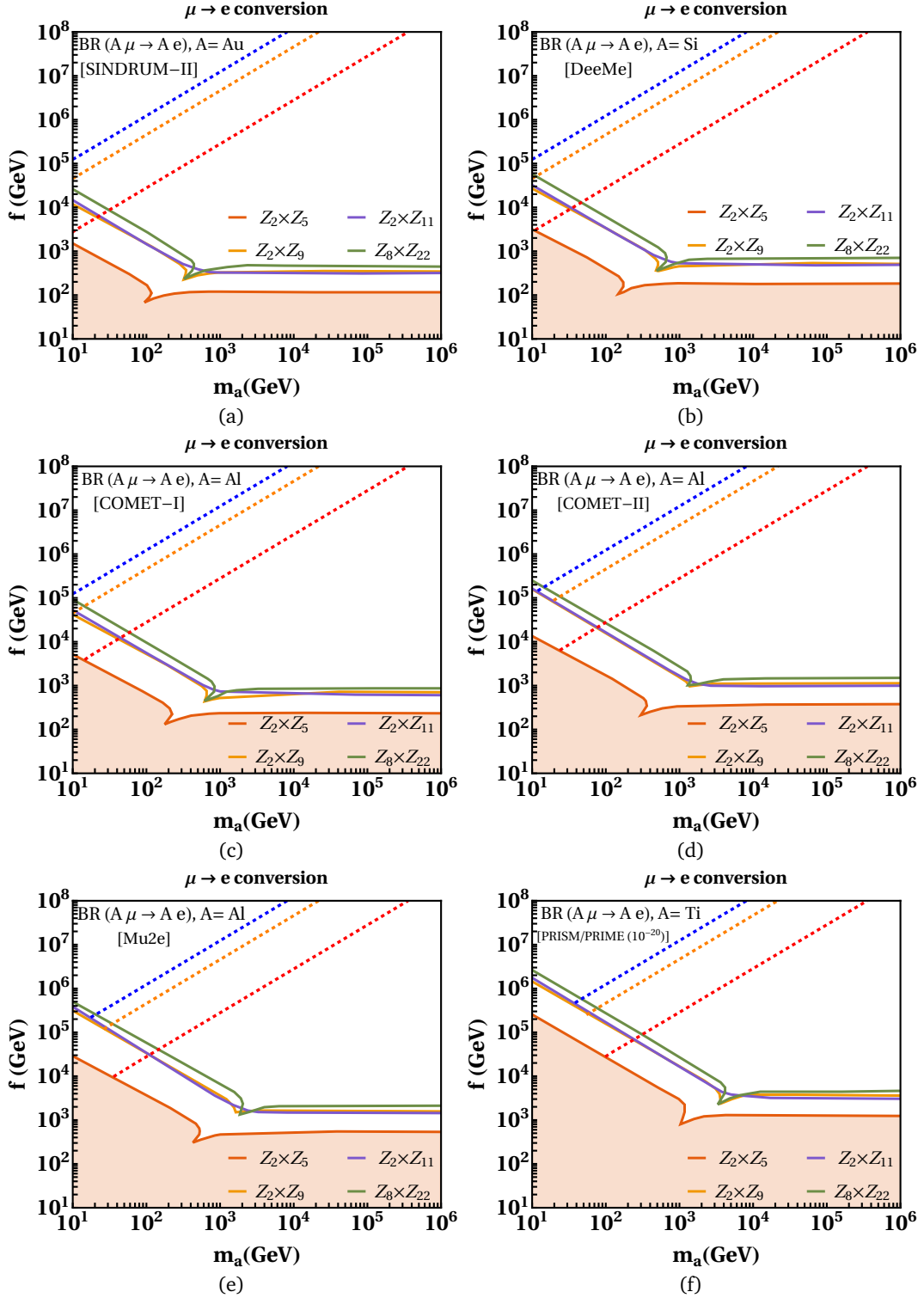


Figure 13: Bounds on the $f - m_a$ parameter space of the flavon of different $\mathcal{Z}_N \times \mathcal{Z}_M$ symmetries by BR($A\mu \rightarrow Ae$) for the current as well as projected sensitivities of the experiments given in table 9. The coloured region represents the excluded parameter space by all four $\mathcal{Z}_N \times \mathcal{Z}_M$ symmetries in the soft symmetry-breaking scenario, while the dashed lines represent the allowed parameter space in the symmetry-conserving scenario.

5.3 $\mu \rightarrow 3e$ and $\tau \rightarrow 3\mu$ decays

The additional probes of the dipole operators given in equation (70) can emerge from the three body flavour violating leptonic decays $\mu \rightarrow 3e$ and $\tau \rightarrow 3\ell$ where $\ell = e, \mu$. The decay width of these decays is given by [33],

$$\Gamma(\ell' \rightarrow 3\ell) = \frac{\alpha m_\ell^5}{12\pi^2} \left| \log \frac{m_\ell^2}{m_\ell'^2} - \frac{11}{4} \right| (|C_T^L|^2 + |C_T^R|^2). \quad (78)$$

where the tree-level contribution is negligible due to the strong chiral-suppression caused by the logarithmic enhancement of the dipole operators[33]. We ignore other contributions, such as Z -mediated penguin, due to their strong suppression [120].

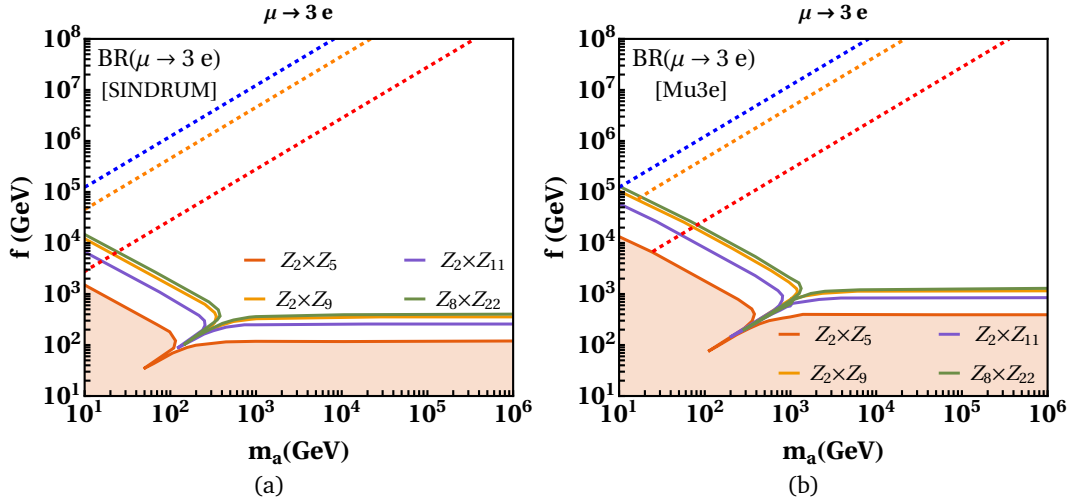


Figure 14: Bounds on the $f - m_a$ parameter space of the flavon of different $\mathcal{Z}_N \times \mathcal{Z}_M$ symmetries by $\text{BR}(\mu \rightarrow 3e)$ for sensitivities of the SINDRUM and Mu3e experiments. The coloured region represents the excluded parameter space by all four $\mathcal{Z}_N \times \mathcal{Z}_M$ symmetries in the soft symmetry-breaking scenario, while the dashed lines represent the allowed parameter space in the symmetry-conserving scenario.

The $\mu \rightarrow 3e$ decays places the most stringent bounds on the parameter space of flavon of the $\mathcal{Z}_8 \times \mathcal{Z}_{22}$ flavour symmetry for the soft symmetry-breaking case as shown in figure 14 for the SINDRUM and Mu3e experiments. The bounds on the flavour symmetry $\mathcal{Z}_2 \times \mathcal{Z}_9$ are almost similar to that of the $\mathcal{Z}_8 \times \mathcal{Z}_{22}$ flavour symmetry. This is followed by the $\mathcal{Z}_2 \times \mathcal{Z}_5$ flavour symmetry. For the symmetry-conserving scenario, the strongest bounds are for the $\mathcal{Z}_2 \times \mathcal{Z}_{11}$ flavour symmetry, followed by the $\mathcal{Z}_2 \times \mathcal{Z}_{9,5}$ flavour symmetries.

In figure 15, we present the summary of the most significant bounds on the parameter space of the flavon of different $\mathcal{Z}_N \times \mathcal{Z}_M$ flavour symmetries. We notice that in the soft symmetry-breaking scenario the most stringent bound for the $\mathcal{Z}_2 \times \mathcal{Z}_5$ flavour symmetry arise from the observable $|M_{12}^D|$, while for the $\mathcal{Z}_2 \times \mathcal{Z}_9$ and $\mathcal{Z}_8 \times \mathcal{Z}_{22}$ flavour symmetries, bounds from the observable C_{ϵ_K} are most stringent, and in the case of the $\mathcal{Z}_2 \times \mathcal{Z}_{11}$ the observable C_{B_d} in the phase-II of the LHCb places the strongest constraint. For the symmetry-conserving scenario, the most significant bounds for every $\mathcal{Z}_N \times \mathcal{Z}_M$ flavour symmetry are shown with the dashed straight-lines in figure 15.

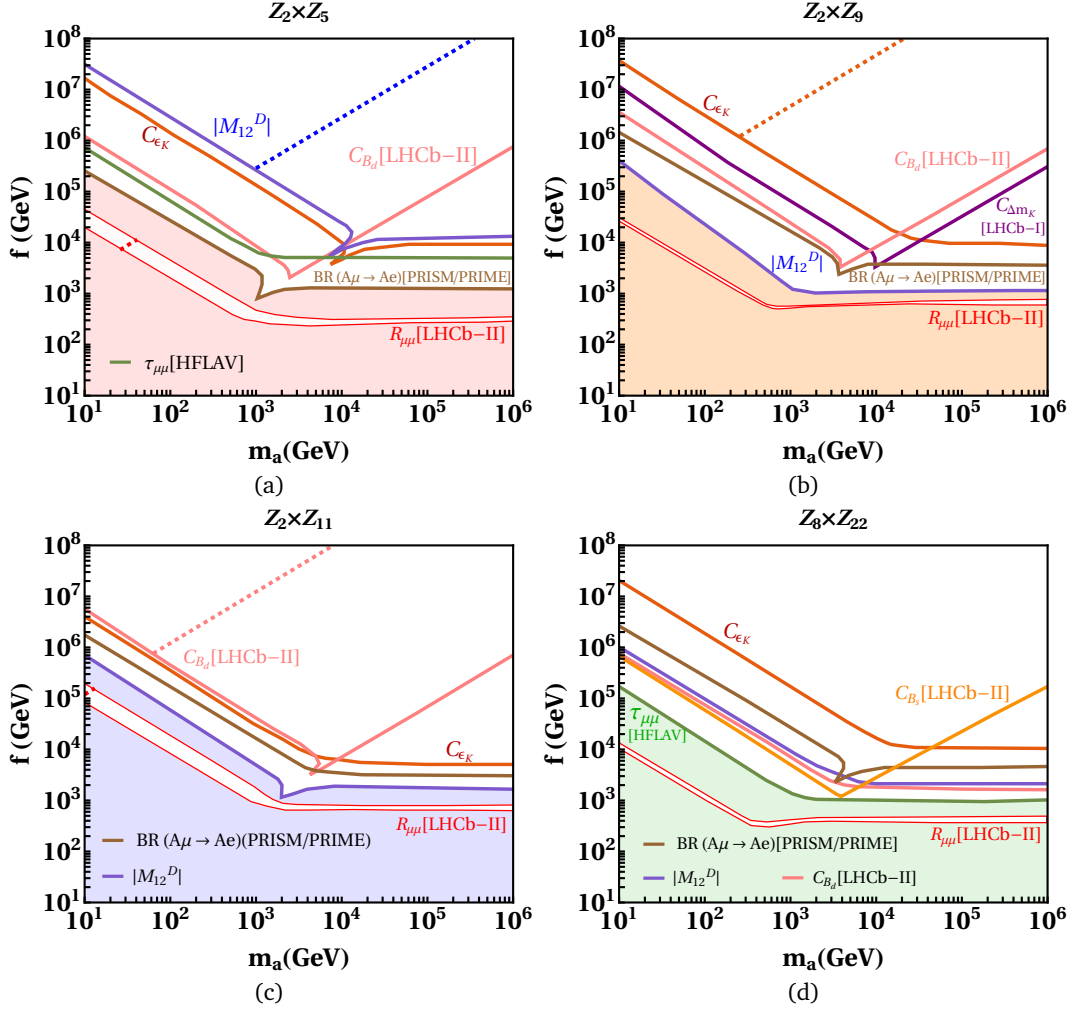


Figure 15: Summary of the excluded parameter space constrained significantly by the quark and leptonic flavour observables for different $\mathcal{Z}_N \times \mathcal{Z}_M$ flavour symmetries are shown with the coloured region in the soft symmetry-breaking scenario. The dashed line represents the allowed parameter space, which is most stringently constrained by the corresponding flavour observable in the symmetry-conserving scenario, except for the $\mathcal{Z}_8 \times \mathcal{Z}_{22}$ flavour symmetry.

6 Hadron collider physics of the flavon of the $\mathcal{Z}_N \times \mathcal{Z}_M$ flavour symmetries

We now discuss the collider signatures of the flavon of the $\mathcal{Z}_N \times \mathcal{Z}_M$ flavour symmetries through its decays and production processes. We first discuss the decays of flavon to a pair of fermions, as well as decays of top quark involving flavon. After this, we investigate the production mechanisms of the flavon of the $\mathcal{Z}_N \times \mathcal{Z}_M$ flavour symmetries. Our aim is to identify different $\mathcal{Z}_N \times \mathcal{Z}_M$ flavour symmetries as much as possible through the collider signatures. Therefore, we shall finally discuss the sensitivity of signatures of different $\mathcal{Z}_N \times \mathcal{Z}_M$ flavour symmetries to the HL-LHC, the HE-LHC, and a 100 TeV collider. We use the square root of the luminosity to scale the sensitivity of the HL-LHC, HE-LHC, and 100 TeV collider, which is a conservative estimate.

For collider investigation, we employ the parameter space of the flavon of the $\mathcal{Z}_N \times \mathcal{Z}_M$ flavour symmetries provided by the observable $R_{\mu\mu}$ in figure 7c. The observable $R_{\mu\mu}$ is sufficiently capable of differentiating the $\mathcal{Z}_N \times \mathcal{Z}_M$ flavour symmetries investigated in this work. For instance, we use the lower boundary of the allowed

region of the parameter space corresponding to the $\mathcal{Z}_2 \times \mathcal{Z}_5$ flavour symmetry, which does not overlap with the parameter space corresponding to the $\mathcal{Z}_2 \times \mathcal{Z}_9$ flavour symmetry.

We notice that in our framework, there is no Higgs-flavon mixing. Therefore, the flavon does not directly couple to the gauge bosons. This fact leads to no constraints on low masses of flavon from the direct LHC searches [121]. The WW and ZZ final states searches set limits on masses above 300 GeV from ATLAS [122] and 200 GeV from CMS [123]. The searches in the di-photon channel place bounds on the masses above 200 GeV from the ATLAS [124], and above 500 GeV from the CMS [125].

6.1 Flavon decays to a pair of fermions

The flavon of the $\mathcal{Z}_N \times \mathcal{Z}_M$ flavour symmetries decays to a pair of fermions at tree-level, while the decays $a \rightarrow gg$ and $a \rightarrow \gamma\gamma$ are loop-induced. This is due to the non-zero off-diagonal couplings of the flavon to fermions. The partial decay width of the decay $a \rightarrow f_i \bar{f}_j$ at the tree-level can be written as,

$$\Gamma(a \rightarrow f_i \bar{f}_j) = \frac{N_c m_a}{16\pi} \left[\frac{(m_a^2 - (m_i + m_j)^2)(m_a^2 - (m_i - m_j)^2)}{m_a^4} \right]^{1/2} \left[(|y_{ij}|^2 + |y_{ji}|^2) \left(1 - \frac{m_i^2 + m_j^2}{m_a^2} \right) - 2(y_{ij}y_{ji} + y_{ij}^*y_{ji}^*) \frac{m_i m_j}{m_a^2} \right], \quad (79)$$

where N_c is the number of colors.

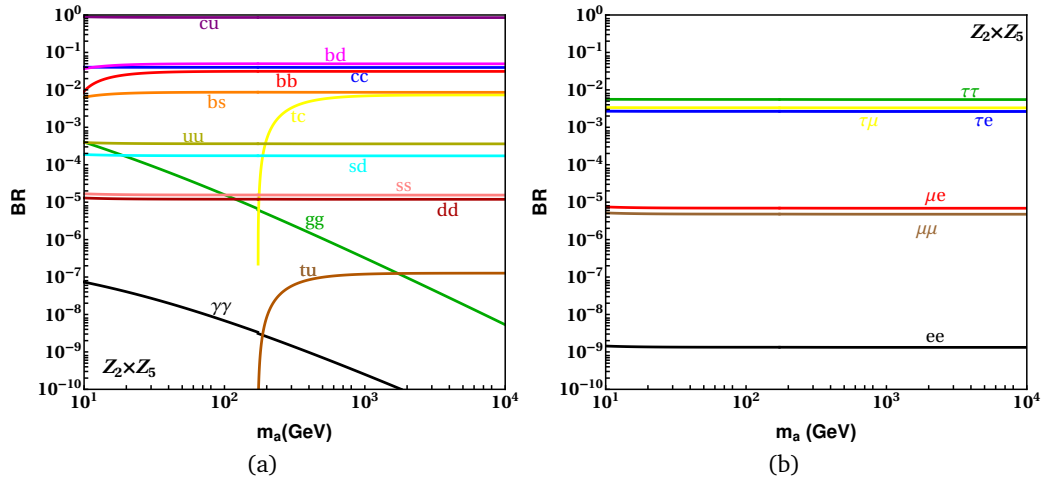


Figure 16: Branching ratios of the various possible decay modes of the flavon into quark and lepton pairs for $\mathcal{Z}_2 \times \mathcal{Z}_5$, $\mathcal{Z}_2 \times \mathcal{Z}_9$, and $\mathcal{Z}_2 \times \mathcal{Z}_{11}$ flavour symmetries.

We present the branching ratios of $a \rightarrow f_i \bar{f}_j$, $a \rightarrow gg$ and $a \rightarrow \gamma\gamma$ in figure 16 for the $\mathcal{Z}_2 \times \mathcal{Z}_5$ flavour symmetry, and in figure 17 for the $\mathcal{Z}_2 \times \mathcal{Z}_{9,11}$, as well as $\mathcal{Z}_8 \times \mathcal{Z}_{22}$ flavour symmetries. In the quark sector, the dominant decay mode is $a \rightarrow b\bar{b}$ below the top quark threshold except for the minimal $\mathcal{Z}_2 \times \mathcal{Z}_5$ symmetry. For the minimal $\mathcal{Z}_2 \times \mathcal{Z}_5$ symmetry the mode $cu(c\bar{u}, \bar{c}u)$ prevails over other modes. This is due to the specific flavour structure of models based on the $\mathcal{Z}_N \times \mathcal{Z}_M$ flavour symmetries and the corresponding Yukawa couplings given in the appendix. As m_a approaches m_t , decay modes involving top quark, particularly, $tc(t\bar{c}, \bar{t}c)$, become increasingly significant for both the $\mathcal{Z}_2 \times \mathcal{Z}_{11}$ and $\mathcal{Z}_8 \times \mathcal{Z}_{22}$ models. These top quark related decay modes, however, remain comparatively less prominent than the decay modes of the flavon involving bottom and charm quark, such as, bd, bs, cc, cu , and bb for $\mathcal{Z}_2 \times \mathcal{Z}_5$ as well as $\mathcal{Z}_2 \times \mathcal{Z}_9$ symmetries, even beyond the top-threshold. Among the leptonic decay modes, the decay channels involving at least one τ dominate for all $\mathcal{Z}_N \times \mathcal{Z}_M$ flavour symmetries.

At $m_a > m_t$, in contrast to the other three $\mathcal{Z}_N \times \mathcal{Z}_M$ flavour symmetries, the $\mathcal{Z}_8 \times \mathcal{Z}_{22}$ model exhibits a dominant decay of the flavon into top quark pairs ($t\bar{t}$), as shown by the dashed-blue line in figure 17e. This

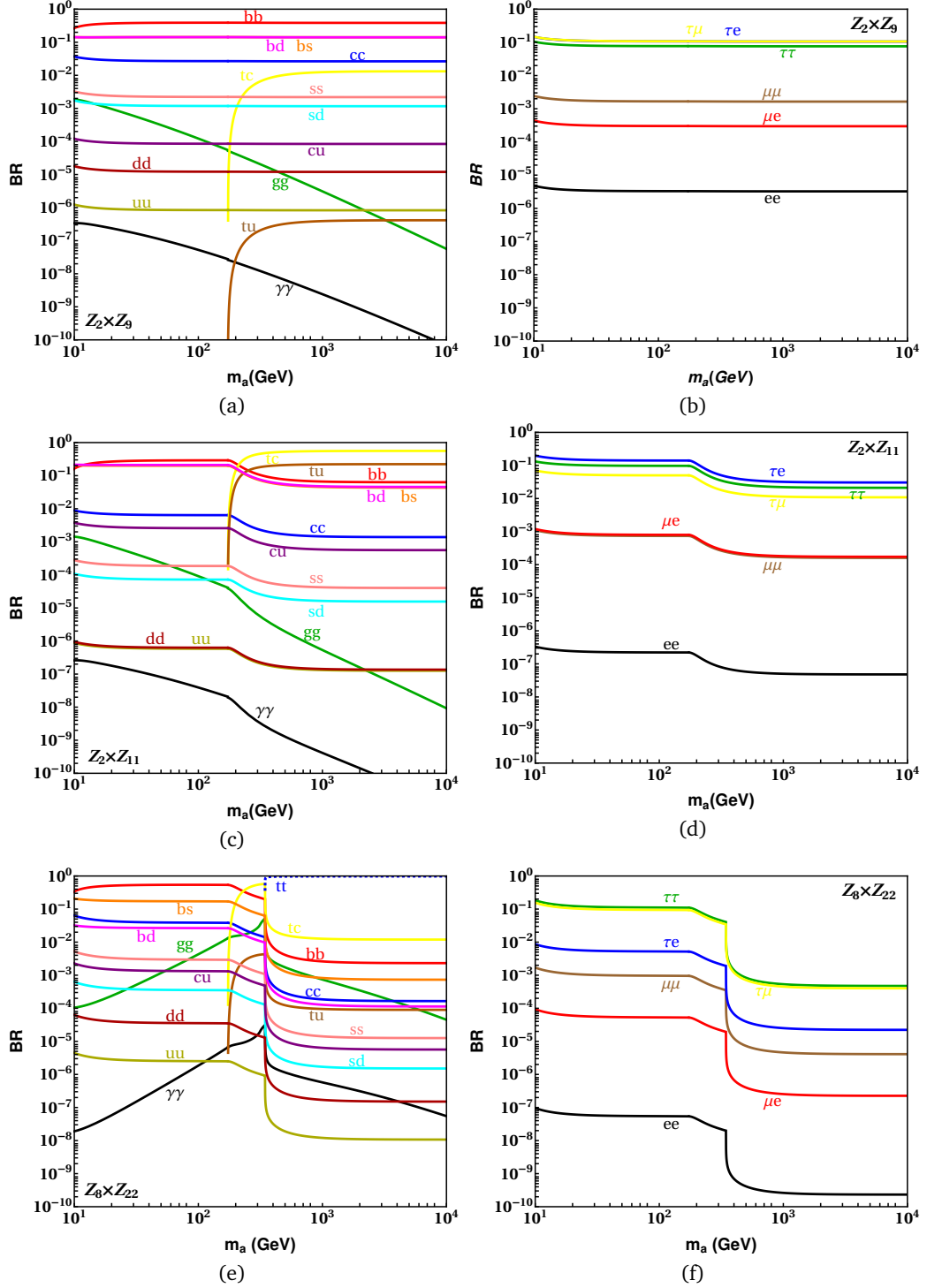


Figure 17: Branching ratios of the various possible decay modes of the flavon into quark and lepton pairs for $Z_2 \times Z_9$, $Z_2 \times Z_{11}$, and $Z_8 \times Z_{22}$ flavour symmetries.

striking feature arises from the construction of the $Z_8 \times Z_{22}$ model, where the top quark couples to the flavon with a suppression factor of order ϵ . Notably, this feature is absent in the remaining three $Z_N \times Z_M$ symmetry-based models under investigation. This feature keeps apart the $Z_8 \times Z_{22}$ based model from the other models in

terms of collider signatures, which are discussed in the later part of this work.

6.2 Top quark decays to flavon

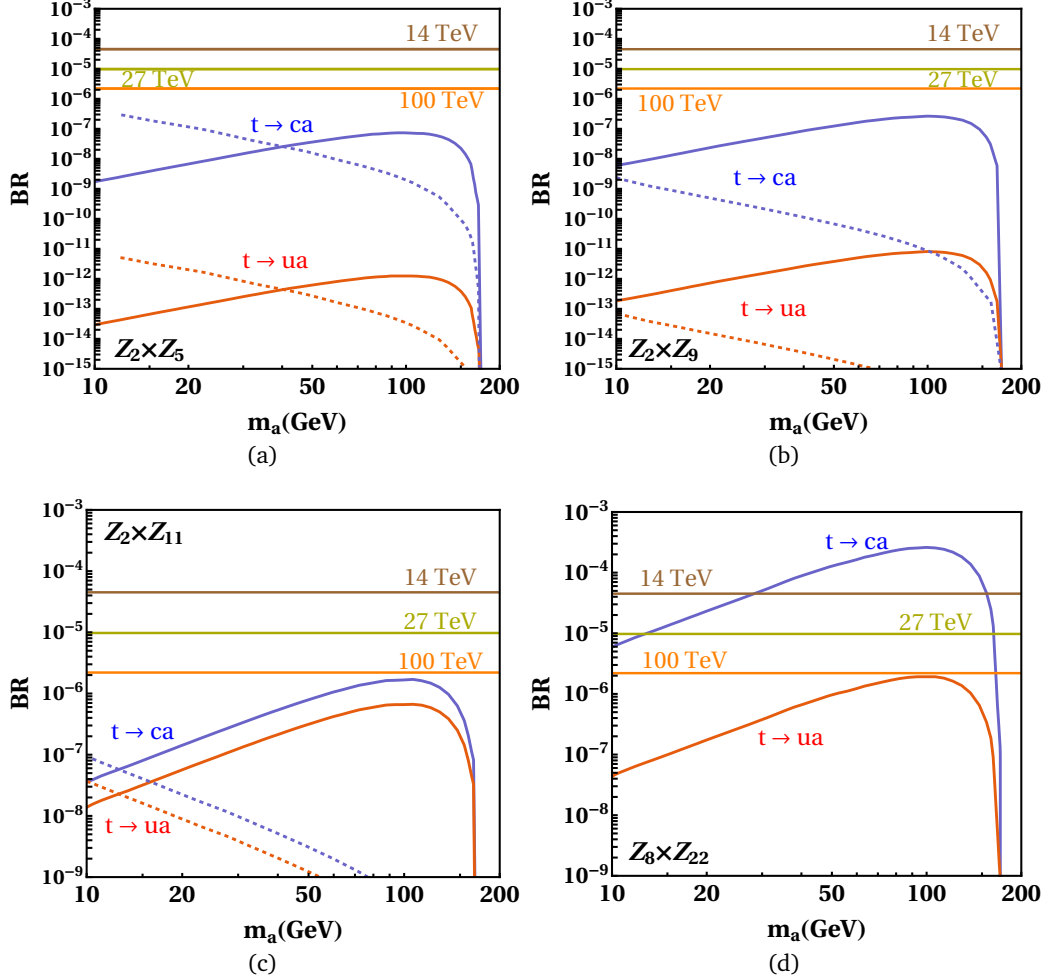


Figure 18: The branching ratios of top quark decays into flavon of $\mathcal{Z}_N \times \mathcal{Z}_M$ flavour symmetries as a function of the flavon mass (m_a) along the parameter space allowed by the observable $R_{\mu\mu}$ in the phase-II of the LHCb for soft-symmetry breaking scenario, and $BR(K_L \rightarrow \mu^+ \mu^-)$ for symmetry-conserving scenario.

The top quark decays to flavon play an important role in constraining a low-mass flavon. For the flavon mass, which is less than the mass of the top quark, anomalous top decays $t \rightarrow ac(au)$ provide distinguished signatures of flavon at hadron colliders. For Higgs production via such anomalous top-quark decays, the limits for the expected reach of the current 14 TeV LHC, HE-LHC, as well as a future high luminosity 100 TeV hadron collider are known, which can also be utilized for the flavon production. The current and expected limits on such processes at the LHC and a 100 TeV hadron collider are [126, 34],

$$\begin{aligned}
 BR_{8 \text{ TeV}}(t \rightarrow Hc) &< 5.6 \cdot 10^{-3}, \\
 BR_{14 \text{ TeV}, 3 \text{ ab}^{-1}}(t \rightarrow Hc) &< 4.5 \cdot 10^{-5}, \\
 BR_{27 \text{ TeV}, 15 \text{ ab}^{-1}}(t \rightarrow Hc) &< 9.7 \cdot 10^{-6}, \\
 BR_{100 \text{ TeV}, 30 \text{ ab}^{-1}}(t \rightarrow Hc) &< 2.2 \cdot 10^{-6}.
 \end{aligned} \tag{80}$$

In figure 18, we show the predictions of branching ratios for decays $t \rightarrow (c, u)a$ in the framework of different $\mathcal{Z}_N \times \mathcal{Z}_M$ flavour symmetries. We note that in the case of the soft symmetry-breaking scenario, shown by the solid continuous curves, the top decays to the flavon are investigated along the boundaries of parameter space allowed by the observable $R_{\mu\mu}$ in the phase-II of the LHCb, shown in figure 7c. With mass range m_a lying between 10 up to 200 GeV, the corresponding ranges for the VEV of the flavon f varies approximately as $\sim (2 \times 10^3, 4 \times 10^4)$ GeV for $\mathcal{Z}_2 \times \mathcal{Z}_5$, $\sim (10^3, 2 \times 10^4)$ GeV for $\mathcal{Z}_2 \times \mathcal{Z}_9$, $\sim (9 \times 10^3 - 1.4 \times 10^5)$ GeV for $\mathcal{Z}_2 \times \mathcal{Z}_{11}$, and $\sim (4 \times 10^2 - 10^4)$ GeV for $\mathcal{Z}_8 \times \mathcal{Z}_{22}$ flavour symmetry. We observe that only the flavon of the $\mathcal{Z}_8 \times \mathcal{Z}_{22}$ has the potential to reach the sensitivity of the 14 TeV LHC, the HE-LHC, and a 100 TeV future hadron collider. This prediction is very specific to test the $\mathcal{Z}_8 \times \mathcal{Z}_{22}$ flavour symmetry.

For the symmetry-conserving scenario, represented by the dashed curves in figure 18, we analyze $t \rightarrow (c, u)a$ decays along the parameter space allowed by the observable $BR(K_L \rightarrow \mu^+ \mu^-)$, where VEV f ranges approximately as $\sim (3 \times 10^3, 6 \times 10^4)$ GeV for $\mathcal{Z}_2 \times \mathcal{Z}_5$, $\sim (4 \times 10^4, 9 \times 10^5)$ GeV for $\mathcal{Z}_2 \times \mathcal{Z}_9$, and $\sim (1.2 \times 10^5, 2 \times 10^6)$ GeV for $\mathcal{Z}_2 \times \mathcal{Z}_{11}$ flavour symmetry. It turns out that the decays $t \rightarrow ac(au)$ in the case of symmetry-conserving scenario for a light flavon are beyond the reach of the LHC, the HE-LHC, and a future 100 TeV hadron collider.

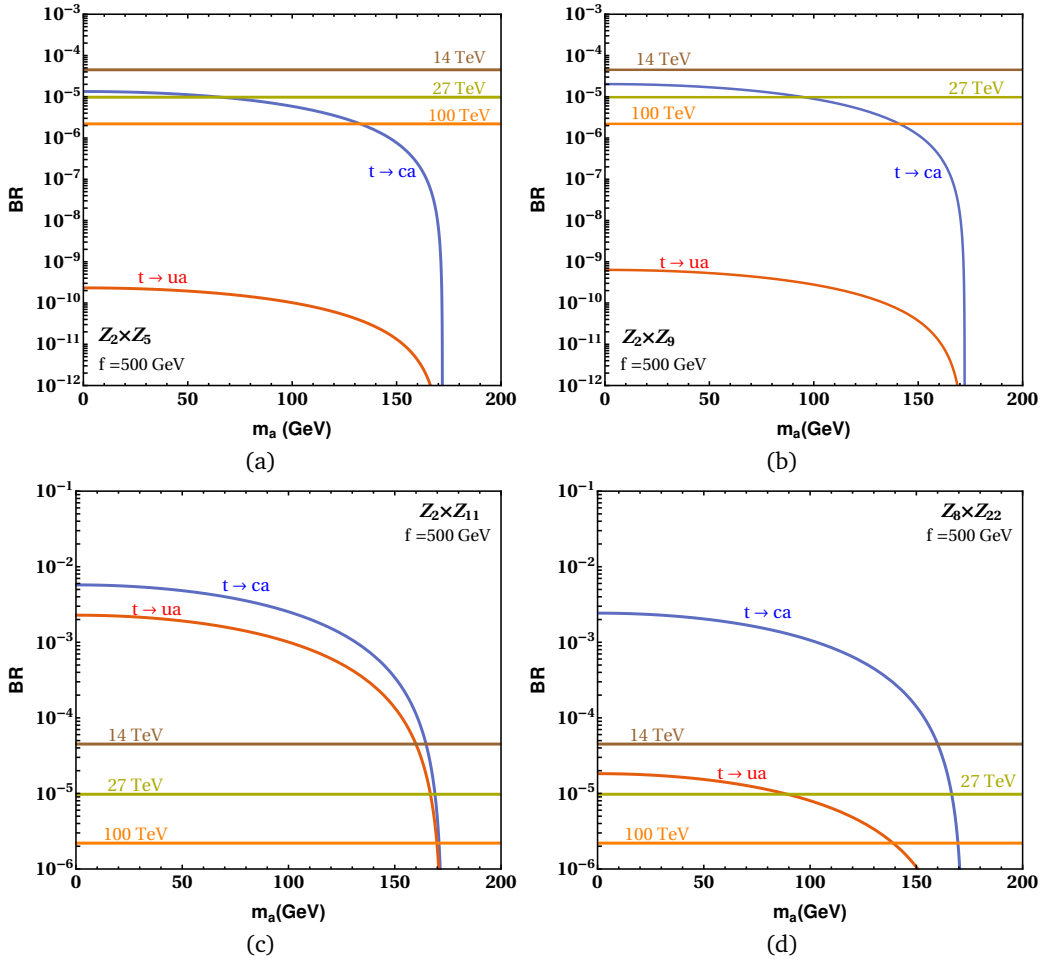


Figure 19: Branching ratios of top quark decays into flavon of $\mathcal{Z}_2 \times \mathcal{Z}_5$, $\mathcal{Z}_2 \times \mathcal{Z}_9$, $\mathcal{Z}_2 \times \mathcal{Z}_{11}$ and $\mathcal{Z}_8 \times \mathcal{Z}_{22}$ flavour symmetries as a function of m_a for a fixed value of the VEV $f = 500$ GeV.

In figure 19, we show the prediction of branching ratios of decays $t \rightarrow (c, u)a$ for different $\mathcal{Z}_N \times \mathcal{Z}_M$ flavour symmetries for the flavon VEV $f = 500$ GeV in the soft symmetry-breaking case. This is a conventional choice in literature [34]. In this scenario, the branching ratio of the decay $t \rightarrow ca$ is accessible to a future 100 TeV hadron collider in a certain mass range for all $\mathcal{Z}_N \times \mathcal{Z}_M$ flavour symmetries discussed in this work. For the symmetries

$\mathcal{Z}_2 \times \mathcal{Z}_{5,9}$, the branching ratio of the decay $t \rightarrow ca$ is of the order $10^{-6} - 10^{-5}$ for $m_a \leq 150$ GeV. The branching ratio of the decay $t \rightarrow ca$ is larger, and is maximally of the order of 10^{-3} for the $\mathcal{Z}_2 \times \mathcal{Z}_{11}$ and $\mathcal{Z}_8 \times \mathcal{Z}_{22}$ flavour symmetries.

The decay $t \rightarrow ca$ can be within the limits of the LHC, HE-LHC and a 100 TeV future hadron collider for the $\mathcal{Z}_2 \times \mathcal{Z}_{11}$ and $\mathcal{Z}_8 \times \mathcal{Z}_{22}$ flavour symmetries. This is a remarkable prediction of this work. The decay $t \rightarrow ca$ is within the reach of the limits of the HE-LHC for the $\mathcal{Z}_2 \times \mathcal{Z}_{5,9}$ flavour symmetries. We notice another important prediction of this work for the branching ratio of the decay $t \rightarrow ua$, which is in the reach of LHC, HE-LHC and a 100 TeV collider only for the $\mathcal{Z}_2 \times \mathcal{Z}_{11}$ flavour symmetry. This decay is accessible to the HE-LHC only for the $\mathcal{Z}_8 \times \mathcal{Z}_{22}$ flavour symmetry. Thus, we conclude that the decays $t \rightarrow (c, u)a$ can be a good test ground for different $\mathcal{Z}_N \times \mathcal{Z}_M$ flavour symmetries for a low mass flavon.

The limits in equation 80 can be used to place bounds on the parameter space of the flavon of the $\mathcal{Z}_N \times \mathcal{Z}_M$ flavour symmetries, as shown in figure 20. We must note that dashed straight lines denote our predictions for the symmetry-conserving scenarios, which are beyond the reach of the sensitivities given in equation 80.

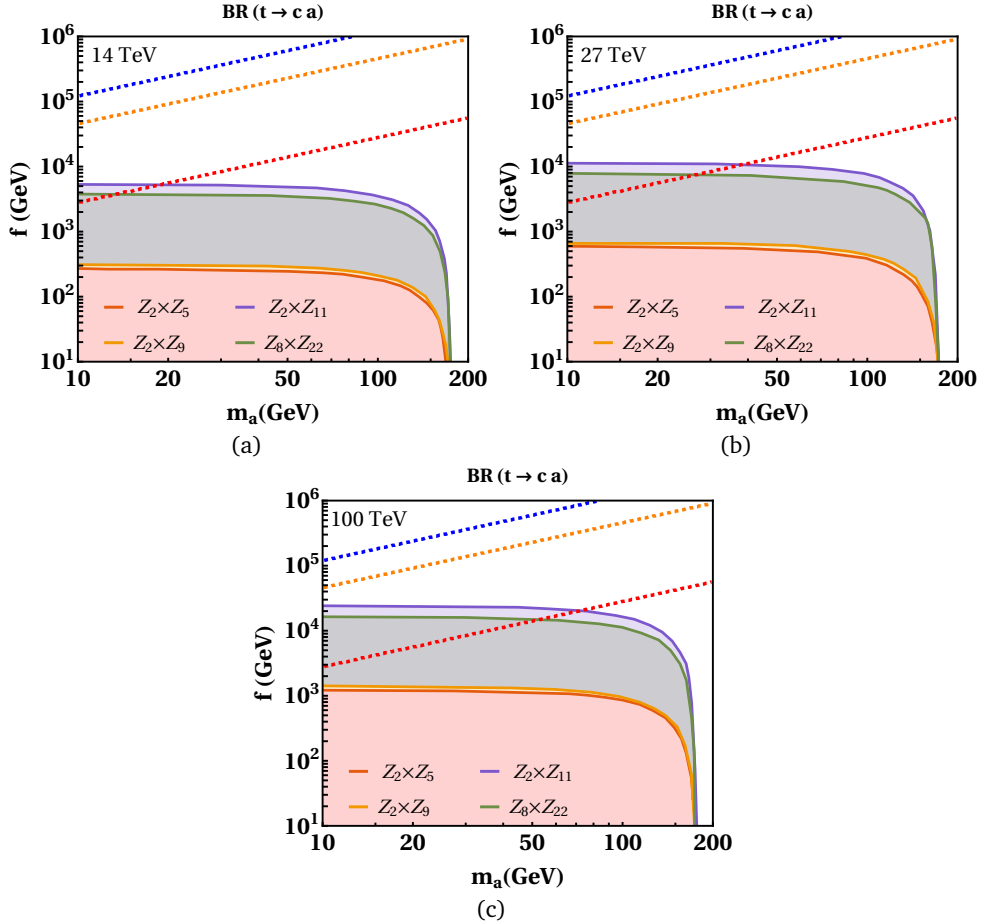


Figure 20: The parameter space excluded by the limits on $BR(t \rightarrow Hc)$ from 14 TeV LHC, 27 TeV HE-LHC, and a 100 TeV collider for $\mathcal{Z}_2 \times \mathcal{Z}_5$, $\mathcal{Z}_2 \times \mathcal{Z}_9$, $\mathcal{Z}_2 \times \mathcal{Z}_{11}$ and $\mathcal{Z}_8 \times \mathcal{Z}_{22}$ flavour symmetries in the soft symmetry-breaking scenario is shown with the coloured regions. The dashed lines represents the allowed parameter space in the symmetry-conserving scenario.

6.3 Flavon production at the LHC, HE-LHC, and a 100 TeV hadron collider

We now discuss the production of the flavon of the $\mathcal{Z}_N \times \mathcal{Z}_M$ flavour symmetries at the LHC, HE-LHC, and at a 100 TeV future hadron collider. The analytical results for the production cross-sections of the flavon in various

channels have been derived using the MSTW2008 PDF [127]. Additionally, FeynRules [128] has been utilized to produce the model UFO files for all four $\mathcal{Z}_N \times \mathcal{Z}_M$ flavour symmetries discussed in this work. We used these files to perform production cross-section calculations with MadGraph [129], and verify our analytical results.

The inclusive production cross-sections of flavon of the $\mathcal{Z}_N \times \mathcal{Z}_M$ flavour symmetries at the LHC, HE-LHC, and at a 100 TeV future hadron collider are shown in figures 21 and 22 for the $\mathcal{Z}_2 \times \mathcal{Z}_{5,9,11}$ and the $\mathcal{Z}_8 \times \mathcal{Z}_{22}$ flavour symmetries. For the soft symmetry-breaking scenario, the boundaries of parameter space allowed by the observable $R_{\mu\mu}$ in the phase-II of the LHCb, shown in figure 7c, are used. The dashed curves are the cross-sections for the symmetry-conserving scenarios using the parameter space allowed by the observable $BR(K_L \rightarrow \mu^+ \mu^-)$.

In the soft symmetry-breaking scenario, the observable $R_{\mu\mu}$ allows the mass range m_a lying between 10 up to 10^4 GeV, the corresponding ranges for the VEV of the flavon f vary approximately as $\sim (3 \times 10^2, 4 \times 10^4)$ GeV for $\mathcal{Z}_2 \times \mathcal{Z}_5$, $\sim (6 \times 10^2, 2.6 \times 10^4)$ GeV for $\mathcal{Z}_2 \times \mathcal{Z}_9$, $\sim (7.8 \times 10^2, 1.4 \times 10^5)$ GeV for $\mathcal{Z}_2 \times \mathcal{Z}_{11}$, and $\sim (3.6 \times 10^2, 10^4)$ GeV for $\mathcal{Z}_8 \times \mathcal{Z}_{22}$ flavour symmetry. For the symmetry-conserving scenario, we analyze flavon production channels with the parameter space allowed the observable $BR(K_L \rightarrow \mu^+ \mu^-)$, where VEV f ranges approximately as $\sim (3 \times 10^3, 3 \times 10^6)$ GeV for $\mathcal{Z}_2 \times \mathcal{Z}_5$, $\sim (4 \times 10^4, 4 \times 10^7)$ GeV for $\mathcal{Z}_2 \times \mathcal{Z}_9$, and $\sim (10^5, 9 \times 10^7)$ GeV for $\mathcal{Z}_2 \times \mathcal{Z}_{11}$ flavour symmetry.

6.3.1 Inclusive production

A flavon can be produced through the inclusive channels,

$$gg, b\bar{b} \rightarrow a. \quad (81)$$

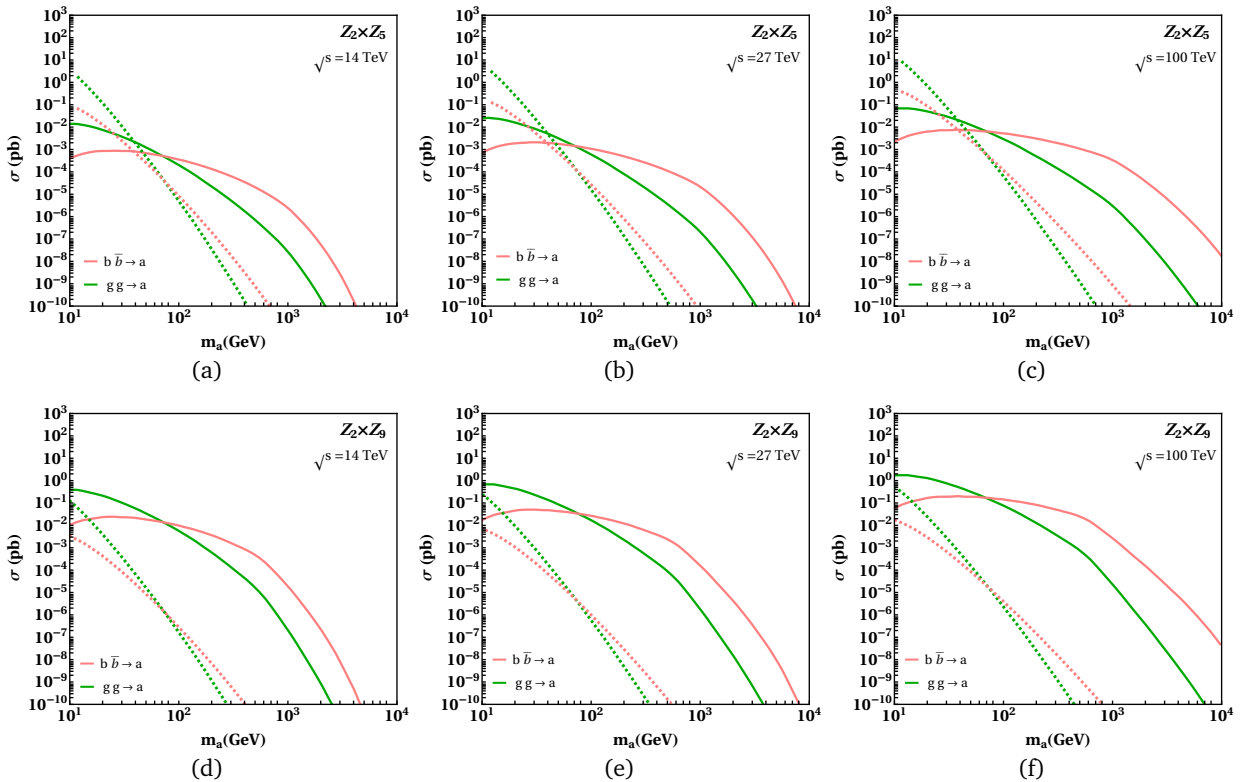


Figure 21: Production cross-sections of the flavon of $\mathcal{Z}_2 \times \mathcal{Z}_5$, $\mathcal{Z}_2 \times \mathcal{Z}_9$ flavour symmetries with respect to its mass through different channels for the 14 TeV HL-LHC, 27 TeV HE-LHC, and future 100 TeV hadron collider. The solid lines represents the production cross section along the boundaries of parameter space allowed by the observable $R_{\mu\mu}$ for soft symmetry-breaking scenario, while the dashed lines correspond to that in the symmetry-conserving scenario along the allowed parameter space by the observable $BR(K_L \rightarrow \mu\mu)_{SD}$.

As it can be noted from figure 21 and 22, the gluon-fusion production cross-sections for the soft symmetry-breaking scenario, is very small for the $\mathcal{Z}_2 \times \mathcal{Z}_{5,9,11}$ flavour symmetries due to the absence of the flavour-diagonal coupling of the flavon to top quarks. However, this observation dramatically changes for the $\mathcal{Z}_8 \times \mathcal{Z}_{22}$ flavour symmetry, where the flavour-diagonal coupling of the flavon to top quarks is allowed. This can be seen in figures 22d-22f. In the case of symmetry-conserving scenario, the gluon-fusion production cross-section turns out to be very small and, as will be shown later, is beyond the reach of the LHC, HE-LHC, and a 100 TeV future collider.

In figures 23 and 24, we show the production cross-sections of the flavon of different $\mathcal{Z}_N \times \mathcal{Z}_M$ flavour symmetries for the VEV $f = 500$ GeV for the soft symmetry-breaking scenario. In this scenario, the production cross-sections can be sufficiently large for the $\mathcal{Z}_2 \times \mathcal{Z}_{5,9,11}$ and $\mathcal{Z}_8 \times \mathcal{Z}_{22}$ flavour symmetries. Therefore, our investigation of the inclusive modes will be performed only for this choice from now on for the heavy mass flavon.

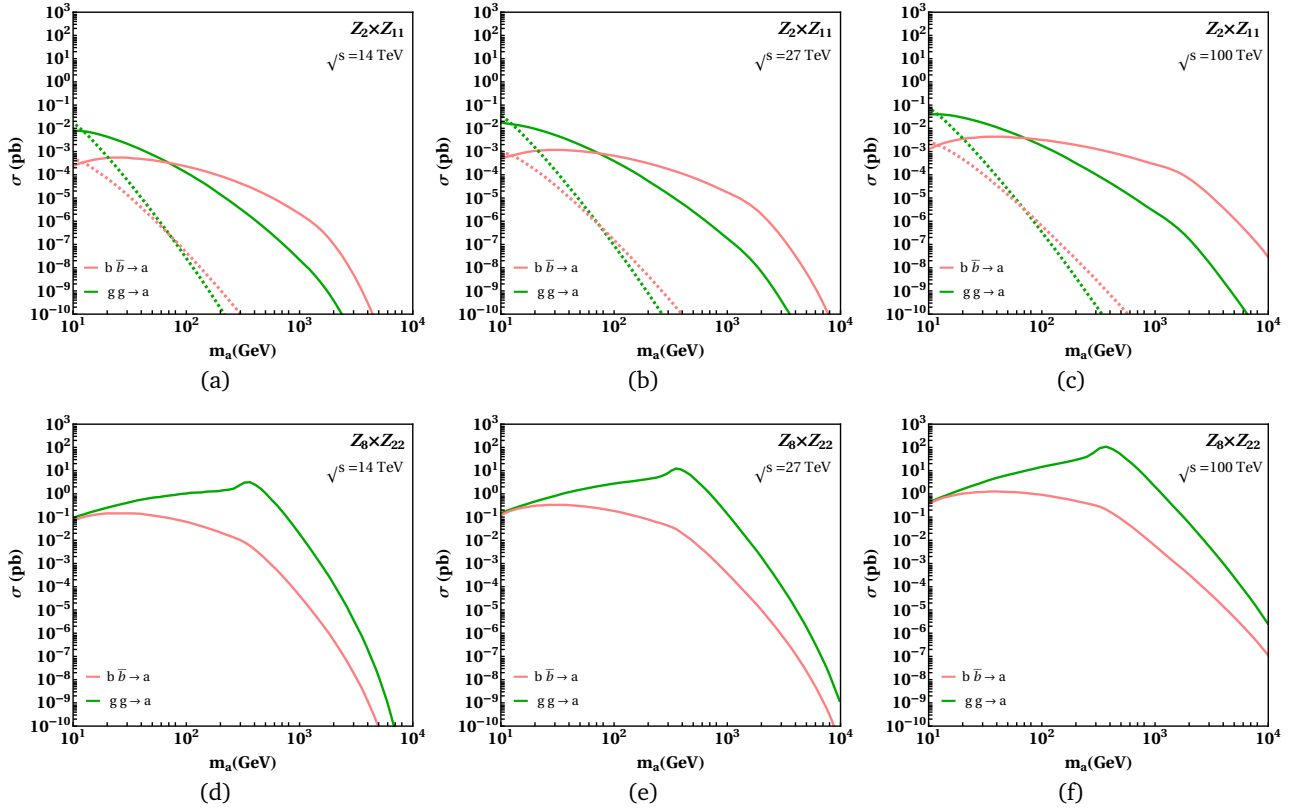


Figure 22: Production cross-sections of the flavon of $\mathcal{Z}_2 \times \mathcal{Z}_{11}$, and $\mathcal{Z}_8 \times \mathcal{Z}_{22}$ flavour symmetries with respect to its mass through different channels for the 14 TeV HL-LHC, 27 TeV HE-LHC, and future 100 TeV hadron collider. The solid lines represents the production cross section along the boundaries of parameter space allowed by the observable $R_{\mu\mu}$ for soft symmetry-breaking scenario, while the dashed lines correspond to that in the symmetry-conserving scenario along the allowed parameter space by the observable $BR(K_L \rightarrow \mu\mu)_{SD}$.

The above results can be used to look for resonance searches of the flavon. For example, a generic search is of the type,

$$pp \rightarrow a \rightarrow b\bar{b}/\ell_i\bar{\ell}_i/\gamma\gamma. \quad (82)$$

On the other side, due to the off-diagonal flavon couplings of flavon to a fermionic pair, searches with a specific signature of the $\mathcal{Z}_N \times \mathcal{Z}_M$ flavour symmetries are,

$$pp \rightarrow a \rightarrow t\bar{c}/t\bar{u}. \quad (83)$$

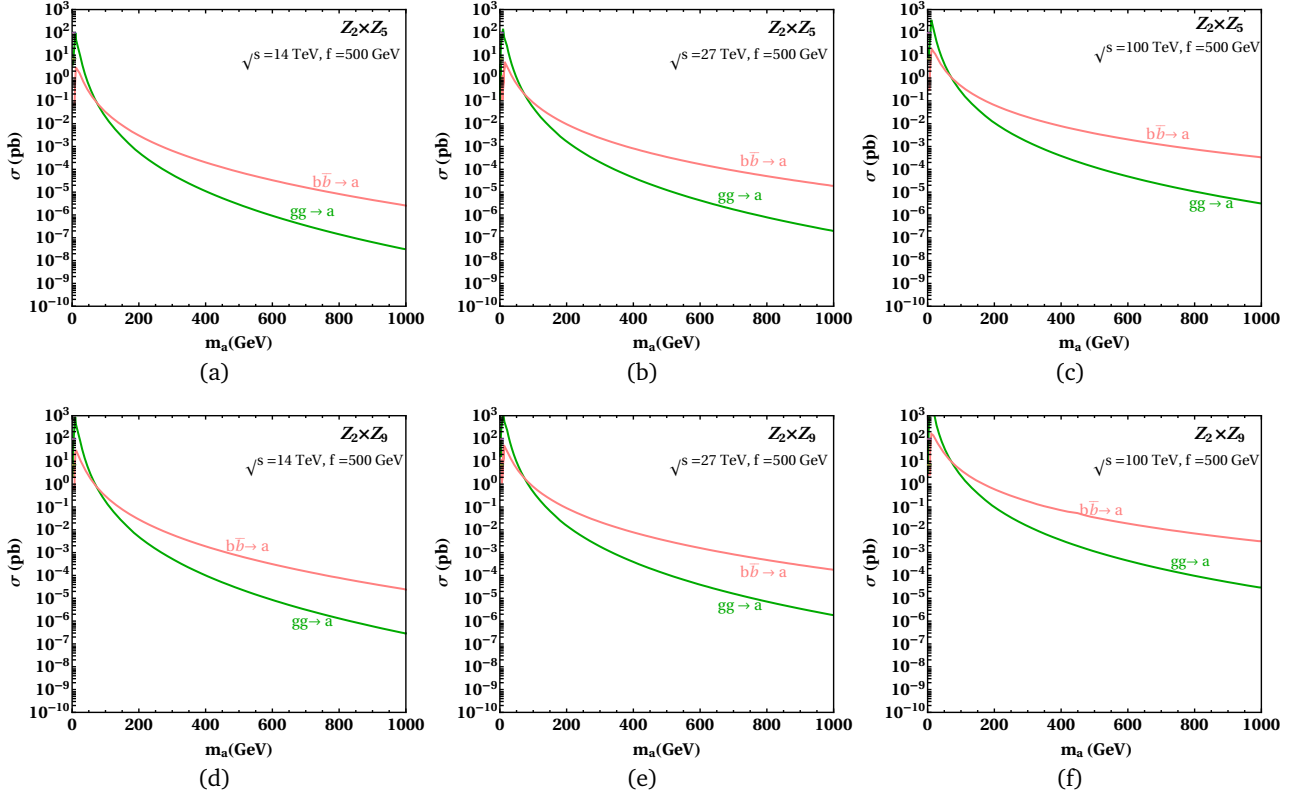


Figure 23: Production cross-sections of the flavon of $Z_2 \times Z_5$, and $Z_2 \times Z_9$ flavour symmetries with respect to its mass through different channels for 14 TeV HL-LHC, 27 TeV HE-LHC, and future 100 TeV hadron collider, where the flavon VEV $f = 500$ GeV.

m_a [GeV]	$\mathcal{L}[fb^{-1}]$ [References]		ATLAS 13 TeV		CMS 13 TeV	
	ATLAS	CMS	500	1000	500	1000
jet-jet [pb]	139 [130]	137 [131]		0.1		0.2
$\tau\tau$ [pb]	36.1 [132]	35.9 [133]	$8 \cdot 10^{-2}$	10^{-2}	$6 \cdot 10^{-2}$	10^{-2}
$ee, \mu\mu$ [pb]	139 [134]	140 [135]	$8 \cdot 10^{-4}$	$2 \cdot 10^{-4}$	$2 \cdot 10^{-3}$	$4 \cdot 10^{-4}$
μe [pb]	138 [136]	139 [137]		$3 \cdot 10^{-4}$	$4 \cdot 10^{-3}$	$3 \cdot 10^{-4}$
$\mu\tau$ [pb]	138 [136]	139 [137]		$1 \cdot 10^{-3}$	$7 \cdot 10^{-3}$	$1 \cdot 10^{-3}$
$e\tau$ [pb]	138 [136]	139 [137]		$1 \cdot 10^{-3}$	$5 \cdot 10^{-3}$	$1 \cdot 10^{-3}$
$b\bar{b}$ [pb]	139 [130]	138 [138]		$1 \cdot 10^{-2}$		$4 \cdot 10^{-2}$
$\gamma\gamma$ [pb]	139 [124]	35.9 [125]	$5 \cdot 10^{-4}$	$1 \cdot 10^{-4}$	$4 \cdot 10^{-3}$	$8 \cdot 10^{-4}$
$t\bar{t}$ [pb]	36.1 [139, 140]	35.9 [141]	$2 \cdot 10^2$	2	30	0.4

Table 11: Current limits for production cross section times branching ratio ($\sigma \times BR$) at 13 TeV LHC by ATLAS and CMS in high mass resonance searches for inclusive flavon production channels.

In table 11, we show the present sensitivities of different inclusive flavon production channels at the 14 TeV LHC. These results will be used to estimate the sensitivities of the HL-LHC, HE-LHC, and a 100 TeV collider for a heavy flavon production and decay. We show these sensitivities in table 12. These sensitivities are estimated using simple square root scaling of the luminosity of the LHC by,

$$S \simeq \frac{S}{\sqrt{B}} \simeq \sqrt{\mathcal{L}} \frac{\sigma_s}{\sqrt{\sigma_B}}, \quad (84)$$

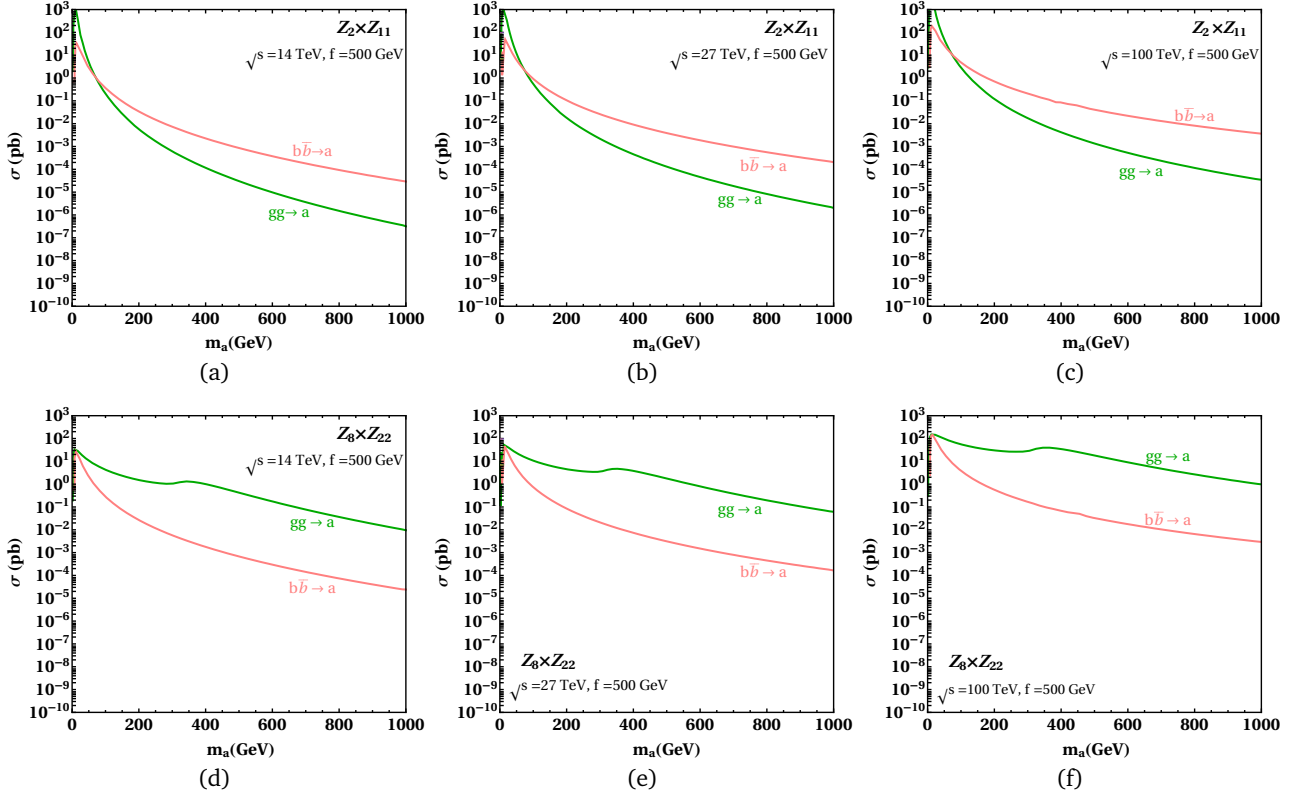


Figure 24: Production cross-sections of the flavon of $\mathcal{Z}_2 \times \mathcal{Z}_{11}$, and $\mathcal{Z}_8 \times \mathcal{Z}_{22}$ flavour symmetries with respect to its mass through different channels for 14 TeV HL-LHC, 27 TeV HE-LHC, and future 100 TeV high-luminosity hadron collider, where the flavon VEV $f = 500$ GeV.

where S is the number of signal events, B denotes the background events, σ_s is the signal cross-section, and σ_B stands for the background cross-section.

m_a [GeV]	HL-LHC [14 TeV, 3 ab^{-1}]		HE-LHC [27 TeV, 15 ab^{-1}]		100 TeV, 30 ab^{-1}	
	500	1000	500	1000	500	1000
jet-jet [pb]		$4 \cdot 10^{-2}$		$3 \cdot 10^{-2}$		$4 \cdot 10^{-2}$
$\tau\tau$ [pb]	$7 \cdot 10^{-3}$	$1 \cdot 10^{-3}$	$4 \cdot 10^{-3}$	$7 \cdot 10^{-4}$	$5 \cdot 10^{-3}$	$8 \cdot 10^{-4}$
$ee, \mu\mu$ [pb]	$2 \cdot 10^{-4}$	$4 \cdot 10^{-5}$	$1 \cdot 10^{-4}$	$3 \cdot 10^{-5}$	$1 \cdot 10^{-4}$	$3 \cdot 10^{-5}$
μe [pb]	$9 \cdot 10^{-4}$	$7 \cdot 10^{-5}$	$7 \cdot 10^{-4}$	$5 \cdot 10^{-5}$	$1 \cdot 10^{-3}$	$1 \cdot 10^{-4}$
$\mu\tau$ [pb]	$2 \cdot 10^{-3}$	$2 \cdot 10^{-4}$	$1 \cdot 10^{-3}$	$2 \cdot 10^{-4}$	$2 \cdot 10^{-3}$	$3 \cdot 10^{-4}$
$e\tau$ [pb]	$1 \cdot 10^{-3}$	$2 \cdot 10^{-4}$	$8 \cdot 10^{-4}$	$2 \cdot 10^{-4}$	$1 \cdot 10^{-3}$	$3 \cdot 10^{-4}$
$b\bar{b}$ [pb]		$9 \cdot 10^{-3}$		$5 \cdot 10^{-3}$		$7 \cdot 10^{-3}$
$\gamma\gamma$ [pb]	$1 \cdot 10^{-4}$	$2 \cdot 10^{-5}$	$6 \cdot 10^{-5}$	$1 \cdot 10^{-5}$	$7 \cdot 10^{-5}$	$1 \cdot 10^{-5}$
$t\bar{t}$ [pb]	4	$5 \cdot 10^{-2}$	3	$4 \cdot 10^{-2}$	8	0.1

Table 12: Estimated reach ($\sigma \times BR$) of the HL-LHC, HE-LHC and a 100 TeV hadron collider for high flavon mass (m_a) in inclusive flavon production channels.

We show our benchmark predictions for the processes given in table 11, for different $\mathcal{Z}_N \times \mathcal{Z}_M$ flavour symmetries in tables 13- 15 for $f = 500$ GeV and $m_a = 500, 1000$ for the soft symmetry-breaking scenarios. The modes that are accessible to the HL-LHC, HE-LHC, and a 100 TeV collider are marked with a box \square .

From table 13, we observe that only the $\mathcal{Z}_2 \times \mathcal{Z}_5$ and the $\mathcal{Z}_8 \times \mathcal{Z}_{22}$ flavour symmetries are accessible to the HL-LHC, and both the symmetries can be differentiated due to the distinct accessible processes. This situation changes sufficiently for the HE-LHC as shown in table 14, as more processes are under the reach of the HE-LHC. However, even now, mainly the $\mathcal{Z}_2 \times \mathcal{Z}_5$ and the $\mathcal{Z}_8 \times \mathcal{Z}_{22}$ flavour symmetries are under the reach of the HE-LHC. The $\mathcal{Z}_2 \times \mathcal{Z}_9$ flavour symmetry can be probed through the $e\tau$ channel.

m_a [GeV]	Benchmark $\mathcal{Z}_2 \times \mathcal{Z}_5$		Benchmark $\mathcal{Z}_2 \times \mathcal{Z}_9$		Benchmark $\mathcal{Z}_2 \times \mathcal{Z}_{11}$		Benchmark $\mathcal{Z}_8 \times \mathcal{Z}_{22}$	
	500	1000	500	1000	500	1000	500	1000
jet-jet [pb]		$3.6 \cdot 10^{-2}$		$1.5 \cdot 10^{-6}$		$2.3 \cdot 10^{-7}$		$1.4 \cdot 10^{-3}$
$\tau\tau$ [pb]	$1.2 \cdot 10^{-3}$	$9.2 \cdot 10^{-5}$	$8.0 \cdot 10^{-5}$	$3.4 \cdot 10^{-6}$	$2.9 \cdot 10^{-5}$	$1.6 \cdot 10^{-6}$	$3.4 \cdot 10^{-3}$	$6.1 \cdot 10^{-5}$
$\mu\tau$ [pb]	$1.4 \cdot 10^{-3}$	$1.1 \cdot 10^{-4}$	$2.3 \cdot 10^{-4}$	$9.5 \cdot 10^{-6}$	$3 \cdot 10^{-5}$	$1.7 \cdot 10^{-6}$	$5.8 \cdot 10^{-3}$	$1 \cdot 10^{-4}$
$e\tau$ [pb]	$1.1 \cdot 10^{-3}$	$8.9 \cdot 10^{-5}$	$2.2 \cdot 10^{-4}$	$9.4 \cdot 10^{-6}$	$8.5 \cdot 10^{-5}$	$4.7 \cdot 10^{-6}$	$3.2 \cdot 10^{-4}$	$5.8 \cdot 10^{-6}$
$\mu\mu$ [pb]	$1.1 \cdot 10^{-6}$	$8.3 \cdot 10^{-8}$	$1.7 \cdot 10^{-6}$	$7.3 \cdot 10^{-8}$	$2.2 \cdot 10^{-7}$	$1.2 \cdot 10^{-8}$	$2.9 \cdot 10^{-5}$	$5.3 \cdot 10^{-7}$
μe [pb]	$2.9 \cdot 10^{-6}$	$2.3 \cdot 10^{-7}$	$6.3 \cdot 10^{-7}$	$2.6 \cdot 10^{-8}$	$4.8 \cdot 10^{-7}$	$2.7 \cdot 10^{-8}$	$3.3 \cdot 10^{-6}$	$5.8 \cdot 10^{-8}$
ee [pb]	$2.5 \cdot 10^{-10}$	$2 \cdot 10^{-11}$	$3.4 \cdot 10^{-9}$	$1.4 \cdot 10^{-10}$	$6.7 \cdot 10^{-11}$	$3.7 \cdot 10^{-12}$	$1.7 \cdot 10^{-9}$	$3 \cdot 10^{-11}$
$\gamma\gamma$ [pb]	$1.3 \cdot 10^{-7}$	$3.6 \cdot 10^{-9}$	$8.2 \cdot 10^{-10}$	$1.2 \cdot 10^{-11}$	$1.5 \cdot 10^{-10}$	$3 \cdot 10^{-12}$	$6.6 \cdot 10^{-4}$	$1 \cdot 10^{-5}$
$b\bar{b}$ [pb]	$9.8 \cdot 10^{-3}$	$6.3 \cdot 10^{-4}$	$4.7 \cdot 10^{-4}$	$1.9 \cdot 10^{-5}$	$1.2 \cdot 10^{-4}$	$5.7 \cdot 10^{-6}$	$1.9 \cdot 10^{-2}$	$3.2 \cdot 10^{-4}$
tc [pb]	$3.6 \cdot 10^{-3}$	$2.8 \cdot 10^{-4}$	$2.5 \cdot 10^{-5}$	$1.2 \cdot 10^{-6}$	$1.5 \cdot 10^{-3}$	$8.5 \cdot 10^{-5}$	0.152	$3.1 \cdot 10^{-3}$
tu [pb]	$6.5 \cdot 10^{-8}$	$5.1 \cdot 10^{-9}$	$7.8 \cdot 10^{-10}$	$3.8 \cdot 10^{-11}$	$6.6 \cdot 10^{-4}$	$3.8 \cdot 10^{-5}$	$1.1 \cdot 10^{-3}$	$2.3 \cdot 10^{-5}$
$t\bar{t}$ [pb]							4.42	0.12

Table 13: Benchmark points for different $\mathcal{Z}_N \times \mathcal{Z}_M$ flavour symmetries for inclusive flavon production channels with high flavon mass (m_a) in case of the soft symmetry-breaking scenario at the 14 TeV HL-LHC, assuming $\text{VEV}(f) = 500$ GeV. Accessible channels are represented within the box.

m_a [GeV]	Benchmark $\mathcal{Z}_2 \times \mathcal{Z}_5$		Benchmark $\mathcal{Z}_2 \times \mathcal{Z}_9$		Benchmark $\mathcal{Z}_2 \times \mathcal{Z}_{11}$		Benchmark $\mathcal{Z}_8 \times \mathcal{Z}_{22}$	
	500	1000	500	1000	500	1000	500	1000
jet-jet [pb]		0.133		$8.2 \cdot 10^{-6}$		$9.4 \cdot 10^{-7}$		$9.8 \cdot 10^{-3}$
$\tau\tau$ [pb]	$2.6 \cdot 10^{-3}$	$2.8 \cdot 10^{-4}$	$2.9 \cdot 10^{-4}$	$1.7 \cdot 10^{-5}$	$8 \cdot 10^{-5}$	$5.6 \cdot 10^{-6}$	$1.5 \cdot 10^{-2}$	$4 \cdot 10^{-4}$
$\mu\tau$ [pb]	$3.2 \cdot 10^{-3}$	$3.5 \cdot 10^{-4}$	$8.3 \cdot 10^{-4}$	$4.8 \cdot 10^{-5}$	$8.4 \cdot 10^{-5}$	$5.8 \cdot 10^{-6}$	$2.5 \cdot 10^{-2}$	$6.8 \cdot 10^{-4}$
$e\tau$ [pb]	$2.6 \cdot 10^{-3}$	$2.8 \cdot 10^{-4}$	$8.2 \cdot 10^{-4}$	$4.8 \cdot 10^{-5}$	$2.3 \cdot 10^{-4}$	$1.6 \cdot 10^{-5}$	$1.4 \cdot 10^{-3}$	$3.8 \cdot 10^{-5}$
$\mu\mu$ [pb]	$2.4 \cdot 10^{-6}$	$2.6 \cdot 10^{-7}$	$6.4 \cdot 10^{-6}$	$3.7 \cdot 10^{-7}$	$6.2 \cdot 10^{-7}$	$4.3 \cdot 10^{-8}$	$1.3 \cdot 10^{-4}$	$3.5 \cdot 10^{-6}$
μe [pb]	$6.6 \cdot 10^{-6}$	$7.1 \cdot 10^{-7}$	$2.3 \cdot 10^{-6}$	$1.4 \cdot 10^{-7}$	$1.3 \cdot 10^{-6}$	$9.3 \cdot 10^{-8}$	$1.4 \cdot 10^{-5}$	$3.8 \cdot 10^{-7}$
ee [pb]	$5.6 \cdot 10^{-10}$	$6.1 \cdot 10^{-11}$	$1.3 \cdot 10^{-8}$	$7.4 \cdot 10^{-10}$	$1.8 \cdot 10^{-10}$	$1.3 \cdot 10^{-11}$	$7.2 \cdot 10^{-9}$	$1.9 \cdot 10^{-10}$
$\gamma\gamma$ [pb]	$2.9 \cdot 10^{-7}$	$1.1 \cdot 10^{-8}$	$3 \cdot 10^{-9}$	$6.3 \cdot 10^{-11}$	$4.2 \cdot 10^{-10}$	$1.1 \cdot 10^{-11}$	$2.8 \cdot 10^{-3}$	$6.7 \cdot 10^{-5}$
$b\bar{b}$ [pb]	$2.7 \cdot 10^{-2}$	$2.3 \cdot 10^{-3}$	$1.9 \cdot 10^{-3}$	$1 \cdot 10^{-4}$	$3.8 \cdot 10^{-4}$	$2.3 \cdot 10^{-5}$	$8.8 \cdot 10^{-2}$	$2.2 \cdot 10^{-3}$
tc [pb]	$1 \cdot 10^{-2}$	$1 \cdot 10^{-3}$	$1 \cdot 10^{-4}$	$6.6 \cdot 10^{-6}$	$4.6 \cdot 10^{-3}$	$3.4 \cdot 10^{-4}$	0.702	$2.1 \cdot 10^{-2}$
tu [pb]	$1.8 \cdot 10^{-7}$	$1.9 \cdot 10^{-8}$	$3.1 \cdot 10^{-9}$	$2 \cdot 10^{-10}$	$2 \cdot 10^{-3}$	$1.5 \cdot 10^{-4}$	$5.3 \cdot 10^{-3}$	$1.6 \cdot 10^{-4}$
$t\bar{t}$ [pb]							20.46	0.83

Table 14: Benchmark points for different $\mathcal{Z}_N \times \mathcal{Z}_M$ flavour symmetries for inclusive flavon production channels with high flavon mass (m_a) in case of the soft symmetry-breaking scenario at the 27 TeV HE-LHC, assuming $f = 500$ GeV.

A 100 TeV collider provides a more dramatic scenario for the $\mathcal{Z}_N \times \mathcal{Z}_M$ flavour symmetries. As shown in table 15, all symmetries except the $\mathcal{Z}_2 \times \mathcal{Z}_{11}$ become sensitive in most of the inclusive processes. The $\mathcal{Z}_2 \times \mathcal{Z}_{11}$ flavour symmetry is accessible only through the $e\tau$ channel.

m_a [GeV]	Benchmark $\mathcal{Z}_2 \times \mathcal{Z}_5$		Benchmark $\mathcal{Z}_2 \times \mathcal{Z}_9$		Benchmark $\mathcal{Z}_2 \times \mathcal{Z}_{11}$		Benchmark $\mathcal{Z}_8 \times \mathcal{Z}_{22}$	
	500	1000	500	1000	500	1000	500	1000
jet-jet [pb]		0.95		$1.1 \cdot 10^{-4}$		$8.1 \cdot 10^{-6}$		0.18
$\tau\tau$ [pb]	$1.1 \cdot 10^{-2}$	$1.4 \cdot 10^{-3}$	$2.2 \cdot 10^{-3}$	$1.9 \cdot 10^{-4}$	$4.8 \cdot 10^{-4}$	$3.8 \cdot 10^{-5}$	0.14	$6.2 \cdot 10^{-3}$
$\mu\tau$ [pb]	$1.3 \cdot 10^{-2}$	$1.7 \cdot 10^{-3}$	$6.3 \cdot 10^{-3}$	$5.5 \cdot 10^{-4}$	$5 \cdot 10^{-4}$	$3.9 \cdot 10^{-5}$	0.23	$1.0 \cdot 10^{-2}$
$e\tau$ [pb]	$1.1 \cdot 10^{-2}$	$1.4 \cdot 10^{-3}$	$6.2 \cdot 10^{-3}$	$5.4 \cdot 10^{-4}$	$1.3 \cdot 10^{-3}$	$1.1 \cdot 10^{-4}$	$1.3 \cdot 10^{-2}$	$5.9 \cdot 10^{-4}$
$\mu\mu$ [pb]	$9.9 \cdot 10^{-5}$	$1.3 \cdot 10^{-6}$	$4.8 \cdot 10^{-5}$	$4.2 \cdot 10^{-6}$	$3.7 \cdot 10^{-6}$	$2.9 \cdot 10^{-7}$	$1.2 \cdot 10^{-3}$	$5.4 \cdot 10^{-5}$
μe [pb]	$2.8 \cdot 10^{-5}$	$3.5 \cdot 10^{-6}$	$1.7 \cdot 10^{-5}$	$1.5 \cdot 10^{-6}$	$8 \cdot 10^{-6}$	$6.3 \cdot 10^{-7}$	$1.3 \cdot 10^{-4}$	$5.9 \cdot 10^{-6}$
ee [pb]	$2.4 \cdot 10^{-9}$	$3.0 \cdot 10^{-10}$	$9.6 \cdot 10^{-8}$	$8.4 \cdot 10^{-9}$	$1.1 \cdot 10^{-9}$	$8.8 \cdot 10^{-11}$	$6.9 \cdot 10^{-8}$	$3.0 \cdot 10^{-9}$
$\gamma\gamma$ [pb]	$1.2 \cdot 10^{-6}$	$5.6 \cdot 10^{-8}$	$2.3 \cdot 10^{-8}$	$7.2 \cdot 10^{-10}$	$2.5 \cdot 10^{-9}$	$7.2 \cdot 10^{-11}$	$2.7 \cdot 10^{-2}$	$1 \cdot 10^{-3}$
$b\bar{b}$ [pb]	0.15	$1.7 \cdot 10^{-2}$	$1.7 \cdot 10^{-2}$	$1.3 \cdot 10^{-3}$	$2.7 \cdot 10^{-3}$	$2 \cdot 10^{-4}$	1.03	$4.1 \cdot 10^{-2}$
tc [pb]	$5.4 \cdot 10^{-2}$	$7.6 \cdot 10^{-3}$	$9.2 \cdot 10^{-4}$	$8.9 \cdot 10^{-5}$	$3.2 \cdot 10^{-2}$	$3 \cdot 10^{-3}$	8.26	0.39
tu [pb]	$9.8 \cdot 10^{-7}$	$1.4 \cdot 10^{-7}$	$2.8 \cdot 10^{-8}$	$2.7 \cdot 10^{-9}$	$1.4 \cdot 10^{-2}$	$1.3 \cdot 10^{-3}$	$6.2 \cdot 10^{-2}$	$2.9 \cdot 10^{-3}$
$t\bar{t}$ [pb]							241.4	15.4

Table 15: Benchmark points for different $\mathcal{Z}_N \times \mathcal{Z}_M$ flavour symmetries for inclusive flavon production channels with high flavon mass (m_a) in case of the soft symmetry-breaking scenario at a 100 TeV hadron collider, assuming $f = 500$ GeV.

The LHC is actively searching for light pseudoscalar particles. For a light flavon, present sensitivities of the LHC are given in table 16. Using these sensitivities given in table 16, the estimated sensitivities for the HL-LHC, HE-LHC, and a 100 TeV collider are given in table 17. The benchmark predictions for the processes given in table 16, for different $\mathcal{Z}_N \times \mathcal{Z}_M$ flavour symmetries, are given in tables 18- 20 for $m_a = 20, 60$ GeV for the soft symmetry-breaking scenario.

m_a [GeV]	$\mathcal{L}[fb^{-1}]$ [References]		ATLAS 13 TeV		CMS 13 TeV	
	ATLAS	CMS	20	60	20	60
$\tau\tau$ [pb]		138 [142]			4	
$\gamma\gamma$ [pb]	138 [143, 144]	[145]	6	7		

Table 16: Current limits of $\sigma \times BR$ at 13 TeV LHC by ATLAS and CMS in low mass resonance searches for inclusive flavon production channels.

m_a [GeV]	HL-LHC [14 TeV, 3 ab $^{-1}$]		HE-LHC [27 TeV, 15 ab $^{-1}$]		100 TeV, 30 ab $^{-1}$	
	20	60	20	60	20	60
$\tau\tau$ [pb]		0.9		0.5		0.6
$\gamma\gamma$ [pb]	1.3	1.5	0.7	0.8	0.8	0.9

Table 17: Estimated reach ($\sigma \times BR$) of the HL-LHC, HE-LHC and a 100 TeV collider for low flavon mass (m_a) in inclusive flavon production channels.

We observe from table 18 that the HL-LHC provides access only to probe the $\mathcal{Z}_8 \times \mathcal{Z}_{22}$ flavour symmetry through the $\tau\tau$ channel for the mass $m_a = 60$ GeV. The situation changes greatly as we approach the HE-LHC

and a 100 TeV hadron collider, as shown in tables 19 and 20. Now, the $\tau\tau$ channel is accessible for all $\mathcal{Z}_N \times \mathcal{Z}_M$ flavour symmetries. The $\gamma\gamma$ channel and the flavon mass $m_a = 20$ GeV remain beyond the reach of the HL-LHC, HE-LHC and a 100 TeV collider for all flavour symmetries.

m_a [GeV]	Benchmark $\mathcal{Z}_2 \times \mathcal{Z}_5$		Benchmark $\mathcal{Z}_2 \times \mathcal{Z}_9$		Benchmark $\mathcal{Z}_2 \times \mathcal{Z}_{11}$		Benchmark $\mathcal{Z}_8 \times \mathcal{Z}_{22}$	
	20	60	20	60	20	60	20	60
$\tau\tau$ [pb]	$4.7 \cdot 10^{-3}$	0.58	$1.1 \cdot 10^{-2}$	0.62	$2.2 \cdot 10^{-2}$	0.69	$7.7 \cdot 10^{-3}$	9.62
$\gamma\gamma$ [pb]	$5.6 \cdot 10^{-4}$	$1 \cdot 10^{-3}$	$1.5 \cdot 10^{-4}$	$9.9 \cdot 10^{-5}$	$1.1 \cdot 10^{-4}$	$5.8 \cdot 10^{-5}$	$9 \cdot 10^{-5}$	$1.7 \cdot 10^{-2}$

Table 18: Benchmark points for different $\mathcal{Z}_N \times \mathcal{Z}_M$ flavour symmetries for inclusive flavon production channels with low flavon mass (m_a) in case of the soft symmetry-breaking scenario at the 14 TeV HL-LHC, assuming $f = 500$ GeV.

m_a [GeV]	Benchmark $\mathcal{Z}_2 \times \mathcal{Z}_5$		Benchmark $\mathcal{Z}_2 \times \mathcal{Z}_9$		Benchmark $\mathcal{Z}_2 \times \mathcal{Z}_{11}$		Benchmark $\mathcal{Z}_8 \times \mathcal{Z}_{22}$	
	20	60	20	60	20	60	20	60
$\tau\tau$ [pb]	$8 \cdot 10^{-3}$	1.06	$2.2 \cdot 10^{-2}$	1.38	$4.2 \cdot 10^{-2}$	1.55	$1.5 \cdot 10^{-2}$	21.78
$\gamma\gamma$ [pb]	$9.4 \cdot 10^{-4}$	$1.8 \cdot 10^{-3}$	$2.9 \cdot 10^{-4}$	$2.2 \cdot 10^{-4}$	$2.2 \cdot 10^{-4}$	$1.3 \cdot 10^{-4}$	$1.7 \cdot 10^{-4}$	$3.8 \cdot 10^{-2}$

Table 19: Benchmark points for different $\mathcal{Z}_N \times \mathcal{Z}_M$ flavour symmetries for inclusive flavon production channels with low flavon mass (m_a) in case of the soft symmetry-breaking scenario at the 27 TeV HE-LHC, assuming $f = 500$ GeV.

m_a [GeV]	Benchmark $\mathcal{Z}_2 \times \mathcal{Z}_5$		Benchmark $\mathcal{Z}_2 \times \mathcal{Z}_9$		Benchmark $\mathcal{Z}_2 \times \mathcal{Z}_{11}$		Benchmark $\mathcal{Z}_8 \times \mathcal{Z}_{22}$	
	20	60	20	60	20	60	20	60
$\tau\tau$ [pb]	$2.2 \cdot 10^{-2}$	3.29	$7.5 \cdot 10^{-2}$	5.72	0.15	6.43	$5.1 \cdot 10^{-2}$	92.23
$\gamma\gamma$ [pb]	$2.6 \cdot 10^{-3}$	$5.7 \cdot 10^{-3}$	$9.5 \cdot 10^{-4}$	$9.1 \cdot 10^{-4}$	$7.5 \cdot 10^{-4}$	$5.3 \cdot 10^{-4}$	$5.5 \cdot 10^{-4}$	0.16

Table 20: Benchmark points for different $\mathcal{Z}_N \times \mathcal{Z}_M$ flavour symmetries for inclusive flavon production channels with low flavon mass (m_a) in case of the soft symmetry-breaking scenario at a 100 TeV collider, assuming $f = 500$ GeV.

m_a [GeV]	Benchmark $\mathcal{Z}_2 \times \mathcal{Z}_5$		Benchmark $\mathcal{Z}_2 \times \mathcal{Z}_9$		Benchmark $\mathcal{Z}_2 \times \mathcal{Z}_{11}$	
	20	60	20	60	20	60
$\tau\tau$ [pb]	$1.9 \cdot 10^{-7}$	$5.1 \cdot 10^{-4}$	$1.1 \cdot 10^{-11}$	$2 \cdot 10^{-6}$	$2.4 \cdot 10^{-13}$	$3.3 \cdot 10^{-7}$
$\gamma\gamma$ [pb]	$3.8 \cdot 10^{-7}$	$8.8 \cdot 10^{-7}$	$4.5 \cdot 10^{-10}$	$3.2 \cdot 10^{-10}$	$3.8 \cdot 10^{-11}$	$2.7 \cdot 10^{-11}$

Table 21: Benchmark points for different $\mathcal{Z}_N \times \mathcal{Z}_M$ flavour symmetries for inclusive flavon production channels with low flavon mass (m_a) in case of the symmetry-conserving scenario at the 14 TeV HL-LHC.

In the symmetry-conserving case, we observe from figures 21 and 22 that the cross-section can be relatively significant only for a low flavon mass. Therefore, we investigate the symmetry-conserving scenario only for

$m_a = 20, 60$ GeV. We show benchmark predictions of symmetry-conserving scenario for different $\mathcal{Z}_N \times \mathcal{Z}_M$ flavour symmetries in tables 21- 23 for $m_a = 20, 60$ GeV. It turns out that the inclusive processes in this scenario are beyond the reach of the HL-LHC, HE-LHC, and even a 100 TeV collider.

m_a [GeV]	Benchmark $\mathcal{Z}_2 \times \mathcal{Z}_5$		Benchmark $\mathcal{Z}_2 \times \mathcal{Z}_9$		Benchmark $\mathcal{Z}_2 \times \mathcal{Z}_{11}$	
	20	60	20	60	20	60
$\tau\tau$ [pb]	$2 \cdot 10^{-7}$	$9.2 \cdot 10^{-4}$	$1.8 \cdot 10^{-11}$	$4.5 \cdot 10^{-6}$	$4 \cdot 10^{-13}$	$7.3 \cdot 10^{-7}$
$\gamma\gamma$ [pb]	$6.3 \cdot 10^{-7}$	$1.6 \cdot 10^{-6}$	$8.8 \cdot 10^{-10}$	$7.2 \cdot 10^{-10}$	$7.4 \cdot 10^{-11}$	$6 \cdot 10^{-11}$

Table 22: Benchmark points for different $\mathcal{Z}_N \times \mathcal{Z}_M$ flavour symmetries for inclusive flavon production channels with low flavon mass (m_a) in case of the symmetry-conserving scenario at the 27 TeV HE-LHC.

m_a [GeV]	Benchmark $\mathcal{Z}_2 \times \mathcal{Z}_5$		Benchmark $\mathcal{Z}_2 \times \mathcal{Z}_9$		Benchmark $\mathcal{Z}_2 \times \mathcal{Z}_{11}$	
	20	60	20	60	20	60
$\tau\tau$ [pb]	$2.7 \cdot 10^{-10}$	$2.8 \cdot 10^{-3}$	$4.9 \cdot 10^{-11}$	$1.9 \cdot 10^{-5}$	$1.1 \cdot 10^{-12}$	$3 \cdot 10^{-6}$
$\gamma\gamma$ [pb]	$1.7 \cdot 10^{-6}$	$4.9 \cdot 10^{-6}$	$2.8 \cdot 10^{-9}$	$2.9 \cdot 10^{-9}$	$2.4 \cdot 10^{-10}$	$2.5 \cdot 10^{-10}$

Table 23: Benchmark points for different $\mathcal{Z}_N \times \mathcal{Z}_M$ flavour symmetries for inclusive flavon production channels with low flavon mass (m_a) in case of the symmetry-conserving scenario at a 100 TeV collider.

6.3.2 Associative production

We notice that there are other channels through which flavon can be produced, as shown in figure 25. For instance, the following associated production processes can be used to produce the flavon,

$$bg \rightarrow ba, ug, cg \rightarrow ta, \bar{b}\bar{b}a \rightarrow \bar{b}\bar{b}\tau^+\tau^-, \bar{t}\bar{t}a \rightarrow \bar{t}\bar{t}\bar{t}, \quad (85)$$

where the first process undergoes through the flavour-diagonal coupling of the flavon to the $b\bar{b}$, and the second process occurs through the flavour-violating flavon-quark coupling.

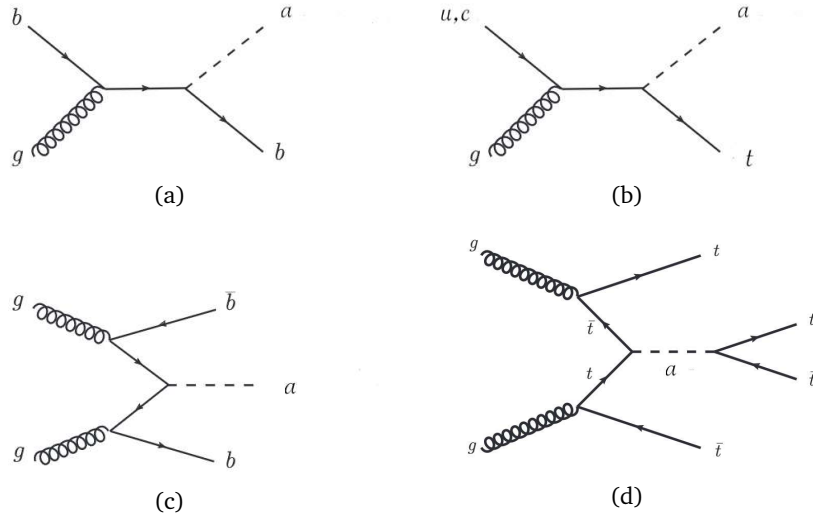


Figure 25: Feynman diagrams for the production of the flavon through different associative channels.

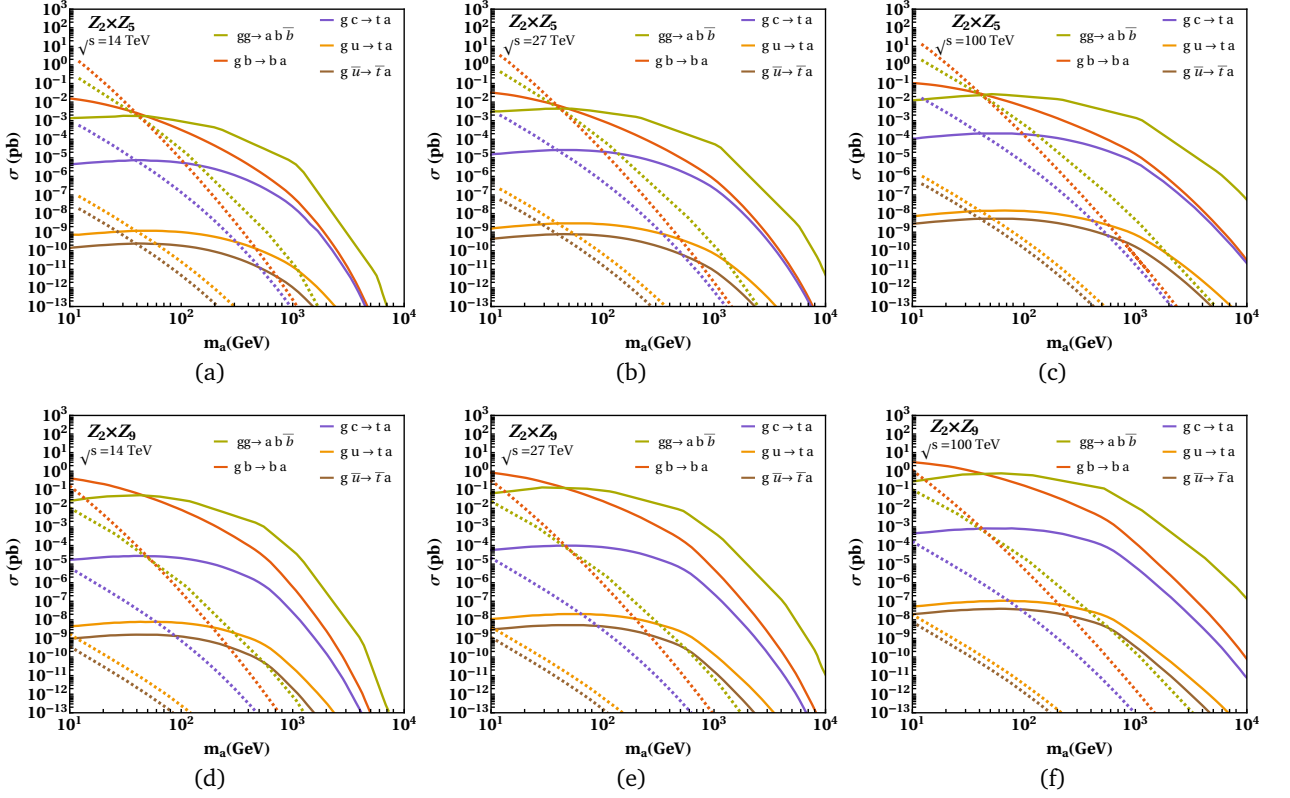


Figure 26: Production cross-sections of the flavon of $\mathcal{Z}_2 \times \mathcal{Z}_5$, and $\mathcal{Z}_2 \times \mathcal{Z}_9$ flavour symmetries with respect to its mass through different channels for 14 TeV HL-LHC, 27 TeV HE-LHC and future 100 TeV collider. The solid lines represents the production cross section along the boundaries of parameter space allowed by the observable $R_{\mu\mu}$ for soft symmetry-breaking scenario, while the dashed lines correspond to that in the symmetry-conserving scenario along the allowed parameter space by the observable $BR(K_L \rightarrow \mu\mu)_{SD}$.

The cross-sections of different associative production channels are also shown in figures 26 and 27. We observe that the production cross sections are, in general, smaller for the soft symmetry-breaking as well as symmetry-conserving scenarios, and can be relatively large only for low flavon mass.

The process $t\bar{t}a \rightarrow t\bar{t}t\bar{t}$ can occur only for the $\mathcal{Z}_8 \times \mathcal{Z}_{22}$ flavour symmetry where the flavour-diagonal coupling of the flavon to top quarks is allowed. This results in a relatively large cross-section involving $t\bar{t}$ channels. Thus, the $\mathcal{Z}_8 \times \mathcal{Z}_{22}$ flavour symmetry is very special in this sense.

As noticed in the case of inclusive production of the heavy flavon mass, we observe from figures 28 and 29 that the associative production cross-sections of the flavon of different $\mathcal{Z}_N \times \mathcal{Z}_M$ flavour symmetries for the VEV $f = 500$ GeV for the soft symmetry-breaking scenario can be sufficiently large. Therefore, we continue to use this choice even for the associative production of the heavy flavon of different $\mathcal{Z}_N \times \mathcal{Z}_M$ flavour symmetries.

m_a [GeV]	$\mathcal{L}[fb^{-1}]$ [References]		ATLAS 13 TeV		CMS 13 TeV	
	ATLAS	CMS	500	1000	500	1000
$t\bar{t}a \rightarrow t\bar{t}t\bar{t}$ [pb]	139 [146]	137 [147]	$1 \cdot 10^{-2}$	$6 \cdot 10^{-3}$	$2 \cdot 10^{-2}$	
$gg \rightarrow ab\bar{b} \rightarrow \tau\tau b\bar{b}$ [pb]	36.1 [132]	35.9 [133]	$8 \cdot 10^{-2}$	$9 \cdot 10^{-3}$	$6 \cdot 10^{-2}$	$1 \cdot 10^{-2}$
$gb \rightarrow ab \rightarrow \tau\tau b$ [pb]	36.1 [132]	35.9 [133]	$3 \cdot 10^{-2}$	$4 \cdot 10^{-3}$	$3 \cdot 10^{-2}$	$4 \cdot 10^{-3}$

Table 24: Current limits of $\sigma \times BR$ at 13 TeV LHC by ATLAS and CMS in resonance searches for associative flavon production channels.

The present reach of the LHC for the associative production channels is shown in table 24. We show the sensitivities of these modes at the HL-LHC, HE-LHC, and a 100 TeV collider in table 25. Our benchmark predictions for different $\mathcal{Z}_N \times \mathcal{Z}_M$ flavour symmetries, are given in tables 26- 28 for the soft symmetry-breaking scenario.

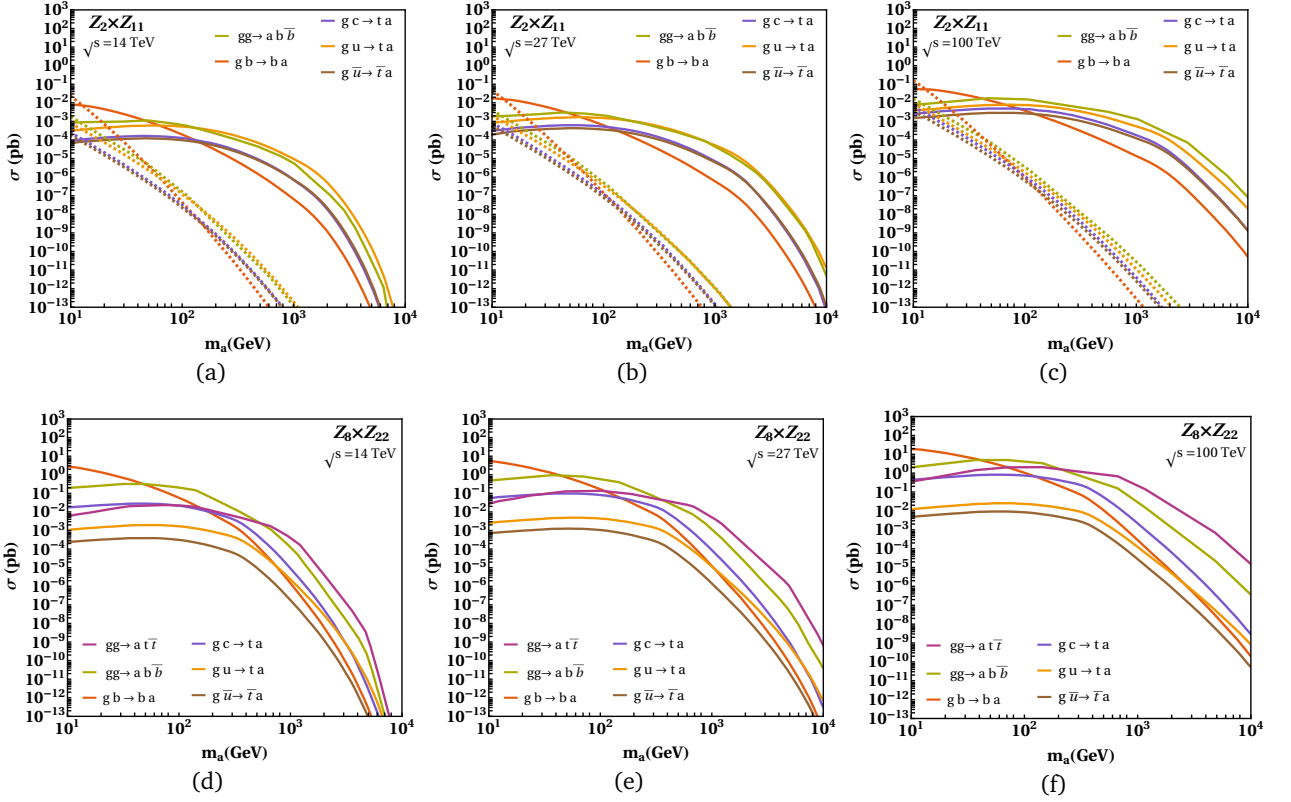


Figure 27: Production cross-sections of the flavon of $\mathcal{Z}_2 \times \mathcal{Z}_{11}$, and $\mathcal{Z}_8 \times \mathcal{Z}_{22}$ flavour symmetries with respect to its mass through different channels for 14 TeV HL-LHC, 27 TeV HE-LHC and future 100 TeV collider. The solid lines represents the production cross section along the boundaries of parameter space allowed by the observable $R_{\mu\mu}$ for soft symmetry-breaking scenario, while the dashed lines correspond to that in the symmetry-conserving scenario along the allowed parameter space by the observable $BR(K_L \rightarrow \mu\mu)_{SD}$.

m_a [GeV]	HL-LHC [14 TeV, 3 ab^{-1}]		HE-LHC [27 TeV, 15 ab^{-1}]		100 TeV, 30 ab^{-1}	
	500	1000	500	1000	500	1000
$t\bar{t}a \rightarrow t\bar{t}t\bar{t}$ [pb]	$2 \cdot 10^{-3}$	$1 \cdot 10^{-3}$	$3 \cdot 10^{-3}$	$2 \cdot 10^{-3}$	$1 \cdot 10^{-2}$	$9 \cdot 10^{-3}$
$gg \rightarrow ab\bar{b} \rightarrow \tau\tau b\bar{b}$ [pb]	$7 \cdot 10^{-3}$	$1 \cdot 10^{-3}$	$5 \cdot 10^{-3}$	$8 \cdot 10^{-4}$	$8 \cdot 10^{-3}$	$1 \cdot 10^{-3}$
$gb \rightarrow ab \rightarrow \tau\tau b$ [pb]	$3 \cdot 10^{-3}$	$5 \cdot 10^{-4}$	$2 \cdot 10^{-3}$	$3 \cdot 10^{-4}$	$4 \cdot 10^{-3}$	$5 \cdot 10^{-4}$

Table 25: Estimated reach ($\sigma \times BR$) of HL-LHC, HE-LHC and the 100 TeV collider for high flavon mass (m_a) in associative flavon production channels.

We observe from table 26 that only the mode $t\bar{t}a \rightarrow t\bar{t}t\bar{t}$ is within the reach of the HL-LHC for the flavon mass $m_a = 500$ GeV for the $\mathcal{Z}_8 \times \mathcal{Z}_{22}$ flavour symmetry. This scenario improves slightly at the HE-LHC and at a 100 TeV collider for the $\mathcal{Z}_8 \times \mathcal{Z}_{22}$ flavour symmetry such that the flavon mass $m_a = 1000$ GeV becomes also accessible. The symmetry-conserving scenario remains beyond the reach of the HL-LHC, HE-LHC and a 100 TeV collider for the associative production modes. Therefore, we do not discuss it anymore in this case.

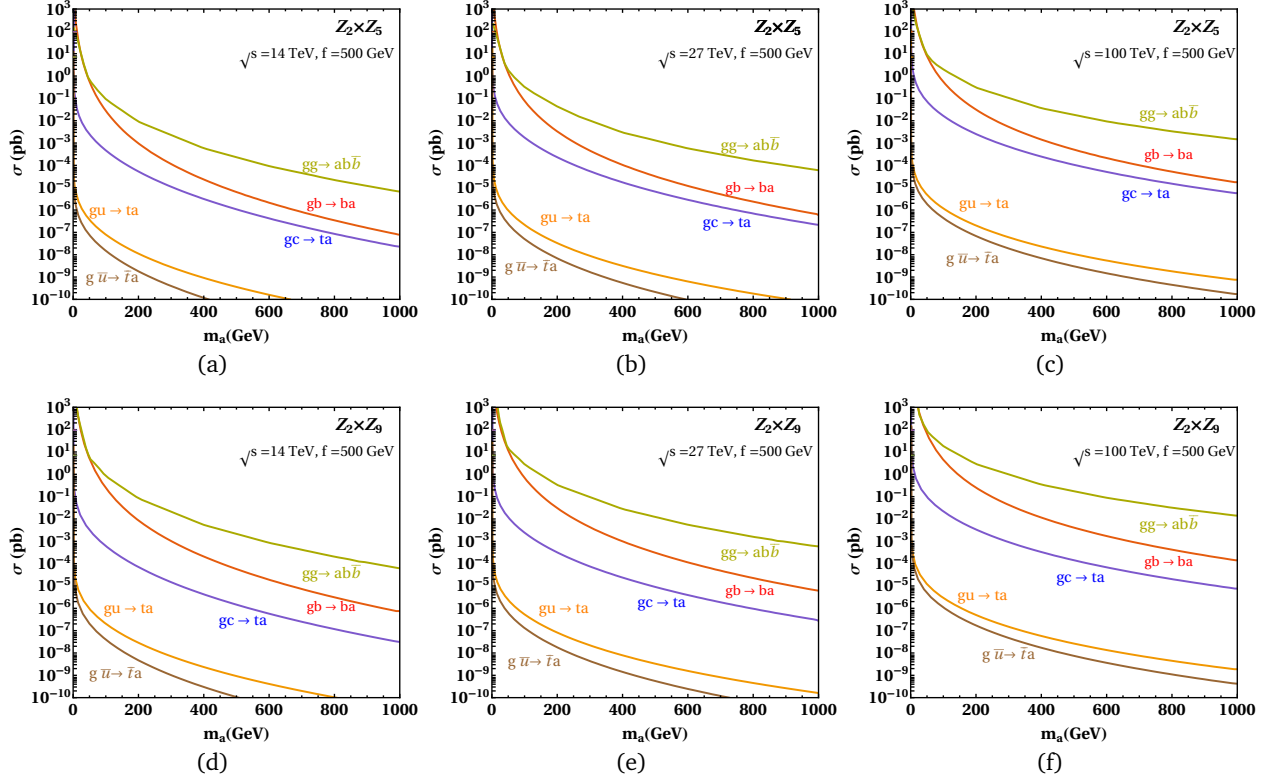


Figure 28: Production cross-sections of the flavon of $Z_2 \times Z_5$, and $Z_2 \times Z_9$ flavour symmetries with respect to its mass through different channels for 14 TeV HL-LHC, 27 TeV HE-LHC, and future 100 TeV hadron collider, where the flavon VEV $f = 500$ GeV.

m_a [GeV]	Benchmark $Z_2 \times Z_5$		Benchmark $Z_2 \times Z_9$		Benchmark $Z_2 \times Z_{11}$		Benchmark $Z_8 \times Z_{22}$	
	500	1000	500	1000	500	1000	500	1000
$t\bar{t}a \rightarrow t\bar{t}t\bar{t}$ [pb]							$1.6 \cdot 10^{-3}$	$1.6 \cdot 10^{-4}$
$gg \rightarrow ab\bar{b} \rightarrow \tau\tau b\bar{b}$ [pb]	$6 \cdot 10^{-7}$	$1.8 \cdot 10^{-8}$	$1 \cdot 10^{-4}$	$3.2 \cdot 10^{-6}$	$3.4 \cdot 10^{-5}$	$8.9 \cdot 10^{-7}$	$1.6 \cdot 10^{-6}$	$3.2 \cdot 10^{-8}$
$gb \rightarrow ab \rightarrow \tau\tau b$ [pb]	$1.7 \cdot 10^{-7}$	$5.6 \cdot 10^{-9}$	$2.9 \cdot 10^{-5}$	$9.7 \cdot 10^{-7}$	$9.4 \cdot 10^{-6}$	$2.7 \cdot 10^{-7}$	$4.5 \cdot 10^{-7}$	$9.7 \cdot 10^{-9}$

Table 26: Benchmark points for different $Z_N \times Z_M$ flavour symmetries for associative flavon production channels with high flavon mass (m_a) in case of the soft symmetry-breaking at the 14 TeV HL-LHC, with $f = 500$ GeV.

m_a [GeV]	Benchmark $Z_2 \times Z_5$		Benchmark $Z_2 \times Z_9$		Benchmark $Z_2 \times Z_{11}$		Benchmark $Z_8 \times Z_{22}$	
	500	1000	500	1000	500	1000	500	1000
$t\bar{t}a \rightarrow t\bar{t}t\bar{t}$ [pb]							$1.5 \cdot 10^{-2}$	$2.3 \cdot 10^{-3}$
$gg \rightarrow ab\bar{b} \rightarrow \tau\tau b\bar{b}$ [pb]	$3.3 \cdot 10^{-6}$	$1.6 \cdot 10^{-7}$	$5.8 \cdot 10^{-4}$	$2.8 \cdot 10^{-5}$	$1.9 \cdot 10^{-4}$	$7.9 \cdot 10^{-6}$	$9 \cdot 10^{-6}$	$2.8 \cdot 10^{-7}$
$gb \rightarrow ab \rightarrow \tau\tau b$ [pb]	$9.3 \cdot 10^{-7}$	$5.1 \cdot 10^{-8}$	$1.6 \cdot 10^{-4}$	$8.8 \cdot 10^{-6}$	$5.3 \cdot 10^{-5}$	$2.5 \cdot 10^{-6}$	$2.5 \cdot 10^{-6}$	$8.8 \cdot 10^{-8}$

Table 27: Benchmark points for different $Z_N \times Z_M$ flavour symmetries for associative flavon production channels with high flavon mass (m_a) in case of the soft symmetry-breaking at the 27 TeV HE-LHC, with $f = 500$ GeV.

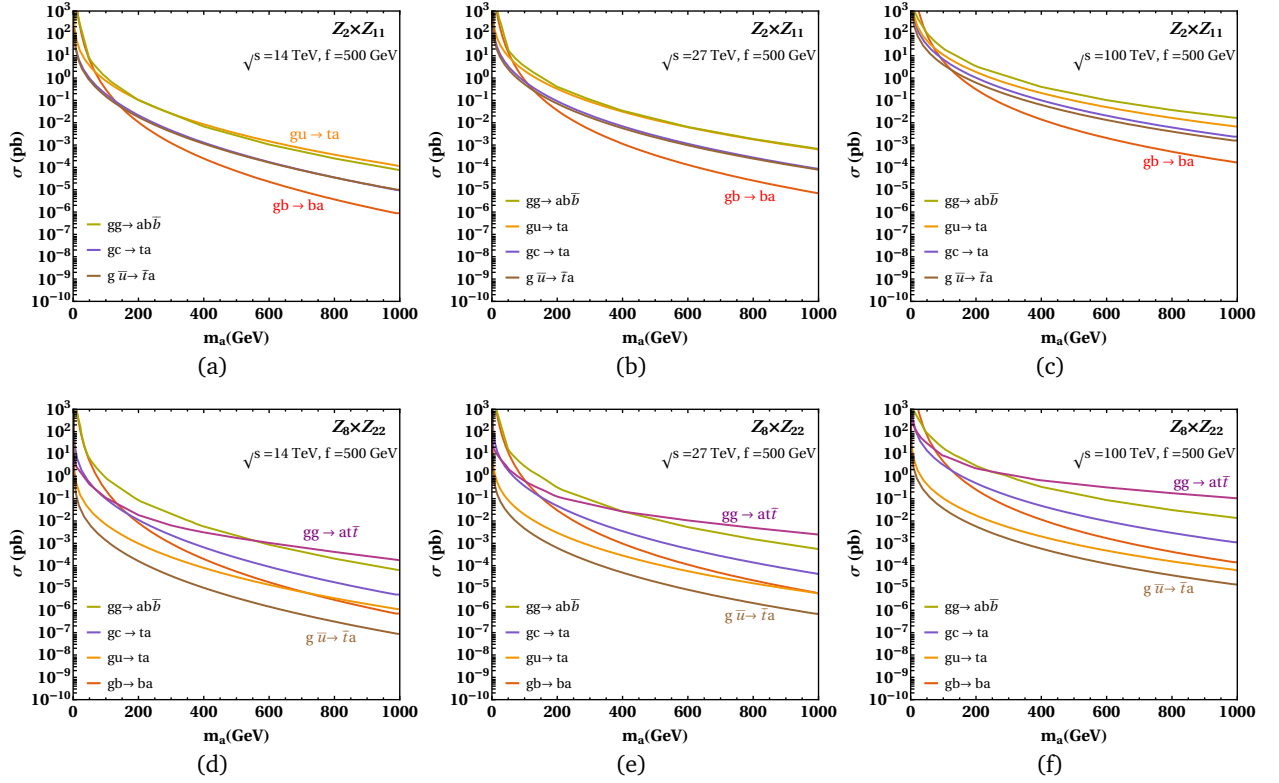


Figure 29: Production cross-sections of the flavon of $Z_2 \times Z_{11}$, and $Z_8 \times Z_{22}$ flavour symmetries with respect to its mass through different channels for 14 TeV HL-LHC, 27 TeV HE-LHC, and future 100 TeV hadron collider, where the flavon VEV $f = 500$ GeV.

m_a [GeV]	Benchmark $Z_2 \times Z_5$		Benchmark $Z_2 \times Z_9$		Benchmark $Z_2 \times Z_{11}$		Benchmark $Z_8 \times Z_{22}$	
	500	1000	500	1000	500	1000	500	1000
$t\bar{t}a \rightarrow t\bar{t}t\bar{t}$ [pb]							0.41	$9.6 \cdot 10^{-2}$
$gg \rightarrow ab\bar{b} \rightarrow \tau\tau b\bar{b}$ [pb]	$4.7 \cdot 10^{-5}$	$4.0 \cdot 10^{-6}$	$8.2 \cdot 10^{-3}$	$6.9 \cdot 10^{-4}$	$2.7 \cdot 10^{-3}$	$1.9 \cdot 10^{-4}$	$1.3 \cdot 10^{-4}$	$6.8 \cdot 10^{-6}$
$gb \rightarrow ab \rightarrow \tau\tau b$ [pb]	$1.34 \cdot 10^{-5}$	$1.23 \cdot 10^{-6}$	$2.3 \cdot 10^{-3}$	$2.1 \cdot 10^{-4}$	$7.5 \cdot 10^{-4}$	$6.0 \cdot 10^{-5}$	$3.6 \cdot 10^{-5}$	$2.1 \cdot 10^{-6}$

Table 28: Benchmark points for different $Z_N \times Z_M$ flavour symmetries for associative flavon production channels with high flavon mass (m_a) in case of the soft symmetry-breaking scenario at a 100 TeV collider, assuming $f = 500$ GeV.

6.3.3 Di-flavon production

In this section, we discuss the production of di-flavon, which is an important mode to explore the flavon physics of different $Z_N \times Z_M$ flavour symmetries. We show the present LHC sensitivities of di-flavon channels in table 29. The reach of the HL-LHC, HE-LHC and a 100 TeV collider is given in table 30. The di-flavon production cross-sections for different $Z_N \times Z_M$ flavour symmetries are shown in figure 30 in the case of soft symmetry-breaking scenario.

The benchmark predictions for different $Z_N \times Z_M$ flavour symmetries, are given in tables 31- 33 for the soft symmetry-breaking scenario and heavy flavon masses. We observe from tables 31- 33 that the di-flavon

production for heavy flavon mass is insensitive to the HL-LHC, HE-LHC and even to a 100 TeV collider for all $\mathcal{Z}_N \times \mathcal{Z}_M$ flavour symmetries.

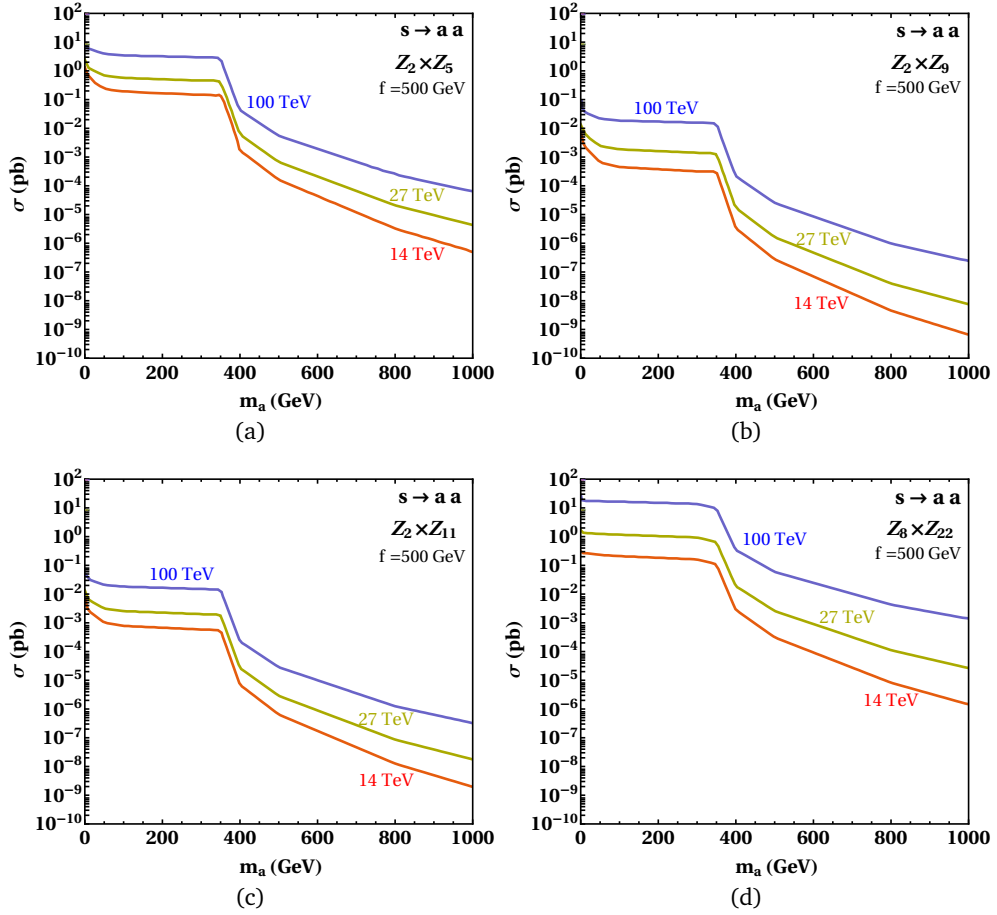


Figure 30: Production cross-sections of the di-flavon in $\mathcal{Z}_2 \times \mathcal{Z}_5$, $\mathcal{Z}_2 \times \mathcal{Z}_9$, $\mathcal{Z}_2 \times \mathcal{Z}_{11}$, and $\mathcal{Z}_8 \times \mathcal{Z}_{22}$ flavour symmetries with respect to its mass for 14 TeV HL-LHC, 27 TeV HE-LHC, and 100 TeV hadron collider, where the flavon VEV $f = 500$ GeV.

m_a [GeV]	$\mathcal{L}[fb^{-1}]$ [References]		ATLAS 13 TeV		CMS 13 TeV	
	ATLAS	CMS	500	1000	500	1000
$s \rightarrow aa \rightarrow b\bar{b}l\bar{l}$ [pb]	36.1 [148]	19.7 [149] ^{aa}	$2 \cdot 10^{-2}$	$1 \cdot 10^{-2}$	$2 \cdot 10^{-1}$	$2 \cdot 10^{-2}$
$s \rightarrow aa \rightarrow b\bar{b}b\bar{b}$ [pb]	36.1 [150]	35.9 [151]	$4 \cdot 10^{-2}$	$9 \cdot 10^{-3}$	$7 \cdot 10^{-2}$	$1 \cdot 10^{-2}$

^aThe reference [149] is at $\sqrt{s} = 8$ TeV.

Table 29: Current limits of $\sigma \times BR$ at 13 TeV LHC by ATLAS and CMS in high mass resonance searches for di-flavon production channels.

m_a [GeV]	HL-LHC [14 TeV, 3 ab ⁻¹]		HE-LHC [27 TeV, 15 ab ⁻¹]		100 TeV, 30 ab ⁻¹	
	500	1000	500	1000	500	1000
$s \rightarrow aa \rightarrow b\bar{b}\tau\tau$ [pb]	$2 \cdot 10^{-3}$	$1 \cdot 10^{-3}$	$2 \cdot 10^{-3}$	$8 \cdot 10^{-4}$	$3 \cdot 10^{-3}$	$1 \cdot 10^{-3}$
$s \rightarrow aa \rightarrow b\bar{b}b\bar{b}$ [pb]	$5 \cdot 10^{-3}$	$1 \cdot 10^{-3}$	$3 \cdot 10^{-3}$	$7 \cdot 10^{-4}$	$5 \cdot 10^{-3}$	$1 \cdot 10^{-3}$

Table 30: Estimated reach ($\sigma \times BR$) of HL-LHC, HE-LHC and the 100 TeV collider for high flavon mass (m_a) in di-flavon production channels.

m_a [GeV]	Benchmark $\mathcal{Z}_2 \times \mathcal{Z}_5$		Benchmark $\mathcal{Z}_2 \times \mathcal{Z}_9$		Benchmark $\mathcal{Z}_2 \times \mathcal{Z}_{11}$		Benchmark $\mathcal{Z}_8 \times \mathcal{Z}_{22}$	
	500	1000	500	1000	500	1000	500	1000
$s \rightarrow aa \rightarrow b\bar{b}\tau\tau$ [pb]	$1.4 \cdot 10^{-8}$	$4.4 \cdot 10^{-11}$	$7 \cdot 10^{-9}$	$1.7 \cdot 10^{-11}$	$7.5 \cdot 10^{-10}$	$1.7 \cdot 10^{-12}$	$2 \cdot 10^{-9}$	$3.7 \cdot 10^{-12}$
$s \rightarrow aa \rightarrow b\bar{b}\mu\mu$ [pb]	$1.3 \cdot 10^{-11}$	$4 \cdot 10^{-14}$	$1.5 \cdot 10^{-10}$	$3.6 \cdot 10^{-13}$	$5.8 \cdot 10^{-12}$	$1.3 \cdot 10^{-14}$	$1.8 \cdot 10^{-11}$	$3.2 \cdot 10^{-14}$
$s \rightarrow aa \rightarrow b\bar{b}b\bar{b}$ [pb]	$4 \cdot 10^{-8}$	$1.3 \cdot 10^{-10}$	$1.8 \cdot 10^{-8}$	$4.3 \cdot 10^{-11}$	$1.1 \cdot 10^{-9}$	$2.6 \cdot 10^{-12}$	$4.9 \cdot 10^{-9}$	$9.1 \cdot 10^{-12}$

Table 31: Benchmark points for different $\mathcal{Z}_N \times \mathcal{Z}_M$ flavour symmetries for di-flavon production channels with high flavon mass (m_a) in case of the soft symmetry-breaking scenario at the 14 TeV HL-LHC, assuming $f = 500$ GeV.

m_a [GeV]	Benchmark $\mathcal{Z}_2 \times \mathcal{Z}_5$		Benchmark $\mathcal{Z}_2 \times \mathcal{Z}_9$		Benchmark $\mathcal{Z}_2 \times \mathcal{Z}_{11}$		Benchmark $\mathcal{Z}_8 \times \mathcal{Z}_{22}$	
	500	1000	500	1000	500	1000	500	1000
$s \rightarrow aa \rightarrow b\bar{b}\tau\tau$ [pb]	$5.9 \cdot 10^{-8}$	$3.7 \cdot 10^{-10}$	$4.2 \cdot 10^{-8}$	$1.9 \cdot 10^{-10}$	$3.4 \cdot 10^{-9}$	$1.5 \cdot 10^{-11}$	$1.6 \cdot 10^{-8}$	$6.9 \cdot 10^{-11}$
$s \rightarrow aa \rightarrow b\bar{b}\mu\mu$ [pb]	$5.3 \cdot 10^{-11}$	$3.4 \cdot 10^{-13}$	$9.1 \cdot 10^{-10}$	$4.2 \cdot 10^{-12}$	$2.6 \cdot 10^{-11}$	$1.2 \cdot 10^{-13}$	$1.4 \cdot 10^{-10}$	$5.9 \cdot 10^{-13}$
$s \rightarrow aa \rightarrow b\bar{b}b\bar{b}$ [pb]	$1.7 \cdot 10^{-7}$	$1.1 \cdot 10^{-9}$	$1.1 \cdot 10^{-7}$	$4.9 \cdot 10^{-10}$	$5.1 \cdot 10^{-9}$	$2.3 \cdot 10^{-11}$	$4 \cdot 10^{-8}$	$1.7 \cdot 10^{-10}$

Table 32: Benchmark points for different $\mathcal{Z}_N \times \mathcal{Z}_M$ flavour symmetries for di-flavon production channels with high flavon mass (m_a) in case of the soft symmetry-breaking scenario at the 27 TeV HE-LHC, assuming $f = 500$ GeV.

m_a [GeV]	Benchmark $\mathcal{Z}_2 \times \mathcal{Z}_5$		Benchmark $\mathcal{Z}_2 \times \mathcal{Z}_9$		Benchmark $\mathcal{Z}_2 \times \mathcal{Z}_{11}$		Benchmark $\mathcal{Z}_8 \times \mathcal{Z}_{22}$	
	500	1000	500	1000	500	1000	500	1000
$s \rightarrow aa \rightarrow b\bar{b}\tau\tau$ [pb]	$4.8 \cdot 10^{-7}$	$5.5 \cdot 10^{-9}$	$6.5 \cdot 10^{-7}$	$6.2 \cdot 10^{-9}$	$3.3 \cdot 10^{-8}$	$2.8 \cdot 10^{-10}$	$3.7 \cdot 10^{-7}$	$3.5 \cdot 10^{-9}$
$s \rightarrow aa \rightarrow b\bar{b}\mu\mu$ [pb]	$4.2 \cdot 10^{-10}$	$4.9 \cdot 10^{-12}$	$1.4 \cdot 10^{-8}$	$1.3 \cdot 10^{-10}$	$2.5 \cdot 10^{-10}$	$2.2 \cdot 10^{-12}$	$3.2 \cdot 10^{-9}$	$3.1 \cdot 10^{-11}$
$s \rightarrow aa \rightarrow b\bar{b}b\bar{b}$ [pb]	$1.4 \cdot 10^{-6}$	$1.6 \cdot 10^{-8}$	$1.7 \cdot 10^{-6}$	$1.6 \cdot 10^{-8}$	$5 \cdot 10^{-8}$	$4.3 \cdot 10^{-10}$	$9.1 \cdot 10^{-7}$	$8.6 \cdot 10^{-9}$

Table 33: Benchmark points for different $\mathcal{Z}_N \times \mathcal{Z}_M$ flavour symmetries for di-flavon production channels with high flavon mass (m_a) in case of the soft symmetry-breaking scenario at a 100 TeV collider, assuming $f = 500$ GeV.

We observed earlier that the di-flavon production of a heavy mass flavon is beyond the reach of HL-LHC, HE-LHC, and a 100 TeV collider for different $\mathcal{Z}_N \times \mathcal{Z}_M$ flavour symmetries. However, this scenario changes in the case of a light flavon. We show the present sensitivities of the light di-flavon searches of the LHC in table

34. The sensitivities of the HL-LHC, HE-LHC, and a 100 TeV collider for a light di-flavon productions are shown in table 35.

m_a [GeV]	$\mathcal{L}[fb^{-1}]$ [References]		ATLAS 13 TeV		CMS 13 TeV	
	ATLAS	CMS	20	60	20	60
$s \rightarrow aa \rightarrow b\bar{b}\ell\ell$ [pb]	139 [152]	138 [153]	$1 \cdot 10^{-4}$	$1 \cdot 10^{-4}$	$9 \cdot 10^{-5}$	$8 \cdot 10^{-5}$
$s \rightarrow aa \rightarrow b\bar{b}b\bar{b}$ [pb]	36.1 [154]	138 [155]	3	1	1	$3 \cdot 10^{-1}$

Table 34: Current limits of $\sigma \times BR$ at 13 TeV LHC by ATLAS and CMS in low mass resonance searches for di-flavon channels.

m_a [GeV]	HL-LHC [14 TeV, 3 ab $^{-1}$]		HE-LHC [27 TeV, 15 ab $^{-1}$]		100 TeV, 30 ab $^{-1}$	
	20	60	20	60	20	60
$s \rightarrow aa \rightarrow b\bar{b}\ell\ell$ [pb]	$2 \cdot 10^{-5}$	$2 \cdot 10^{-5}$	$1 \cdot 10^{-5}$	$1 \cdot 10^{-5}$	$2 \cdot 10^{-5}$	$2 \cdot 10^{-5}$
$s \rightarrow aa \rightarrow b\bar{b}b\bar{b}$ [pb]	0.2	$7 \cdot 10^{-2}$	0.16	$5 \cdot 10^{-2}$	0.2	$7 \cdot 10^{-2}$

Table 35: Estimated reach ($\sigma \times BR$) of HL-LHC, HE-LHC and the 100 TeV collider for low flavon mass (m_a) in di-flavon production channels.

We show our benchmark predictions of di-flavon production cross-sections in tables 36-38 for low flavon masses in the soft symmetry-breaking scenario. We observe that $aa \rightarrow b\bar{b}\tau\tau$ mode is accessible for all $\mathcal{Z}_N \times \mathcal{Z}_M$ flavour symmetries at the HL-LHC, HE-LHC, and a 100 TeV collider. All three channels are sensitive to the HL-LHC, HE-LHC, and a 100 TeV collider only for the $\mathcal{Z}_8 \times \mathcal{Z}_{22}$ flavour symmetry. The production cross-sections in the symmetry-conserving scenario are too small to be under the reach of any collider, as observed in tables 39-41.

m_a [GeV]	Benchmark $\mathcal{Z}_2 \times \mathcal{Z}_5$		Benchmark $\mathcal{Z}_2 \times \mathcal{Z}_9$		Benchmark $\mathcal{Z}_2 \times \mathcal{Z}_{11}$		Benchmark $\mathcal{Z}_8 \times \mathcal{Z}_{22}$	
	20	60	20	60	20	60	20	60
$s \rightarrow aa \rightarrow b\bar{b}\tau\tau$ [pb]	$2.7 \cdot 10^{-5}$	$1.9 \cdot 10^{-5}$	$3.2 \cdot 10^{-5}$	$1.5 \cdot 10^{-5}$	$3.3 \cdot 10^{-5}$	$2 \cdot 10^{-5}$	$1.8 \cdot 10^{-2}$	$1.6 \cdot 10^{-2}$
$s \rightarrow aa \rightarrow b\bar{b}\mu\mu$ [pb]	$2.5 \cdot 10^{-8}$	$1.7 \cdot 10^{-8}$	$7.2 \cdot 10^{-7}$	$3.3 \cdot 10^{-7}$	$2.7 \cdot 10^{-7}$	$1.5 \cdot 10^{-7}$	$1.6 \cdot 10^{-4}$	$1.3 \cdot 10^{-4}$
$s \rightarrow aa \rightarrow b\bar{b}b\bar{b}$ [pb]	$6.8 \cdot 10^{-5}$	$5.4 \cdot 10^{-5}$	$6.1 \cdot 10^{-5}$	$3.7 \cdot 10^{-5}$	$4.1 \cdot 10^{-5}$	$2.9 \cdot 10^{-5}$	$3.6 \cdot 10^{-2}$	$3.7 \cdot 10^{-2}$

Table 36: Benchmark points for different $\mathcal{Z}_N \times \mathcal{Z}_M$ flavour symmetries for di-flavon production channels with low flavon mass (m_a) in case of the soft symmetry-breaking scenario at the 14 TeV HL-LHC, assuming $f = 500$ GeV.

m_a [GeV]	Benchmark $\mathcal{Z}_2 \times \mathcal{Z}_5$		Benchmark $\mathcal{Z}_2 \times \mathcal{Z}_9$		Benchmark $\mathcal{Z}_2 \times \mathcal{Z}_{11}$		Benchmark $\mathcal{Z}_8 \times \mathcal{Z}_{22}$	
	20	60	20	60	20	60	20	60
$s \rightarrow aa \rightarrow b\bar{b}\tau\tau$ [pb]	$6.8 \cdot 10^{-5}$	$5.5 \cdot 10^{-5}$	$9.5 \cdot 10^{-5}$	$5.8 \cdot 10^{-5}$	$8.9 \cdot 10^{-5}$	$6.1 \cdot 10^{-5}$	$8.8 \cdot 10^{-2}$	$8.1 \cdot 10^{-2}$
$s \rightarrow aa \rightarrow b\bar{b}\mu\mu$ [pb]	$6.4 \cdot 10^{-8}$	$5 \cdot 10^{-8}$	$2.2 \cdot 10^{-6}$	$1.3 \cdot 10^{-6}$	$7.1 \cdot 10^{-7}$	$4.7 \cdot 10^{-7}$	$8 \cdot 10^{-4}$	$7 \cdot 10^{-4}$
$s \rightarrow aa \rightarrow b\bar{b}b\bar{b}$ [pb]	$1.7 \cdot 10^{-4}$	$1.6 \cdot 10^{-4}$	$1.8 \cdot 10^{-4}$	$1.4 \cdot 10^{-4}$	$1.1 \cdot 10^{-4}$	$9.2 \cdot 10^{-5}$	0.18	0.19

Table 37: Benchmark points for different $\mathcal{Z}_N \times \mathcal{Z}_M$ flavour symmetries for di-flavon production channels with high flavon mass (m_a) in case of the soft symmetry-breaking scenario at the 27 TeV HE-LHC, assuming $f = 500$ GeV.

m_a [GeV]	Benchmark $\mathcal{Z}_2 \times \mathcal{Z}_5$		Benchmark $\mathcal{Z}_2 \times \mathcal{Z}_9$		Benchmark $\mathcal{Z}_2 \times \mathcal{Z}_{11}$		Benchmark $\mathcal{Z}_8 \times \mathcal{Z}_{22}$	
	20	60	20	60	20	60	20	60
$s \rightarrow aa \rightarrow b\bar{b}\tau\tau$ [pb]	$3.5 \cdot 10^{-4}$	$3.2 \cdot 10^{-4}$	$6.9 \cdot 10^{-4}$	$5.5 \cdot 10^{-4}$	$5.2 \cdot 10^{-4}$	$4.2 \cdot 10^{-4}$	1.17	1.11
$s \rightarrow aa \rightarrow b\bar{b}\mu\mu$ [pb]	$3.3 \cdot 10^{-7}$	$2.9 \cdot 10^{-7}$	$1.6 \cdot 10^{-5}$	$1.2 \cdot 10^{-5}$	$4.2 \cdot 10^{-6}$	$3.2 \cdot 10^{-6}$	$1.1 \cdot 10^{-2}$	$9.7 \cdot 10^{-3}$
$s \rightarrow aa \rightarrow b\bar{b}b\bar{b}$ [pb]	$8.8 \cdot 10^{-4}$	$9.2 \cdot 10^{-4}$	$1.3 \cdot 10^{-3}$	$1.3 \cdot 10^{-3}$	$6.4 \cdot 10^{-4}$	$6.3 \cdot 10^{-4}$	2.35	2.65

Table 38: Benchmark points for different $\mathcal{Z}_N \times \mathcal{Z}_M$ flavour symmetries for di-flavon production channels with high flavon mass (m_a) in case of the soft symmetry-breaking scenario at a 100 TeV collider, assuming $f = 500$ GeV.

m_a [GeV]	Benchmark $\mathcal{Z}_2 \times \mathcal{Z}_5$		Benchmark $\mathcal{Z}_2 \times \mathcal{Z}_9$		Benchmark $\mathcal{Z}_2 \times \mathcal{Z}_{11}$	
	20	60	20	60	20	60
$s \rightarrow aa \rightarrow b\bar{b}\tau\tau$ [pb]	$8.7 \cdot 10^{-10}$	$3.5 \cdot 10^{-12}$	$1.9 \cdot 10^{-14}$	$5.4 \cdot 10^{-17}$	$3.4 \cdot 10^{-16}$	$1.1 \cdot 10^{-18}$
$s \rightarrow aa \rightarrow b\bar{b}\mu\mu$ [pb]	$8.2 \cdot 10^{-13}$	$3.2 \cdot 10^{-15}$	$4.2 \cdot 10^{-16}$	$1.2 \cdot 10^{-18}$	$2.7 \cdot 10^{-18}$	$8.8 \cdot 10^{-21}$
$s \rightarrow aa \rightarrow b\bar{b}b\bar{b}$ [pb]	$2.2 \cdot 10^{-9}$	$1 \cdot 10^{-11}$	$3.6 \cdot 10^{-14}$	$1.3 \cdot 10^{-16}$	$4.2 \cdot 10^{-16}$	$1.7 \cdot 10^{-18}$

Table 39: Benchmark points for different $\mathcal{Z}_N \times \mathcal{Z}_M$ flavour symmetries for di-flavon production channels with low flavon mass (m_a) in case of the symmetry-conserving scenario at the 14 TeV HL-LHC.

m_a [GeV]	Benchmark $\mathcal{Z}_2 \times \mathcal{Z}_5$		Benchmark $\mathcal{Z}_2 \times \mathcal{Z}_9$		Benchmark $\mathcal{Z}_2 \times \mathcal{Z}_{11}$	
	20	60	20	60	20	60
$s \rightarrow aa \rightarrow b\bar{b}\tau\tau$ [pb]	$1.9 \cdot 10^{-9}$	$8.8 \cdot 10^{-12}$	$4.7 \cdot 10^{-14}$	$1.6 \cdot 10^{-16}$	$7.7 \cdot 10^{-16}$	$3 \cdot 10^{-18}$
$s \rightarrow aa \rightarrow b\bar{b}\mu\mu$ [pb]	$1.8 \cdot 10^{-12}$	$7.9 \cdot 10^{-15}$	$1.1 \cdot 10^{-15}$	$3.6 \cdot 10^{-18}$	$6.2 \cdot 10^{-18}$	$2.3 \cdot 10^{-20}$
$s \rightarrow aa \rightarrow b\bar{b}b\bar{b}$ [pb]	$4.7 \cdot 10^{-9}$	$2.5 \cdot 10^{-11}$	$9.1 \cdot 10^{-14}$	$4.1 \cdot 10^{-16}$	$9.5 \cdot 10^{-16}$	$3.1 \cdot 10^{-18}$

Table 40: Benchmark points for different $\mathcal{Z}_N \times \mathcal{Z}_M$ flavour symmetries for di-flavon production channels with low flavon mass (m_a) in case of the symmetry-conserving scenario at the 27 TeV HE-LHC.

m_a [GeV]	Benchmark $\mathcal{Z}_2 \times \mathcal{Z}_5$		Benchmark $\mathcal{Z}_2 \times \mathcal{Z}_9$		Benchmark $\mathcal{Z}_2 \times \mathcal{Z}_{11}$	
	20	60	20	60	20	60
$s \rightarrow aa \rightarrow b\bar{b}\tau\tau$ [pb]	$7.8 \cdot 10^{-9}$	$4.5 \cdot 10^{-11}$	$2.4 \cdot 10^{-13}$	$1.2 \cdot 10^{-15}$	$3.4 \cdot 10^{-15}$	$1.7 \cdot 10^{-17}$
$s \rightarrow aa \rightarrow b\bar{b}\mu\mu$ [pb]	$7.4 \cdot 10^{-12}$	$4 \cdot 10^{-14}$	$5.5 \cdot 10^{-15}$	$2.5 \cdot 10^{-17}$	$2.8 \cdot 10^{-17}$	$1.3 \cdot 10^{-19}$
$s \rightarrow aa \rightarrow b\bar{b}b\bar{b}$ [pb]	$2 \cdot 10^{-8}$	$1.3 \cdot 10^{-10}$	$4.7 \cdot 10^{-13}$	$2.8 \cdot 10^{-15}$	$4.2 \cdot 10^{-15}$	$2.6 \cdot 10^{-17}$

Table 41: Benchmark points for different $\mathcal{Z}_N \times \mathcal{Z}_M$ flavour symmetries for di-flavon production channels with low flavon mass (m_a) in case of the symmetry-conserving scenario at a 100 TeV collider.

7 Summary

The $\mathcal{Z}_N \times \mathcal{Z}_M$ flavour symmetry is a unique and novel framework that may have its origin either in a $U(1) \times U(1)$ symmetry or in an anomalous global $U(1)_A \times U(1)_A$ symmetry. This symmetry provides a unique way to realize the FN mechanism, resulting in an explanation to the flavour problem of the SM. In this work, we have thoroughly investigated the flavour phenomenology and the collider signatures of different realizations of the $\mathcal{Z}_N \times \mathcal{Z}_M$ flavour symmetry motivated by different theoretical demands.

In the case of quark flavour physics, the $K^0 - \bar{K}^0$ mixing places the strongest bounds on the parameter space of the flavon of the $\mathcal{Z}_2 \times \mathcal{Z}_9$ flavour symmetry in the case of the soft symmetry-breaking scenario. The $\mathcal{Z}_2 \times \mathcal{Z}_5$ flavour symmetry is subjected to the weakest constraints from the $K^0 - \bar{K}^0$ mixing. This scenario continues to remain the same even for the symmetry-conserving case, where the allowed parameter space is only along a straight dashed line. The $B_s - \bar{B}_s$ mixing better constraints the parameter space of the flavon of the $\mathcal{Z}_2 \times \mathcal{Z}_{11}$ and $\mathcal{Z}_8 \times \mathcal{Z}_{22}$ flavour symmetries for the soft symmetry-breaking scenario. In the case of the symmetry-conserving potential, the $B_s - \bar{B}_s$ mixing provides more stringent bounds on the $\mathcal{Z}_2 \times \mathcal{Z}_{11}$ flavour symmetry. The $B_d - \bar{B}_d$ mixing places more tight bounds on the parameter space of the flavon of the $\mathcal{Z}_2 \times \mathcal{Z}_{11}$ and $\mathcal{Z}_2 \times \mathcal{Z}_{5,9}$ flavour symmetries for the soft symmetry-breaking scenario. This feature continues to hold even for the symmetry-conserving potential. The $D^0 - \bar{D}^0$ mixing works remarkably well in constraining the parameter space of the flavon of the $\mathcal{Z}_2 \times \mathcal{Z}_5$ flavour symmetry for the soft symmetry-breaking scenario. This is also true for the symmetry-conserving case. The $B_{d,s} \rightarrow \mu^+ \mu^-$ decays impose relatively better bounds on the parameter space of the flavon of the $\mathcal{Z}_2 \times \mathcal{Z}_{11}$ symmetry. On the other side, the $K_L \rightarrow \mu^+ \mu^-$ decays are more sensitive to the parameter space of the flavon of the $\mathcal{Z}_2 \times \mathcal{Z}_9$ symmetry. The $B_{d,s} \rightarrow \mu^+ \mu^-$ and $K_L \rightarrow \mu^+ \mu^-$ decays place tighter constraints on the parameter space of the flavon of the $\mathcal{Z}_2 \times \mathcal{Z}_{11}$ symmetry for the symmetry-conserving scenario. The lifetime $\tau_{\mu\mu}$ is important in constraining the parameter space of the flavon of the $\mathcal{Z}_2 \times \mathcal{Z}_5$ symmetry. For the soft symmetry-breaking scenario, the lifetime $\tau_{\mu\mu}$ places more significant bounds on the parameter space of the flavon of the $\mathcal{Z}_2 \times \mathcal{Z}_{11}$ symmetry. The ratio $R_{\mu\mu}$ is a powerful observable to constrain the parameter space of the flavon of all $\mathcal{Z}_N \times \mathcal{Z}_M$ flavour symmetries for the soft symmetry-breaking as well as symmetry-conserving scenarios, and will play a crucial role in determining the parameter space of the flavon of different $\mathcal{Z}_N \times \mathcal{Z}_M$ flavour symmetries. A global fit to diverse data coming from the observables having $b \rightarrow s\mu^+ \mu^-$ transitions is performed, and allowed ranges of the Wilson coefficients are derived. This results in bounds on the parameter space of the flavon of all $\mathcal{Z}_N \times \mathcal{Z}_M$ flavour symmetries for the soft symmetry-breaking as well as symmetry-conserving scenarios. We also predict muon forward-backward asymmetry in $B \rightarrow K\mu^+ \mu^-$ decays for $f < 200$ GeV.

On the leptonic flavour side, the decay $\mu \rightarrow e\gamma$ is able to constrain more the parameter space of the flavon of the $\mathcal{Z}_2 \times \mathcal{Z}_9$ and the $\mathcal{Z}_8 \times \mathcal{Z}_{22}$ flavour symmetries for the soft symmetry-breaking case. However, the parameter space of the flavon of the $\mathcal{Z}_2 \times \mathcal{Z}_{11}$ is more constrained for the symmetry-conserving scenario. The $A \mu \rightarrow A e$ conversion is more effective in constraining the parameter space of the flavon of the $\mathcal{Z}_8 \times \mathcal{Z}_{22}$ flavour symmetry for the soft symmetry-breaking scenario. In the case of symmetry-conserving scenario, the parameter space of the flavon of the $\mathcal{Z}_2 \times \mathcal{Z}_{11}$ is more constrained. Similar results are obtained for the $\mu \rightarrow 3e$ and $\tau \rightarrow 3\mu$ decays.

In the study of collider physics of the flavon of different $\mathcal{Z}_N \times \mathcal{Z}_M$ flavour symmetries, we computed flavon decays as well as $t \rightarrow (c, u)a$ decays. The $t \rightarrow ca$ decays are within the reach of the HL-LHC, HE-LHC, and a 100 TeV collider only for the $\mathcal{Z}_2 \times \mathcal{Z}_{11}$ and the $\mathcal{Z}_8 \times \mathcal{Z}_{22}$ flavour symmetries for the soft symmetry-breaking scenario. Furthermore, we have investigated inclusive, associative, and di-flavon production signatures of flavon for the soft symmetry-breaking as well as symmetry-conserving scenarios. We have predicted the sensitivities of these channels for the HL-LHC, HE-LHC, and a 100 TeV collider in a model-independent way using the square root scaling of luminosity. We compare our benchmark predictions for heavy and light flavon at the HL-LHC, HE-LHC, and a 100 TeV collider to estimated sensitivities of the HL-LHC, HE-LHC and a 100 TeV collider for all the $\mathcal{Z}_N \times \mathcal{Z}_M$ flavour symmetries discussed in this work. In the case of inclusive production channels, a 100 TeV collider can probe the $\mathcal{Z}_2 \times \mathcal{Z}_{5,9}$ and the $\mathcal{Z}_8 \times \mathcal{Z}_{22}$ flavour symmetries for the soft symmetry-breaking scenario for a heavy flavon. The HE-LHC will be able to probe the $\mathcal{Z}_2 \times \mathcal{Z}_5$ and the $\mathcal{Z}_8 \times \mathcal{Z}_{22}$ flavour symmetries better than the HL-LHC for the soft symmetry-breaking scenario. In the case of a light flavon, the HE-LHC and a 100 TeV collider can probe all the $\mathcal{Z}_N \times \mathcal{Z}_M$ flavour symmetries in the $\tau\tau$ channel for the soft symmetry-breaking scenario. A few specific inclusive signatures are within the reach of the 14 TeV high-luminosity LHC only for the $\mathcal{Z}_2 \times \mathcal{Z}_5$ and $\mathcal{Z}_8 \times \mathcal{Z}_{22}$ flavour symmetries. The symmetry-conserving scenario is beyond the reach of detection

capabilities of any collider for the inclusive processes.

For associative production modes, only the parameter space of the flavon of the $\mathcal{Z}_8 \times \mathcal{Z}_{22}$ flavour is accessible to the HL-LHC, HE-LHC, and a 100 TeV collider through the $t\bar{t}a \rightarrow t\bar{t}t\bar{t}$ channel in the soft symmetry-breaking scenario for high flavon mass. The di-flavon production channels for heavy flavon are insensitive to the HL-LHC, HE-LHC, and even to a 100 TeV collider for all the $\mathcal{Z}_N \times \mathcal{Z}_M$ flavour symmetries in the case of soft symmetry-breaking scenario. However, a light flavon scenario can be probed for all the $\mathcal{Z}_N \times \mathcal{Z}_M$ flavour symmetries at the HL-LHC, HE-LHC, and a 100 TeV collider. In the case of the symmetry-conserving scenario, the di-flavon productions cross-sections are too small to be accessible at the HL-LHC, HE-LHC as well as a 100 TeV collider, and can be further constrained through the precision flavour physics in future. Collider simulations for some particular signatures, such as $pp \rightarrow a \rightarrow t\bar{t}$, could be an interesting future investigation, which is an expected sequel to the present work [156].

Acknowledgement

We acknowledge the use of JaxoDraw [157] for creating the Feynman diagrams in this work. This work is supported by the Council of Science and Technology, Govt. of Uttar Pradesh, India through the project ‘‘A new paradigm for flavour problem’’ no. CST/D-1301, and Science and Engineering Research Board, Department of Science and Technology, Government of India through the project ‘‘Higgs Physics within and beyond the Standard Model’’ no. CRG/2022/003237. NS acknowledges the support through the INSPIRE fellowship by the Department of Science and Technology, Government of India.

Benchmark points for the Yukawa couplings

We reproduce the fermion masses using the following values of the fermion masses at 1TeV[158],

$$\begin{aligned} \{m_t, m_c, m_u\} &\simeq \{150.7 \pm 3.4, 0.532^{+0.074}_{-0.073}, (1.10^{+0.43}_{-0.37}) \times 10^{-3}\} \text{ GeV}, \\ \{m_b, m_s, m_d\} &\simeq \{2.43 \pm 0.08, 4.7^{+1.4}_{-1.3} \times 10^{-2}, 2.50^{+1.08}_{-1.03} \times 10^{-3}\} \text{ GeV}, \\ \{m_\tau, m_\mu, m_e\} &\simeq \{1.78 \pm 0.2, 0.105^{+9.4 \times 10^{-9}}_{-9.3 \times 10^{-9}}, 4.96 \pm 0.00000043 \times 10^{-4}\} \text{ GeV}. \end{aligned} \quad (86)$$

The magnitudes and phases of the CKM mixing elements are [50],

$$\begin{aligned} |V_{ud}| &= 0.97370 \pm 0.00014, |V_{cb}| = 0.0410 \pm 0.0014, |V_{ub}| = 0.00382 \pm 0.00024, \\ \sin 2\beta &= 0.699 \pm 0.017, \alpha = (84.9^{+5.1}_{-4.5})^\circ, \gamma = (72.1^{+4.1}_{-4.5})^\circ, \delta = 1.196^{+0.045}_{-0.043} \end{aligned} \quad (87)$$

The dimensionless coefficients $y_{ij}^{u,d,\ell,\nu} = |y_{ij}^{u,d,\ell,\nu}| e^{i\phi_{ij}^{q,\ell,\nu}}$ are scanned with $|y_{ij}^{u,d,\ell,\nu}| \in [0.7, 2\pi]$ and $\phi_{ij}^{q,\ell,\nu} \in [0, 2\pi]$. The fit results are,

The $\mathcal{Z}_2 \times \mathcal{Z}_5$ model

The dimensionless coefficients $y_{ij}^{u,d,\ell,\nu} = |y_{ij}^{u,d,\ell,\nu}| e^{i\phi_{ij}^{q,\ell,\nu}}$ are scanned with $|y_{ij}^{u,d,\ell,\nu}| \in [0.1, 4\pi]$ and $\phi_{ij}^{q,\ell,\nu} \in [0, 2\pi]$. The fit results are,

$$\begin{aligned} Y_u &= \begin{pmatrix} -1.68 - 3.37i & -0.09 + 0.03i & -0.1 - 0.02i \\ 1.53 + 4.95i & -0.57 + 0.55i & 0.48 + 0.002i \\ 0.76 + 0.18i & -1.04 + 0.46i & 0.58 - 0.65i \end{pmatrix}, Y_d = \begin{pmatrix} -4.15 + 3.58i & 2.20 - 0.89i & 2.62 - 4.20i \\ -0.33 - 0.36i & 0.07 - 0.075i & 0.17 + 0.47i \\ -0.24 - 0.07i & -0.06 - 0.084i & -0.07 - 0.12i \end{pmatrix}, \\ Y_l &= \begin{pmatrix} -0.07 - 0.06i & 0.099 - 0.004i & 0.45 - 0.32i \\ -0.14 - 0.09i & 0.08 - 0.06i & -0.63 + 0.24i \\ -0.04 + 0.09i & -0.09 + 0.06i & 0.10 - 0.0003i \end{pmatrix} \end{aligned}$$

with $\epsilon = 0.1$ and $\delta = 1.196$.

The $\mathcal{Z}_2 \times \mathcal{Z}_9$ model

The dimensionless coefficients $y_{ij}^{u,d,\ell,\nu} = |y_{ij}^{u,d,\ell,\nu}| e^{i\phi_{ij}^{q,\ell,\nu}}$ are scanned with $|y_{ij}^{u,d,\ell,\nu}| \in [0.9, 2\pi]$ and $\phi_{ij}^{q,\ell,\nu} \in [0, 2\pi]$. The fit results are,

$$Y_u = \begin{pmatrix} 1 & 0.87 - 0.49i & -0.23 + 0.97i \\ -0.9 + 1.05i & -0.7 - 0.72i & 1 \\ 0.94 - 0.33i & 0.55 + 0.84i & 0.9 \end{pmatrix}, Y_d = \begin{pmatrix} 0.99 - 0.09i & 3.24 - 1.05i & 1 \\ 0.99 - 0.10i & 0.92 + 0.39i & 0.9 \\ 1 & 1 & -1.04 + 0.54i \end{pmatrix},$$

$$Y_l = \begin{pmatrix} 0.9 & 0.9 & 1.5 \\ 0.9 & 1.5 & 1.5 \\ 1.5 & 1.5 & 0.9 \end{pmatrix}$$

with $\epsilon = 0.23$ and $\delta = 1.196$.

The $\mathcal{Z}_2 \times \mathcal{Z}_{11}$ model

The dimensionless coefficients $y_{ij}^{u,d,\ell,\nu} = |y_{ij}^{u,d,\ell,\nu}| e^{i\phi_{ij}^{q,\ell,\nu}}$ are scanned with $|y_{ij}^{u,d,\ell,\nu}| \in [0.7, 2\pi]$ and $\phi_{ij}^{q,\ell,\nu} \in [0, 2\pi]$. The fit results are,

$$Y_u = \begin{pmatrix} 2.19 - 0.18i & 1.40 - 0.09i & 0.70 - 0.002i \\ 2.12 + 0.02i & -1.02 + 2.12i & 4.45 - 1.01i \\ 0.33 - 0.71i & 0.92 + 0.42i & 0.82 - 0.26i \end{pmatrix}, Y_d = \begin{pmatrix} 0.40 + 0.59i & 3.61 - 0.16i & 3.34 - 4.06i \\ 1.02 + 0.01i & -0.36 + 1.18i & 1.29 + 0.36i \\ -0.77 + 0.33i & 0.82 + 0.02i & -0.51 + 0.48i \end{pmatrix}$$

$$Y_l = \begin{pmatrix} -0.73 + 0.001i & -0.58 + 0.53i & 0.001 + 1.29i \\ 6.24 + 0.37i & 3.48 - 2.44i & 1.71 + 1.7 \times 10^{-5}i \\ 0.24 - 1.16i & -0.36 - 0.61i & -0.60 + 0.35i \end{pmatrix}$$

with $\epsilon = 0.28$ and $\delta = 1.196$.

The $\mathcal{Z}_8 \times \mathcal{Z}_{22}$ model

The dimensionless coefficients $y_{ij}^{u,d,\ell,\nu} = |y_{ij}^{u,d,\ell,\nu}| e^{i\phi_{ij}^{q,\ell,\nu}}$ are scanned with $|y_{ij}^{u,d,\ell,\nu}| \in [0.9, 2]$ and $\phi_{ij}^{q,\ell,\nu} \in [0, 2\pi]$. The fit results are,

$$Y_u = \begin{pmatrix} 0.12 + 1.44i & -0.38 - 0.82i & 0.989 + 0.004i \\ -1.27 - 1.38i & -0.56 + 0.82i & -1.22 - 0.24i \\ -1.12 - 0.25i & -1.12 - 0.43i & -2.70 - 2.61i \end{pmatrix}, Y_d = \begin{pmatrix} -1.36 + 0.39i & 0.31 - 1.28i & 0.71 + 0.61i \\ -1.05 + 0.27i & -0.44 + 0.85i & 0.47 - 0.79i \\ -1.11 - 0.37i & -0.81 + 0.42i & 0.80 + 0.82i \end{pmatrix}$$

$$Y_l = \begin{pmatrix} -1.40 - 0.21i & 1.14 - 0.004i & -0.78 + 0.45i \\ -0.88 + 0.16i & -0.54 + 0.78i & -1.16 + 0.11i \\ 0.85 + 0.34i & 0.899 + 0.003i & 0.899 - 0.003i \end{pmatrix}$$

with $\epsilon = 0.23$ and $\delta = 1.196$.

The SM background

Production mode	Channel	SM Backgrounds
Inclusive production	jet-jet	$pp \rightarrow jj$
	$\ell^+\ell^- (\ell = e, \mu, \tau)$	$pp \rightarrow \ell^+\ell^-$
	μe	$pp \rightarrow tt, pp \rightarrow VV (V = W^+, W^-, Z),$ $pp \rightarrow \ell^+\ell^-, pp \rightarrow tWb$
	$\mu\tau, e\tau$	$pp \rightarrow \text{multijets}, pp \rightarrow W + \text{jets},$ $pp \rightarrow t\bar{t}, pp \rightarrow VV (V = W^+, W^-, Z),$ $pp \rightarrow \ell^+\ell^-, pp \rightarrow tWb$
	$b\bar{b}$	$pp \rightarrow b\bar{b}$
	$\gamma\gamma$	$pp \rightarrow \gamma\gamma$
	$t\bar{t}$	$pp \rightarrow t\bar{t}$
Associative production	$t\bar{t}a \rightarrow t\bar{t}t$	$pp \rightarrow t\bar{t}t$
	$ab\bar{b} \rightarrow \tau\tau b\bar{b}$	$pp \rightarrow \tau\tau b\bar{b}$
	$ab \rightarrow \tau\tau b$	$pp \rightarrow \text{multijets}, pp \rightarrow W + \text{jets}, pp \rightarrow t\bar{t}$ $pp \rightarrow \ell^+\ell^-, pp \rightarrow tWb, pp \rightarrow VV$
Di-flavon production	$aa \rightarrow b\bar{b}\ell\ell (\ell = \mu, \tau)$	$pp \rightarrow b\bar{b}\ell\ell$
	$aa \rightarrow b\bar{b}b\bar{b}$	$pp \rightarrow b\bar{b}b\bar{b}$

Table 42: SM Backgrounds for the flavon production through various channels.

The dark-technicolor paradigm

In this appendix, we show how the $\mathcal{Z}_N \times \mathcal{Z}_M$ flavour symmetry and the FN mechanism of the $\mathcal{Z}_8 \times \mathcal{Z}_{22}$ model naturally emerge from a dark-technicolour paradigm [3, 4, 6]. The technicolour paradigm is obtained by $SU(N_{\text{TC}}) \times SU(N_{\text{DTC}}) \times SU(N_{\text{F}})$, where TC denotes the standard technicolour gauge group, DTC is for the dark-technicolour, and the F stands for the strong dynamics of vector-like fermions.

The TC fermions transform under the symmetry $\text{SM} \times \mathcal{G}$ as [4],

$$\begin{aligned}
 T_q^i &\equiv \begin{pmatrix} T \\ B \end{pmatrix}_L : (1, 2, 0, N_{\text{TC}}, 1, 1), \\
 T_R^i &: (1, 1, 1, N_{\text{TC}}, 1, 1), B_R^i : (1, 1, -1, N_{\text{TC}}, 1, 1),
 \end{aligned} \tag{88}$$

where $i = 1, 2, 3 \dots$, and $+\frac{1}{2}$ is the electric charge for T , and $-\frac{1}{2}$ is that of the B .

The transformation of the DTC fermions under the $\text{SM} \times \mathcal{G}$ symmetry is [4],

$$\mathcal{D}_q^i \equiv \mathcal{C}_{L,R}^i : (1, 1, 1, 1, N_{\text{DTC}}, 1), \mathcal{S}_{L,R}^i : (1, 1, -1, 1, N_{\text{DTC}}, 1), \tag{89}$$

where $i = 1, 2, 3 \dots$, and electric charges are $+\frac{1}{2}$ for \mathcal{C} and $-\frac{1}{2}$ for \mathcal{S} .

The fermions of the $SU(N_{\text{F}})$ symmetry have the following behavior under the $\text{SM} \times \mathcal{G}$ symmetry [4],

$$\begin{aligned}
 F_{L,R} &\equiv U_{L,R}^i \equiv (3, 1, \frac{4}{3}, 1, 1, N_{\text{F}}), D_{L,R}^i \equiv (3, 1, -\frac{2}{3}, 1, 1, N_{\text{F}}), \\
 N_{L,R}^i &\equiv (1, 1, 0, 1, 1, N_{\text{F}}), E_{L,R}^i \equiv (1, 1, -2, 1, 1, N_{\text{F}}),
 \end{aligned} \tag{90}$$

where $i = 1, 2, 3 \dots$.

We notice that there are three axial $U(1)_A^{\text{TC,DTC,F}}$ symmetries in the dark-technicolor paradigm. They are broken by instanton effects to a cyclic discrete group as $U(1)_A^{\text{TC,DTC,F}} \rightarrow \mathcal{Z}_{2K_{\text{TC,DTC,F}}}$ [159], where $K_{\text{TC,DTC,F}}$ show the number of massless flavours of the TC, DTC and F gauge symmetries in the N -dimensional representation of the gauge group $SU(N)_{\text{TC,DTC,F}}$. Thus, we observe a natural emergence of a generic $\mathcal{Z}_N \times \mathcal{Z}_M \times \mathcal{Z}_P$ flavour symmetry, whose subset is the $\mathcal{Z}_N \times \mathcal{Z}_M$ flavour symmetry.

- [3] G. Abbas, *Int. J. Mod. Phys. A* **34** (2019) no.20, 1950104 doi:10.1142/S0217751X19501045 [arXiv:1712.08052 [hep-ph]].
- [4] G. Abbas, *Int. J. Mod. Phys. A* **37**, no.11n12, 2250056 (2022) doi:10.1142/S0217751X22500567 [arXiv:2012.11283 [hep-ph]].
- [5] G. Abbas, [arXiv:2310.12915 [hep-ph]].
- [6] G. Abbas and N. Singh, [arXiv:2312.16532 [hep-ph]].
- [7] C. D. Froggatt and H. B. Nielsen, *Nucl. Phys. B* **147**, 277 (1979). doi:10.1016/0550-3213(79)90316-X
- [8] M. Leurer, Y. Nir and N. Seiberg, *Nucl. Phys. B* **398**, 319 (1993); M. Leurer, Y. Nir and N. Seiberg, *Nucl. Phys. B* **420**, 468 (1994).
- [9] E. J. Chun and A. Lukas, *Phys. Lett. B* **387**, 99-106 (1996) doi:10.1016/0370-2693(96)01015-5 [arXiv:hep-ph/9605377 [hep-ph]].
- [10] K. S. Babu and S. Nandi, *Phys. Rev. D* **62**, 033002 (2000) doi:10.1103/PhysRevD.62.033002 [hep-ph/9907213].
- [11] G. G. Ross and L. Velasco-Sevilla, *Nucl. Phys. B* **653**, 3-26 (2003) doi:10.1016/S0550-3213(03)00041-5 [arXiv:hep-ph/0208218 [hep-ph]]. S. F. King, *JHEP* **01**, 119 (2014) doi:10.1007/JHEP01(2014)119 [arXiv:1311.3295 [hep-ph]]. G. F. Giudice and O. Lebedev, *Phys. Lett. B* **665**, 79-85 (2008) doi:10.1016/j.physletb.2008.05.062 [arXiv:0804.1753 [hep-ph]].
- [12] A. Davidson, V. P. Nair and K. C. Wali, *Phys. Rev. D* **29**, 1504 (1984) doi:10.1103/PhysRevD.29.1504
- [13] A. Davidson and K. C. Wali, *Phys. Rev. Lett.* **60**, 1813 (1988) doi:10.1103/PhysRevLett.60.1813
- [14] Z. G. Berezhiani and M. Y. Khlopov, *Sov. J. Nucl. Phys.* **51**, 739-746 (1990)
- [15] Z. G. Berezhiani and M. Y. Khlopov, *Sov. J. Nucl. Phys.* **51**, 935-942 (1990)
- [16] Z. G. Berezhiani and M. Y. Khlopov, *Z. Phys. C* **49**, 73-78 (1991) doi:10.1007/BF01570798
- [17] A. S. Sakharov and M. Y. Khlopov, *Phys. Atom. Nucl.* **57**, 651-658 (1994)
- [18] A. R. Shaikh and R. Adhikari, [arXiv:2404.11570 [hep-ph]].
- [19] J. L. Yang, H. B. Zhang and T. F. Feng, *Eur. Phys. J. C* **84**, no.6, 616 (2024) doi:10.1140/epjc/s10052-024-12958-5 [arXiv:2405.17807 [hep-ph]].
- [20] G. Abbas, *Int. J. Mod. Phys. A* **36**, 2150090 (2021) doi:10.1142/S0217751X21500901 [arXiv:1807.05683 [hep-ph]].
- [21] G. Abbas, V. Singh, N. Singh and R. Sain, *Eur. Phys. J. C* **83**, no.4, 305 (2023) doi:10.1140/epjc/s10052-023-11471-5 [arXiv:2208.03733 [hep-ph]].
- [22] T. Higaki and J. Kawamura, *JHEP* **03**, 129 (2020) doi:10.1007/JHEP03(2020)129 [arXiv:1911.09127 [hep-ph]].
- [23] A. Greljo, A. Smolkovič and A. Valenti, [arXiv:2407.02998 [hep-ph]].
- [24] H. Georgi and S. L. Glashow, *Phys. Rev. D* **7**, 2457 (1973).
- [25] T. Gherghetta and A. Pomarol, *Nucl. Phys. B* **586**, 141 (2000); Y. Grossman and M. Neubert, *Phys. Lett. B* **474**, 361 (2000); M. Blanke, A. J. Buras, B. Duling, S. Gori and A. Weiler, *JHEP* **0903**, 001 (2009); S. Casagrande, F. Goertz, U. Haisch, M. Neubert and T. Pfoh, *JHEP* **0810**, 094 (2008); M. Bauer, S. Casagrande, U. Haisch and M. Neubert, *JHEP* **1009**, 017 (2010).

- [26] D. B. Kaplan, Nucl. Phys. B **365**, 259 (1991).
- [27] J. Fuentes-Martin, G. Isidori, J. M. Lizana, N. Selimovic and B. A. Stefanek, Phys. Lett. B **834**, 137382 (2022) doi:10.1016/j.physletb.2022.137382 [arXiv:2203.01952 [hep-ph]].
- [28] G. Abbas, Phys. Lett. B **773**, 252-257 (2017) doi:10.1016/j.physletb.2017.08.028 [arXiv:1706.02564 [hep-ph]].
- [29] G. Abbas, Mod. Phys. Lett. A **34**, no.15, 1950119 (2019) doi:10.1142/S0217732319501190 [arXiv:1706.01052 [hep-ph]].
- [30] G. Abbas, Phys. Rev. D **95**, no.1, 015029 (2017) doi:10.1103/PhysRevD.95.015029 [arXiv:1609.02899 [hep-ph]].
- [31] G. Abbas, Mod. Phys. Lett. A **31**, no.19, 1650117 (2016) doi:10.1142/S0217732316501170 [arXiv:1605.02497 [hep-ph]].
- [32] I. Dorsner and S. M. Barr, Phys. Rev. D **65**, 095004 (2002) doi:10.1103/PhysRevD.65.095004 [arXiv:hep-ph/0201207 [hep-ph]].
- [33] M. Bauer, M. Carena and K. Gemmler, Phys. Rev. D **94**, no.11, 115030 (2016) doi:10.1103/PhysRevD.94.115030 [arXiv:1512.03458 [hep-ph]].
- [34] M. Bauer, T. Schell and T. Plehn, Phys. Rev. D **94**, no.5, 056003 (2016) doi:10.1103/PhysRevD.94.056003 [arXiv:1603.06950 [hep-ph]].
- [35] L. Calibbi, A. Crivellin and B. Zaldivar, Phys. Rev. D **92**, no.1, 016004 (2015) doi:10.1103/PhysRevD.92.016004 [arXiv:1501.07268 [hep-ph]].
- [36] M. Fedele, A. Mastroddi and M. Valli, JHEP **03**, 135 (2021) doi:10.1007/JHEP03(2021)135 [arXiv:2009.05587 [hep-ph]].
- [37] K. Tsumura and L. Velasco-Sevilla, Phys. Rev. D **81**, 036012 (2010) doi:10.1103/PhysRevD.81.036012 [arXiv:0911.2149 [hep-ph]].
- [38] E. L. Berger, S. B. Giddings, H. Wang and H. Zhang, Phys. Rev. D **90**, no. 7, 076004 (2014) doi:10.1103/PhysRevD.90.076004 [arXiv:1406.6054 [hep-ph]].
- [39] K. Huitu, V. Keus, N. Koivunen and O. Lebedev, JHEP **05**, 026 (2016) doi:10.1007/JHEP05(2016)026 [arXiv:1603.06614 [hep-ph]].
- [40] J. L. Diaz-Cruz and U. J. Saldaña-Salazar, Nucl. Phys. B **913**, 942-963 (2016) doi:10.1016/j.nuclphysb.2016.10.018 [arXiv:1405.0990 [hep-ph]].
- [41] M. A. Arroyo-Ureña, J. L. Díaz-Cruz, G. Tavares-Velasco, A. Bolaños and G. Hernández-Tomé, Phys. Rev. D **98**, no.1, 015008 (2018) doi:10.1103/PhysRevD.98.015008 [arXiv:1801.00839 [hep-ph]].
- [42] M. A. Arroyo-Ureña, A. Fernández-Téllez and G. Tavares-Velasco, [arXiv:1906.07821 [hep-ph]].
- [43] M. A. Arroyo-Ureña, A. Chakraborty, J. L. Díaz-Cruz, D. K. Ghosh, N. Khan and S. Moretti, [arXiv:2205.12641 [hep-ph]].
- [44] A. Chakraborty, D. K. Ghosh, N. Khan and S. Moretti, [arXiv:2405.16939 [hep-ph]].
- [45] A. Abada *et al.* [FCC], Eur. Phys. J. ST **228**, no.5, 1109-1382 (2019) doi:10.1140/epjst/e2019-900088-6
- [46] A. Abada *et al.* [FCC], Eur. Phys. J. C **79**, no.6, 474 (2019) doi:10.1140/epjc/s10052-019-6904-3
- [47] A. Rasin, Phys. Rev. D **58**, 096012 (1998) doi:10.1103/PhysRevD.58.096012 [arXiv:hep-ph/9802356 [hep-ph]].

- [48] G. G. Ross in “flavour Physics for the Millennium”, Editor Jonathan L. Rosner, World Scientific, Singapore, 2001
- [49] G. Abbas, R. Adhikari and E. J. Chun, [arXiv:2303.10125 [hep-ph]].
- [50] P.A. Zyla et al. (Particle Data Group), Prog. Theor. Exp. Phys. 2020, 083C01 (2020) and 2021 update
- [51] Y. Aoki *et al.*, [arXiv:2111.09849v1 [hep-lat]].
- [52] M. Ciuchini *et al.*, JHEP **9810** (1998) 008 doi:10.1088/1126-6708/1998/10/008 [hep-ph/9808328].
- [53] J. Brod and M. Gorbahn, Next-to-next-to-leading-order charm-quark contribution to the CP violation parameter ϵ_K and ΔM_K , Phys.Rev.Lett. 108 (2012) 121801, [1108.2036]
- [54] Buchalla, Gerhard and Buras, Andrzej J. and Lautenbacher, Markus E., doi:10.1103/RevModPhys.68.1125, <https://link.aps.org/doi/10.1103/RevModPhys.68.1125>
- [55] J. Brod and M. Gorbahn, ϵ_K at next-to-next-to-leading order: the charm-top-quark contribution, Phys. Rev. D82 (2010) 094026, [1007.0684].
- [56] D. Becirevic, V. Gimenez, G. Martinelli, M. Papinutto and J. Reyes, JHEP **04** (2002), 025 doi:10.1088/1126-6708/2002/04/025 [arXiv:hep-lat/0110091 [hep-lat]].
- [57] M. Bona *et al.* [UTfit Collaboration], JHEP **0803**, 049 (2008), <http://www.utfit.org/UTfit/>
- [58] Y. Amhis *et al.* [HFLAV], Eur. Phys. J. C **77**, no.12, 895 (2017) doi:10.1140/epjc/s10052-017-5058-4 [arXiv:1612.07233 [hep-ex]].
- [59] A. J. Buras, F. De Fazio, J. Girrbach, R. Kneijens and M. Nagai, JHEP **1306**, 111 (2013).
- [60] A. Crivellin, A. Kokulu and C. Greub, Phys. Rev. D **87**, no. 9, 094031 (2013).
- [61] D. Becirevic, M. Ciuchini, E. Franco, V. Gimenez, G. Martinelli, A. Masiero, M. Papinutto, J. Reyes and L. Silvestrini, Nucl. Phys. B **634** (2002), 105-119 doi:10.1016/S0550-3213(02)00291-2 [arXiv:hep-ph/0112303 [hep-ph]].
- [62] A. Donini, V. Gimenez, L. Giusti and G. Martinelli, Phys. Lett. B **470**, 233-242 (1999) doi:10.1016/S0370-2693(99)01300-3 [arXiv:hep-lat/9910017 [hep-lat]].
- [63] J. Charles, S. Descotes-Genon, Z. Ligeti, S. Monteil, M. Papucci, K. Trabelsi and L. Vale Silva, Phys. Rev. D **102**, no.5, 056023 (2020) doi:10.1103/PhysRevD.102.056023 [arXiv:2006.04824 [hep-ph]].
- [64] J. Charles, S. Descotes-Genon, Z. Ligeti, S. Monteil, M. Papucci and K. Trabelsi, Phys. Rev. D **89**, no.3, 033016 (2014) doi:10.1103/PhysRevD.89.033016 [arXiv:1309.2293 [hep-ph]].
- [65] M. Bona [UTfit], PoS **CKM2016**, 143 (2017) doi:10.22323/1.291.0143
- [66] T. Inami and C. S. Lim, Prog. Theor. Phys. **65**, 297 (1981) [erratum: Prog. Theor. Phys. **65**, 1772 (1981)] doi:10.1143/PTP.65.297
- [67] A. J. Buras, J. Girrbach, D. Guadagnoli and G. Isidori, Eur. Phys. J. C **72**, 2172 (2012) doi:10.1140/epjc/s10052-012-2172-1 [arXiv:1208.0934 [hep-ph]].
- [68] Y. Amhis *et al.* [HFLAV], [arXiv:2206.07501 [hep-ex]].
- [69] R. Aaij *et al.* [LHCb], Phys. Rev. Lett. **128**, no.4, 041801 (2022) doi:10.1103/PhysRevLett.128.041801 [arXiv:2108.09284 [hep-ex]].
- [70] R. Aaij *et al.* [LHCb], Phys. Rev. D **105**, no.1, 012010 (2022) doi:10.1103/PhysRevD.105.012010 [arXiv:2108.09283 [hep-ex]].

- [71] K. De Bruyn, R. Fleischer, R. Kneijens, P. Koppenburg, M. Merk, A. Pellegrino and N. Tuning, Phys. Rev. Lett. **109**, 041801 (2012) doi:10.1103/PhysRevLett.109.041801 [arXiv:1204.1737 [hep-ph]].
- [72] R. Fleischer, [arXiv:1212.4967 [hep-ph]].
- [73] [CMS], CMS-PAS-BPH-21-006.
- [74] W. Altmannshofer and F. Archilli, [arXiv:2206.11331 [hep-ph]].
- [75] K. De Bruyn, R. Fleischer, R. Kneijens, P. Koppenburg, M. Merk and N. Tuning, Phys. Rev. D **86** (2012), 014027 doi:10.1103/PhysRevD.86.014027 [arXiv:1204.1735 [hep-ph]].
- [76] M. Gorbahn and U. Haisch, Phys. Rev. Lett. **97**, 122002 (2006) doi:10.1103/PhysRevLett.97.122002 [arXiv:hep-ph/0605203 [hep-ph]].
- [77] R. Aaij *et al.* [LHCb], Phys. Lett. B **725**, 15-24 (2013) doi:10.1016/j.physletb.2013.06.037 [arXiv:1305.5059 [hep-ex]].
- [78] M. Ciuchini, M. Fedele, E. Franco, A. Paul, L. Silvestrini and M. Valli, Phys. Rev. D **107** (2023) no.5, 055036 [arXiv:2212.10516 [hep-ph]].
- [79] J. P. Lees *et al.* [BaBar Collaboration], Phys. Rev. Lett. **112**, 211802 (2014) [arXiv:1312.5364 [hep-ex]].
- [80] R. Aaij *et al.* [LHCb], JHEP **11** (2016), 047 [arXiv:1606.04731 [hep-ex]].
- [81] CDF Collaboration, CDF public note 10894.
- [82] V. Khachatryan *et al.* [CMS Collaboration], Phys. Lett. B **753**, 424 (2016) [arXiv:1507.08126 [hep-ex]].
- [83] R. Aaij *et al.* [LHCb Collaboration], JHEP **1406**, 133 (2014) [arXiv:1403.8044 [hep-ex]].
- [84] R. Aaij *et al.* [LHCb], Phys. Rev. Lett. **127** (2021) no.15, 151801 [arXiv:2105.14007 [hep-ex]].
- [85] R. Aaij *et al.* [LHCb], Phys. Rev. Lett. **125** (2020) no.1, 011802 [arXiv:2003.04831 [hep-ex]].
- [86] M. Aaboud *et al.* [ATLAS], JHEP **10**, 047 (2018) [arXiv:1805.04000 [hep-ex]].
- [87] A. M. Sirunyan *et al.* [CMS], Phys. Lett. B **781**, 517-541 (2018) [arXiv:1710.02846 [hep-ex]].
- [88] R. Aaij *et al.* [LHCb], Phys. Rev. Lett. **126**, no.16, 161802 (2021) [arXiv:2012.13241 [hep-ex]].
- [89] R. Aaij *et al.* [LHCb], JHEP **11**, 043 (2021) [arXiv:2107.13428 [hep-ex]].
- [90] F. James and M. Roos, Comput. Phys. Commun. **10**, 343-367 (1975)
- [91] D. M. Straub, arXiv:1810.08132 [hep-ph].
- [92] A. Bharucha, D. M. Straub and R. Zwicky, JHEP **08**, 098 (2016) [arXiv:1503.05534 [hep-ph]].
- [93] N. Gubernari, A. Kokulu and D. van Dyk, JHEP **01**, 150 (2019) [arXiv:1811.00983 [hep-ph]].
- [94] A. K. Alok, N. R. Singh Chundawat, S. Gangal and D. Kumar, Eur. Phys. J. C **82** (2022) no.10, 967 [arXiv:2203.13217 [hep-ph]].
- [95] N. R. Singh Chundawat, Phys. Rev. D **107** (2023), 075014 [arXiv:2207.10613 [hep-ph]].
- [96] N. R. Singh Chundawat, Phys. Rev. D **107** (2023) no.5, 055004 [arXiv:2212.01229 [hep-ph]].
- [97] C. Bobeth, G. Hiller and G. Piranishvili, JHEP **12** (2007), 040 [arXiv:0709.4174 [hep-ph]].
- [98] A. K. Alok, A. Dighe and S. U. Sankar, Phys. Rev. D **78** (2008), 114025 [arXiv:0810.3779 [hep-ph]].

- [99] J. Charles, A. Le Yaouanc, L. Oliver, O. Pene and J. C. Raynal, Phys. Rev. D **60** (1999), 014001 [arXiv:hep-ph/9812358 [hep-ph]].
- [100] M. Beneke and T. Feldmann, Nucl. Phys. B **592** (2001), 3-34 [arXiv:hep-ph/0008255 [hep-ph]].
- [101] A. M. Baldini *et al.* [MEG], Eur. Phys. J. C **76**, no.8, 434 (2016) doi:10.1140/epjc/s10052-016-4271-x [arXiv:1605.05081 [hep-ex]].
- [102] A. M. Baldini *et al.* [MEG II], Eur. Phys. J. C **78**, no.5, 380 (2018) doi:10.1140/epjc/s10052-018-5845-6 [arXiv:1801.04688 [physics.ins-det]].
- [103] B. Aubert *et al.* [BaBar], Phys. Rev. Lett. **104**, 021802 (2010) doi:10.1103/PhysRevLett.104.021802 [arXiv:0908.2381 [hep-ex]].
- [104] E. Kou *et al.* [Belle-II], PTEP **2019**, no.12, 123C01 (2019) [erratum: PTEP **2020**, no.2, 029201 (2020)] doi:10.1093/ptep/ptz106 [arXiv:1808.10567 [hep-ex]].
- [105] W. H. Bertl *et al.* [SINDRUM II], Eur. Phys. J. C **47**, 337-346 (2006) doi:10.1140/epjc/s2006-02582-x
- [106] M. L. Wong [COMET], PoS **FPCP2015**, 059 (2015) doi:10.22323/1.248.0059
- [107] Akiro SATO https://indico.fnal.gov/event/46669/contributions/203149/attachments/138299/173056/201210_PRISM_sato.pdf
- [108] R. M. Carey *et al.* [Mu2e], doi:10.2172/952028
- [109] N. Teshima [DeeMe], SciPost Phys. Proc. **1**, 051 (2019) doi:10.21468/SciPostPhysProc.1.051 [arXiv:1811.04235 [physics.ins-det]].
- [110] S. Davidson and B. Echenard, Eur. Phys. J. C **82**, no.9, 836 (2022) doi:10.1140/epjc/s10052-022-10773-4 [arXiv:2204.00564 [hep-ph]].
- [111] Y. Kuno, Nucl. Phys. B Proc. Suppl. **225-227**, 228-231 (2012) doi:10.1016/j.nuclphysbps.2012.02.047
- [112] U. Bellgardt *et al.* [SINDRUM], Nucl. Phys. B **299**, 1-6 (1988) doi:10.1016/0550-3213(88)90462-2
- [113] A. Blondel, A. Bravar, M. Pohl, S. Bachmann, N. Berger, M. Kiehn, A. Schoning, D. Wiedner, B. Windelband and P. Eckert, *et al.* [arXiv:1301.6113 [physics.ins-det]].
- [114] K. Hayasaka, K. Inami, Y. Miyazaki, K. Arinstein, V. Aulchenko, T. Aushev, A. M. Bakich, A. Bay, K. Belous and V. Bhardwaj, *et al.* Phys. Lett. B **687**, 139-143 (2010) doi:10.1016/j.physletb.2010.03.037 [arXiv:1001.3221 [hep-ex]].
- [115] M. A. Shifman, A. I. Vainshtein and V. I. Zakharov, Phys. Lett. B **78**, 443-446 (1978) doi:10.1016/0370-2693(78)90481-1
- [116] A. Crivellin, M. Hoferichter and M. Procura, Phys. Rev. D **89**, 054021 (2014) doi:10.1103/PhysRevD.89.054021 [arXiv:1312.4951 [hep-ph]].
- [117] A. Crivellin, M. Hoferichter and M. Procura, Phys. Rev. D **89**, 093024 (2014) doi:10.1103/PhysRevD.89.093024 [arXiv:1404.7134 [hep-ph]].
- [118] P. Junnarkar and A. Walker-Loud, Phys. Rev. D **87**, 114510 (2013) doi:10.1103/PhysRevD.87.114510 [arXiv:1301.1114 [hep-lat]].
- [119] R. Kitano, M. Koike and Y. Okada, Phys. Rev. D **66**, 096002 (2002) [erratum: Phys. Rev. D **76**, 059902 (2007)] doi:10.1103/PhysRevD.76.059902 [arXiv:hep-ph/0203110 [hep-ph]].
- [120] T. Goto, R. Kitano and S. Mori, Phys. Rev. D **92**, 075021 (2015) doi:10.1103/PhysRevD.92.075021 [arXiv:1507.03234 [hep-ph]].

- [121] A. M. Sirunyan *et al.* [CMS], JHEP **06** (2018), 127 [erratum: JHEP **03** (2019), 128] doi:10.1007/JHEP06(2018)127 [arXiv:1804.01939 [hep-ex]].
- [122] G. Aad *et al.* [ATLAS], JHEP **07**, 200 (2023) doi:10.1007/JHEP07(2023)200 [arXiv:2211.02617 [hep-ex]].
- [123] A. M. Sirunyan *et al.* [CMS], JHEP **03**, 034 (2020) doi:10.1007/JHEP03(2020)034 [arXiv:1912.01594 [hep-ex]].
- [124] G. Aad *et al.* [ATLAS], Phys. Lett. B **822**, 136651 (2021) doi:10.1016/j.physletb.2021.136651 [arXiv:2102.13405 [hep-ex]].
- [125] A. M. Sirunyan *et al.* [CMS], Phys. Rev. D **98** (2018) no.9, 092001 doi:10.1103/PhysRevD.98.092001 [arXiv:1809.00327 [hep-ex]].
- [126] J. A. Aguilar-Saavedra and G. C. Branco, Phys. Lett. B **495**, 347 (2000).
- [127] A. D. Martin, W. J. Stirling, R. S. Thorne and G. Watt, Eur. Phys. J. C **63**, 189-285 (2009) doi:10.1140/epjc/s10052-009-1072-5 [arXiv:0901.0002 [hep-ph]].
- [128] A. Alloul, N. D. Christensen, C. Degrande, C. Duhr and B. Fuks, Comput. Phys. Commun. **185**, 2250-2300 (2014) doi:10.1016/j.cpc.2014.04.012 [arXiv:1310.1921 [hep-ph]].
- [129] J. Alwall, R. Frederix, S. Frixione, V. Hirschi, F. Maltoni, O. Mattelaer, H. S. Shao, T. Stelzer, P. Torrielli and M. Zaro, JHEP **07**, 079 (2014) doi:10.1007/JHEP07(2014)079 [arXiv:1405.0301 [hep-ph]].
- [130] G. Aad *et al.* [ATLAS], JHEP **03**, 145 (2020) doi:10.1007/JHEP03(2020)145 [arXiv:1910.08447 [hep-ex]].
- [131] A. M. Sirunyan *et al.* [CMS], JHEP **05**, 033 (2020) doi:10.1007/JHEP05(2020)033 [arXiv:1911.03947 [hep-ex]].
- [132] M. Aaboud *et al.* [ATLAS], JHEP **01**, 055 (2018) doi:10.1007/JHEP01(2018)055 [arXiv:1709.07242 [hep-ex]].
- [133] A. M. Sirunyan *et al.* [CMS], JHEP **09** (2018), 007 doi:10.1007/JHEP09(2018)007 [arXiv:1803.06553 [hep-ex]].
- [134] G. Aad *et al.* [ATLAS], Phys. Lett. B **796** (2019), 68-87 doi:10.1016/j.physletb.2019.07.016 [arXiv:1903.06248 [hep-ex]].
- [135] A. M. Sirunyan *et al.* [CMS], JHEP **07** (2021), 208 doi:10.1007/JHEP07(2021)208 [arXiv:2103.02708 [hep-ex]].
- [136] G. Aad *et al.* [ATLAS], JHEP **23** (2020), 082 doi:10.1007/JHEP10(2023)082 [arXiv:2307.08567 [hep-ex]].
- [137] A. Tumasyan *et al.* [CMS], JHEP **05** (2023), 227 doi:10.1007/JHEP05(2023)227 [arXiv:2205.06709 [hep-ex]].
- [138] A. Tumasyan *et al.* [CMS], Phys. Rev. D **108** (2023) no.1, 012009 doi:10.1103/PhysRevD.108.012009 [arXiv:2205.01835 [hep-ex]].
- [139] M. Aaboud *et al.* [ATLAS], Phys. Rev. D **99** (2019) no.9, 092004 doi:10.1103/PhysRevD.99.092004 [arXiv:1902.10077 [hep-ex]].
- [140] G. Aad *et al.* [ATLAS], JHEP **10** (2020), 061 doi:10.1007/JHEP10(2020)061 [arXiv:2005.05138 [hep-ex]].
- [141] A. M. Sirunyan *et al.* [CMS], JHEP **04** (2019), 031 doi:10.1007/JHEP04(2019)031 [arXiv:1810.05905 [hep-ex]].

- [142] A. Tumasyan *et al.* [CMS], JHEP **07**, 073 (2023) doi:10.1007/JHEP07(2023)073 [arXiv:2208.02717 [hep-ex]].
- [143] G. Aad *et al.* [ATLAS], JHEP **07**, 155 (2023) doi:10.1007/JHEP07(2023)155 [arXiv:2211.04172 [hep-ex]].
- [144] ATLAS-CONF-2023-035, 15 Jun 2023.
- [145] [CMS], CMS-PAS-HIG-20-002.
- [146] G. Aad *et al.* [ATLAS], JHEP **07**, 203 (2023) doi:10.1007/JHEP07(2023)203 [arXiv:2211.01136 [hep-ex]].
- [147] A. M. Sirunyan *et al.* [CMS], Eur. Phys. J. C **80** (2020) no.2, 75 doi:10.1140/epjc/s10052-019-7593-7 [arXiv:1908.06463 [hep-ex]].
- [148] M. Aaboud *et al.* [ATLAS], Phys. Rev. Lett. **121**, no.19, 191801 (2018) [erratum: Phys. Rev. Lett. **122**, no.8, 089901 (2019)] doi:10.1103/PhysRevLett.121.191801 [arXiv:1808.00336 [hep-ex]].
- [149] A. M. Sirunyan *et al.* [CMS], Phys. Rev. D **96**, no.7, 072004 (2017) doi:10.1103/PhysRevD.96.072004 [arXiv:1707.00350 [hep-ex]].
- [150] M. Aaboud *et al.* [ATLAS], JHEP **01**, 030 (2019) doi:10.1007/JHEP01(2019)030 [arXiv:1804.06174 [hep-ex]].
- [151] A. M. Sirunyan *et al.* [CMS], JHEP **08**, 152 (2018) doi:10.1007/JHEP08(2018)152 [arXiv:1806.03548 [hep-ex]].
- [152] G. Aad *et al.* [ATLAS], Phys. Rev. D **105**, no.1, 012006 (2022) doi:10.1103/PhysRevD.105.012006 [arXiv:2110.00313 [hep-ex]].
- [153] A. Hayrapetyan *et al.* [CMS], [arXiv:2402.13358 [hep-ex]].
- [154] M. Aaboud *et al.* [ATLAS], JHEP **10**, 031 (2018) doi:10.1007/JHEP10(2018)031 [arXiv:1806.07355 [hep-ex]].
- [155] A. Hayrapetyan *et al.* [CMS], [arXiv:2403.10341 [hep-ex]].
- [156] Under progress.
- [157] D. Binosi, J. Collins, C. Kaufhold and L. Theussl, Comput. Phys. Commun. **180**, 1709-1715 (2009) doi:10.1016/j.cpc.2009.02.020 [arXiv:0811.4113 [hep-ph]].
- [158] Z. z. Xing, H. Zhang and S. Zhou, Phys. Rev. D **77**, 113016 (2008) doi:10.1103/PhysRevD.77.113016 [arXiv:0712.1419 [hep-ph]].
- [159] H. Harari and N. Seiberg, Phys. Lett. B **102**, 263-266 (1981) doi:10.1016/0370-2693(81)90871-6
- [160] K. I. Aoki and M. Bando, Prog. Theor. Phys. **70**, 272 (1983) doi:10.1143/PTP.70.272